5-2020

Identification and Quantification of Black Carbon Particulates in Urban River Sediments Involving a Multi-tiered Analytical Approach

Anastasia Figueroa

ABSTRACT

Black Carbon ('BC') is routinely defined as the residual carbon fraction resulting from the incomplete combustion of biomass and/or biofuels (Agarwal et al. 2011). BC is best described as spectrum of carbonaceous combustion by-products, encompassing partially combusted, charred plant tissues, to highly graphitized soot (Shrestha et al. 2010). The highly condensed aromatic structures which exist in the BC matrix are largely responsible for its resistance to further biological or chemical degradation, as well as, its efficient sorption properties in soils and sediments (Forbes et al., 2006; Shrestha et al., 2010). Using a multi-tiered geochemical approach, quantification of BC was coupled with environmental forensics of other contaminants of concern in a highly urbanized/industrialized, tidally influenced river (Lower Hackensack River, New Jersey, USA). This approach allowed for further understanding involving the accumulation and mobility of BC particles in relation to other contaminants of concern and the sedimentation fluxes and hydrodynamic processes which influence them. Review of BC as a potential index parameter for other hydrophobic organic compounds, such as the ever-persistent polycyclic aromatic hydrocarbons (PAHs), was included as part of this research due to their synchronous co-emission inputs and complimentary high sorption capabilities. Analytical quantitative efforts included an array of chemical, thermal and oxidative isolation/extraction techniques including: the Lloyd Kahn method for total organic carbon (TOC) analysis, modified TOC analysis for BC determination, EPA Method 8270 for priority PAHs, loss on ignition (LOI), pyrolysis-gas chromatography mass spectrometry (Py-GC/MS) for evaluation of parent and alkylated PAH assemblages, chemo-thermal oxidation at 375ºC (CTO-375), and major and minor elemental analysis involving scanning electron microscopy (SEM). PAH ratios of various principal masses (m/z 178, 202, 228, etc.,) were also utilized in conjunction with alkyl PAH series ratios to infer potential BC source inputs and to allow for a comprehensive analysis of the chemical characteristics of the historically impacted Lower Hackensack River sediment. Lastly, routine ecological and risk assessment analytical techniques, such as grain size distribution and percent moisture (of sediments) were included as part of this comprehensive sediment study. Historical river-sediment data provided by several federal and state agencies were also evaluated to allow for elucidation of spatial trends relative to heavy metal concentrations, PAHs and other contaminants of concern. Ultimately, the results indicate relatively low concentrations of BC (in comparison to TOC) throughout the lower river sediments, with a general increasing trend observed further downstream adjacent to various petroleum related industries. Qualitative and quantitative analysis of BC particles via SEM further revealed the likely presence of coal fly ash, and various amorphous pyrolytic BC particles. The results of this study also demonstrate the importance of considering different analytical approaches when attempting to quantify BC stocks in an urbanized waterway such as the Lower Hackensack River.

MONTCLAIR STATE UNIVERSITY

Identification and Quantification of Black Carbon Particulates in Urban River Sediments Involving a Multi-tiered Analytical Approach.

By

Anastasia Figueroa

A Master's Thesis Submitted to the Faculty of

Montclair State University

In Partial Fulfillment of the Requirements

For the Degree of

Master of Science

May 2020

School: College of Science and Mathematics

Department: Earth and Environmental Studies

Thesis Committee:

[redacted]

Dr. Gregory Pope
Thesis Sponsor

[redacted]

Dr. Michael Kruge
Committee Member

[redacted]

Dr. Yang Deng
Committee Member

IDENTIFICATION AND QUANTIFICATION OF BLACK CARBON PARTICULATES IN URBAN RIVER SEDIMENTS INVOLVING A MULTI-TIERED ANALYTICAL APPROACH

A THESIS

Submitted in partial fulfillment of the requirements

For the degree of Master of Science

By

Anastasia Figueroa

Montclair State University
Montclair, New Jersey
2020

ACKNOWLEDGEMENTS

Many acknowledgments are due, as this interdisciplinary research involved great coordination. First, thank you to my thesis advisor, Dr. Gregory Pope, and thesis committee members Dr. Michael Kruge and Dr. Yang Deng. Dr. Pope, thank you for providing me with constant support and encouragement. Thank you for mentoring me as I navigated my graduate school experience. Also, thank you for the many pieces of 'freak-out' chocolate. To Dr. Kruge, thank you for also providing mentorship and helping me develop my appreciation and love for organic geochemistry and all things petroleum. To Dr. Deng, thank you for providing support, feedback regarding analytical design, and casual conversations.

To Diane Hagmann, thank you for all the laboratory assistance and support. Without your constant assistance I would not have been able to accomplish this research. Thank you for joining me in sample collection and for method interpretation and analysis. Also, thank you Dr. Xiaona Li and Dr. Laying Wu for the guidance and assistance regarding laboratory analysis. Both of your insights regarding data processing, analysis, and interpretations was very much appreciated. Thank you to Dr. Stefanie Brachfeld and Nichole Anest, Curator at Lamont-Doherty Core Repository, for assisting me with particle size determination and other analytical components. Thank you to all my other Montclair State EAES professors who have guided me and supported me through this research journey.

Thank you to Dr. Michael Leftin, Laboratory Director, at Integrated Analytical Laboratories for your gracious analytical assistance. Thank you to the entire staff at IAL for assisting me with this research endeavor, without your support for higher education this would have not been made possible. Thank you to my former and current employers who allowed me access to sampling equipment and materials.

A very special thank you to the Captain Bill Sheehan and Hugh M. Carola and the Hackensack Riverkeeper Organization. Thank you for providing me access to sampling sites and also a great vast of marine-time knowledge regarding the Lower Hackensack River. Also, thank you for your constant fight defending this beautiful and rich waterway.

Thank you to my loving and supporting parents who have always believed in my research pursuits. Thank you to my siblings, my family, and friends who constantly provided support and encouragement. To Chris Bush, thank you for being at my side this entire journey and for picking up pieces as I consumed myself with this research. I dedicate this thesis to all my mentors who have shaped the environmental scientist I am today. Thank you for teaching me the values of hard work, attention to details, and the importance of having an inquisitive mind.

Table of Contents

FIGURES:

TABLES:

1. INTRODUCTION

Black Carbon (BC) is often defined as the refractory carbon (RC) created during the incomplete combustion of fossil fuels, biofuels and biomass (Shrestha et al., 2010). BC particles encompass a wide spectrum of pyrolytic carbonaceous materials ranging from slightly burned plant tissue (i.e. char) to various aromatic condensates (i.e. soot) (Sanchez-Garcia et al., 2013). BC particles have largely been overlooked in ecological risk assessments and sediment investigations. Such oversight however can be problematic when attempting to quantify total carbon (C) fractions within sediment or soil, resulting in either over-estimation or under-estimation of certain C fractions.

The various carbon fractions of sediments include, inorganic carbon (IC), which refers to the presence of any carbonates (i.e., calcite or aragonite shells , organic carbon (OC) encompassing all organic compounds present and refractory ('residual' or 'resistant' carbon carbon (RC), which is typically defined as relatively inert carbonaceous materials, including BC particles (Oen et al., 2006; Agarwal & Bucheli (2011). Definitional variations exist for all carbon components, owing to the relative analytical difficulty when distinguishing and characterizing the various C components. Generally, sediment studies and investigations focus solely on total organic carbon (TOC) which is routinely defined as the sum of all organic carbon compounds present, including any RC or BC compounds (Oen et al., 2006). The New Jersey Department of Environmental Protection (NJDEP) routinely requires sediment and ground water investigations to include TOC evaluation due to the linear relationship between organic carbon content and various organic contaminants and defines whether the sample area is depositional in nature. (NJDEP, 2013). The TOC analysis required is a non-specific test, meaning it does not distinguish

the individual components of the complex OC mixture present, but rather reports the overall sum (Kahn, 1988). The relative concentration of TOC in sediment or soil provides insight regarding how organic compounds, including hydrophobic organic compounds (i.e., PAHs and BC particles) are distributed, absorbed and move in a dynamic and complex environment (Shrestha et al., 2014). Additionally, the presence of organic matter can provide insight regarding the sulfate/sulfide cycle in tidally influenced estuarine areas and can also serve as a useful predicator for certain metal and HC-related compounds (Konsevick & Bragin, 2010). BC particles are a component of the overall RC content, which is one component of the overall OC content, which is a component of the organic matter present (Killops & Killops, 2005). Therefore, to properly evaluate and quantify BC particles, it is imperative to clearly define what is being measured and how it is being measured and reported to avoid over or under estimation or misidentification (Forbes et al., 2006).

BC particles themselves are largely resistant to further alteration relative to other organic forms and are often described as relatively inert material with the potential of enhancing other chemical and physical properties (Sanchez-Garcia et al., 2013; Shrestha et al., 2010). BC ‘s relative resistance and strength allow it serve as a stable organic indicator of geochemical and ecological conditions over time. The highly condensed aromatic structures and few functional groups which exist in BC are largely responsible for its resistance to further biological or chemical degradation, as well as its efficient pollution sorption properties in soils and sediments (Forbes et al., 2006; Shrestha et al., 2010). Further, the condensed aromatic moieties which exist within BC particles are directly correlated to the different pyrogenic conditions in which they were formed (Sanchez-Garcia et al., 2013; Kruge, 2015, Ulher, 2005). For example, char is often formed as a result of lower temperature flaming and smoldering, while soot is commonly formed

as a result of high temperature flaming and pressure allowing for the re-condensation of fine particles into complex aromatic structures (Sanchez-Garcia et al., 2013). The duration, temperature of combustion, extent of combustion, and presence of oxygen during combustion, influences the extent of polymerization and surface functional group composition of the associated BC particles (Shrestha et al., 2010). Figure 1 summarizes the wide spectrum of BC's physical and chemical characteristics.

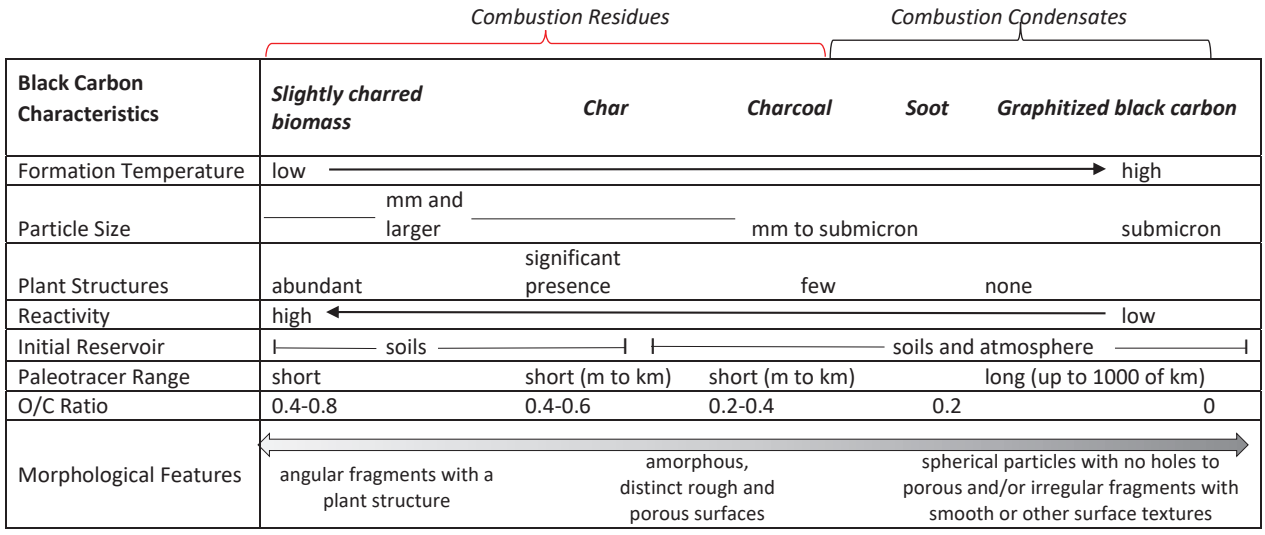

Figure 1. Summary compilation of common BC characteristics. Modified from Schimmelpfennig et al. (2012) and Stoffyn-Egli et al. (1997).

BC particles can cover a spectrum of sizes and shapes, spanning from a few nm for spherical soot particles to several cm for angular, brittle charcoal fragments or charred vegetation pieces (Shrestha et al., 2010). Regardless of particle size and texture, BC particles typically consist of mainly carbon, at approximately 60 % or greater, with accessory elements including H, O, N, and S (Shrestha et al., 2010).

BC resistance to further degradation when coupled with its efficient sorption properties allows it to serve as useful tracer of other organic and/or inorganic contaminants of concern (Sanchez-Garcia et al., 2013). Additionally, through careful manipulation via chemical fingerprinting, BC particles can assist in emission input(s) reconstruction when compared against known aromatic signature profiles or chemical signatures of numerous petroleum or industry related materials (Tobiszewski & Namiesnik, 2012).

BC quantification also provides insight into the physiochemical properties governing BC and OC deposition and accumulation within an environment. As previously stated, BC particles have extremely efficient sorption properties and due to co-emission, are often deposited alongside other organic pollutants (Agarwal & Bucheli, 2011). Fine pollutant particulates when dispersed in the water column can remain suspended before settling. When finer particles, such as silts (<63 μm) and clay (<4 μm), mix with organic matter, cohesive bonding can occur, resulting in 'cohesive sediments' (Shrestha et al., 2014). Hydrodynamic flows influence the dispersion, accumulation, and weathering of sediments. The hydrodynamics of meandering rivers illustrate the effects hydrodynamic flows have on erosion processes, as observed along the outer curves and the accumulation of fine-grained particles along the inner curves (Shrestha et al., 2014, EPA, 2017). Depositional zones are generally classified as being located on the inner bend of the river and characterized by relatively high TOC amounts and higher percentages of fine-grained particles (Konsevick & Bragin, 2010). Additionally, mineral weathering and fine particulate matter or pollutants preferentially absorb to finer particles and organic rich matrixes due to the higher surface area to volume ratio and strong affinity to non-polar substances (Shrestha et al., 2010). Therefore, depositional zones of fine-grained sediments are often the primary focus of any ecological investigation due to their likelihood of being 'hot-spots' for a

multitude of organic and inorganic compounds, and for further investigation regarding the hydrodynamics driving deposition, accumulation and fate transport systems (Konsevick & Bragin, 2010; NJDEP, 2013).

While, BC has been well studied in various terrestrial environments and is often regarded as ubiquitous in deposition, it has not been as extensively researched in aqueous environments. Furthermore, only a limited amount of studies to date have investigated the potential BC has on system fate processes. Therefore, the purpose of this study focuses on not only quantifying BC particles, but also on determining the likely source input(s) responsible for its deposition in a natural environment and the processes which favor BC accumulation in sediment. This study also highlights on the relationship between BC concentrations and other pollutant loads, primarily, PAHs due to their similar physiochemical properties, pyrogenic origin and relative occurrence in urban sediment and soil (Tobiszewski & Namiesnik, 2012; Oen et al., 2006). PAHs and BC should also experience similar fate processes due to BC's strong sorption of PAHs and other planar compounds and relative resistance to decay one settled (Oen et al., 2006; Yanju et al., 2009). Characterization of other organic pollutants (i.e., PAHs) or compounds (i.e., alkanes) will assist when evaluating genetic signatures inherited from the BC parent material (Emsbo-Mattingly et al., 2001); Bucheli et al., 2004). The diagnostic chemical features (biomarkers) of the sediment will be evaluated against various petroleum related reference materials and other organic assemblages to determine whether BC can serve as a potential pollutant indicator for other contaminants of concern.

The Lower Hackensack River was chosen as the study area due to its extensive industrial history and proximity to various industrial and commercial entities (Murphy et al., 2011), as well

as its historically poor ecological scoring due to historic anthropogenic intervention, including but not limited to, navigational dredging, wetland reclamation, and various forms historical pollution over the last 200 years (EPA, 2017). In addition, five Superfund sites, two former power plants, three public sewage treatment plants, 26 combined sewer overflows and various landfills line the Lower Hackensack River shores (EPA, 2017). Furthermore, the Lower Hackensack River is currently under regulatory evaluation by the United States Environmental Protection Agency (EPA) regarding whether the lower river portion (35 km) should be included on the National Priorities List (NPL), also known as the *'Superfund Law'* (Langa, 2017; ATSDR, 2005). The NPL list compiles contaminated or potentially contaminated properties throughout the United States, ranking the relative degree of risk to human, ecological and environmental health pursuant to EPA's Hazard Ranking System (HRS) and regulations set forth under the Comprehensive Environmental (USFWS, 2007). NPL is federal designation of nation-wide hazardous waste sites and allows cooperation between federal entities (i.e., EPA) and individual states regarding investigation and remedial action of contaminated sites and recovery of clean-up related costs (E&E, 2016; EPA, 2017). Further discussion regarding the regulatory process involved for NPL status and the Lower Hackensack River is included in Section 4.1 of this paper. Lastly, a 2017 editorial regarding the Lower Hackensack River describe the current state as 'one large, simmering toxic stew of contamination' (O'Neill, 2017). Based on the complex industrial history of the river and widespread contamination of various hydrophobic pollutants and proximity to various industries, land uses, and environments, and presence of organic-rich sediment and various forms of wetland vegetation, the Lower Hackensack River presented itself as an obvious study area for investigating both the presence and characteristics of BC in an urban waterway. Figure 2 illustrates the proximity of various industrial entities along the lower,

downstream river shores with the dense urbanization of northern New Jersey and New York City skyline in the backdrop.

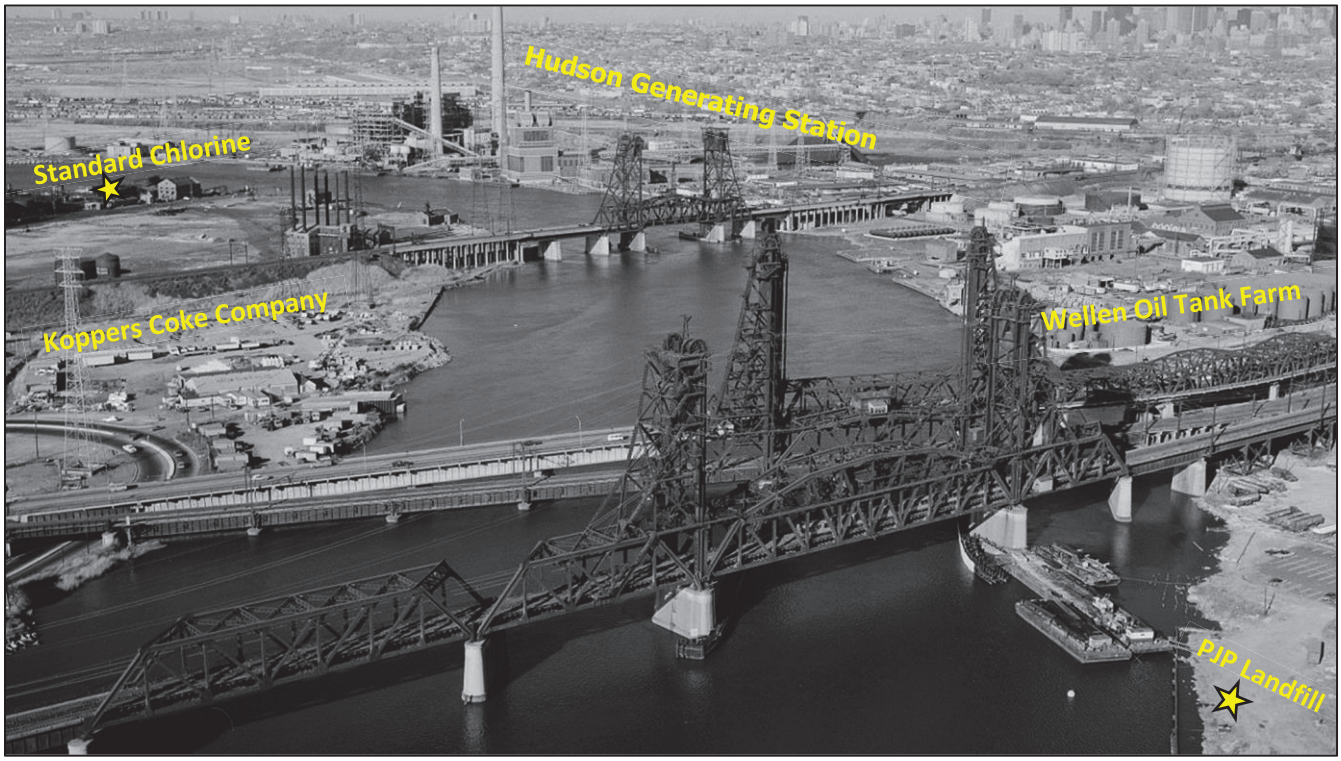

Figure 2. Historical aerial (1978) of the various industries and vertical lift bridges looking northeast on the Lower Hackensack River. 1978 Aerial view of the Lower Hackensack River and the various industries and vertical lift bridges looking northeast (U.S. Library of Congress, 1978). The PATH Transit Bridge is in the foreground, with the Conrail, Newark Turnpike and Erie & Lackawanna Railroad bridges behind it. The New York City skyline is the far eastern corner. Aerial photograph also captures the Kearny portion of the Lower Hackensack River or '*Koppers Coke Peninsula'*. Several former petroleum related and manufacturing related facilities are denoted in yellow bold text. Yellow Stars signify the adjacent properties which have Superfund status (e.g., Standard Chlorine & PJP Landfill). Standard Chlorine located along the western riverbank, is responsible for significant discharges of PCBs, dioxins, naphthalene, benzene, chlorobenzene and other contaminants directly into the river (E&E, 2015). Contaminated soil and lagoons drained directly into the river (E&E, 2015). The PJP Landfill located further downstream, along the eastern bank, is also responsible for substantial releases of organic and inorganic pollutants to the river (E&E, 2015). The former landfill accepted various chemical and industrial wastes during its operational history, resulting in significant contamination of various organic and inorganic compounds (i.e., PAHs, PCBs, lead, mercury) (E&E, 2015).

Going into this study, the initial hypothesis held was that BC concentrations will vary due to tidal influences; however, preference will be shown further downstream adjacent to former and current industries. BC accumulation in sediments is anticipated to favor inner riverbanks due to depositional preference of fine-grained particles (< 0.625 mm), including hydrophobic BC particles and various metal and hydrocarbon (HC) particles (Uhler et al., 2005; Konsevick & Bragin, 2010). Another assumption held is that contaminants of concern will follow similar distribution trends relative to BC concentrations due to favorable BC - contaminant sorption properties and co-emission (Agarwal & Bucheli, 2011). Lastly, environmental forensics of the Lower Hackensack River in the form of chemical fingerprinting supported by high-resolution imaging will reveal specific signatures and assemblages within the observed BC particle matrix which than can be manipulated or used in diagnostic source determinations. Evaluating the morphological and geochemical composition will also aid in understanding the overall relationship between BC and other organic compounds and pollutants.

1.1 Black Carbon & the Environment

Understanding the physiochemical structures of BC and how such features interact with other organic and inorganic contaminants in the environment is crucial for comprehensive environmental risk assessments. Further understanding of BC's physiochemical properties can be accomplished by investigating both the presence and chemical relationship/similarities of BC and other persistent hydrophobic organic compounds (Agarwal & Bucheli, 2011; Emsbo-Mattingly, 2001). Carbon dioxide and water are the major combustion products of fossil fuels, however, during combustion processes more complex compounds are often present in the form of various aromatic hydrocarbons (Killops & Killops, 2005). For example, when various crude

or other refined petroleum products are combusted at moderate (400-600 ºC) to high temperatures (> 700 ºC) in the absence of oxygen, pyrolysis artifacts in the form of condensed aromatic hydrocarbons are created alongside the refractory carbon (RC) particles which were not completely burned (Emsbo-Mattingly, 2001; Killops & Killops, 2005). Because formation temperatures are directly responsible for the chemical complexities present, assessment of such aromatic hydrocarbons are imperative when differentiating carbonaceous particles (including BC) from other RC particles (Boehm & Saba, 2008; Shrestha et al., 2010).

1.1.1 BC and PAHs

Polycyclic aromatic hydrocarbons (PAHs) consist of several fused benzenoid rings (and their alkylated derivatives) and often co-emit along BC particles due to similar formation processes (Agarwal & Bucheli, 2011). PAHs are considered one of the most persistent pollutant groups with deposition in both soil and sediment routinely described as ubiquitous (EPA, 2017; Stout et al., 2015). PAH structures span from simple two fused benzene rings (naphthalene) to highly peri-condensed 6 ring structures and their innumerable derivatives (i.e., benzo[*ghi*]perylene) (Killops & Killops, 2005; Uhler et al., 2005; Kruge, 2018).

As explained by Shrestha et al. (2010), Staniszewska et al (2011), and Agarwal and Bucheli (2011), BC's high surface to volume ratio leads to a strong affinity to non-polar substances such as PAHs. The strong affinity for such non-polar compounds is of important consideration, as PAHs are considered mutagenic and carcinogenic (Shrestha et al*.,* 2010). Sixteen (16) PAH compounds are federally regulated due to their relative risk to human and ecological health; these specific PAH compounds are often referred to as the '16 priority pollutants PAHs' (herein denoted as EPA PAHs) (Stout et al., 2015). EPA PAHs are all parent

PAH compounds, meaning there are no C side chains present, only fused polycyclic aromatic structures (Uhler et al., 2005). EPA PAHs consist of 2- to 6- ring non-alkylated structures (Uhler et al., 2005). Figure 3 is an example of the distribution and chromatographic profile of parent EPA PAHs in study sample HACK19_03. Figure 4 includes the chemical structures of several regulated organic contaminant compounds.

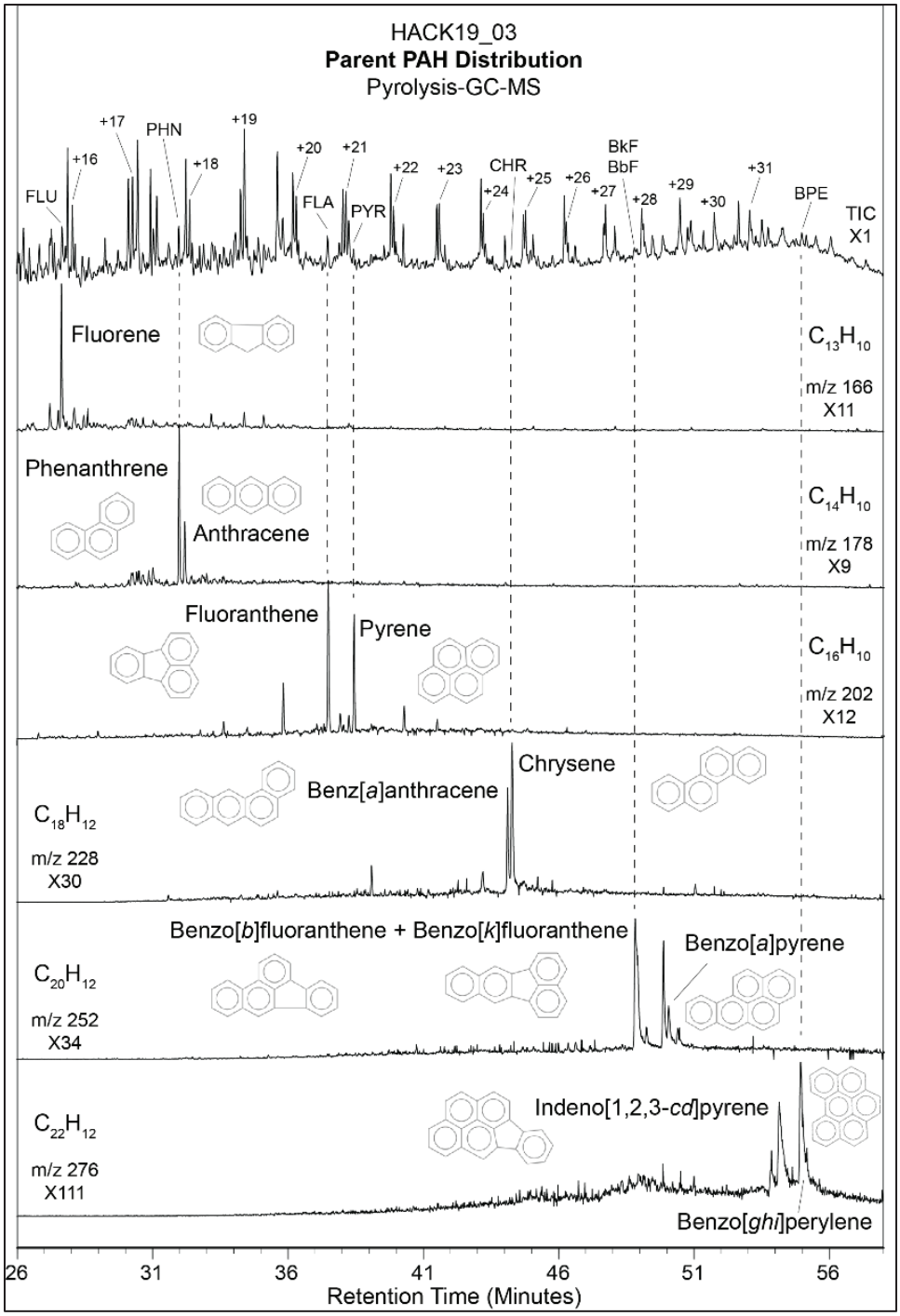

Figure 3. Distribution and chromatographic profile of parent (2- and 6- ring) EPA PAHs in sample HACK19_03. The associated ionization mass spectrum and parent fused ring structure are also included for quick reference (Kruge, 2015). Parent PAHs are more thermochemically resistant than their alkylated derivatives, therefore, predominance of parent or EPA PAHs is usually indicative of pyrogenic sources.

Several other hydrocarbon contaminants exist and are of equal concern regarding their potential presence and distribution in urban waterways, examples include various crude and refined petroleum products, pesticides, polychlorinated biphenyls (PCBs), dioxins and furans (USFWS, 2007). Hydrocarbon pollutants generally have varying physiochemical properties influencing bioavailability and toxicity USFWS, 2007). However, the presence of any aromatic byproducts including polyhalogenated organic contaminants (e.g., PCBs, dioxins or furans) and polycyclic compounds (PAHs) are of concern due to their relative toxicity, accumulation rates, and interference with natural system processes (Shrestha et al., 2010; USFWS, 2007).

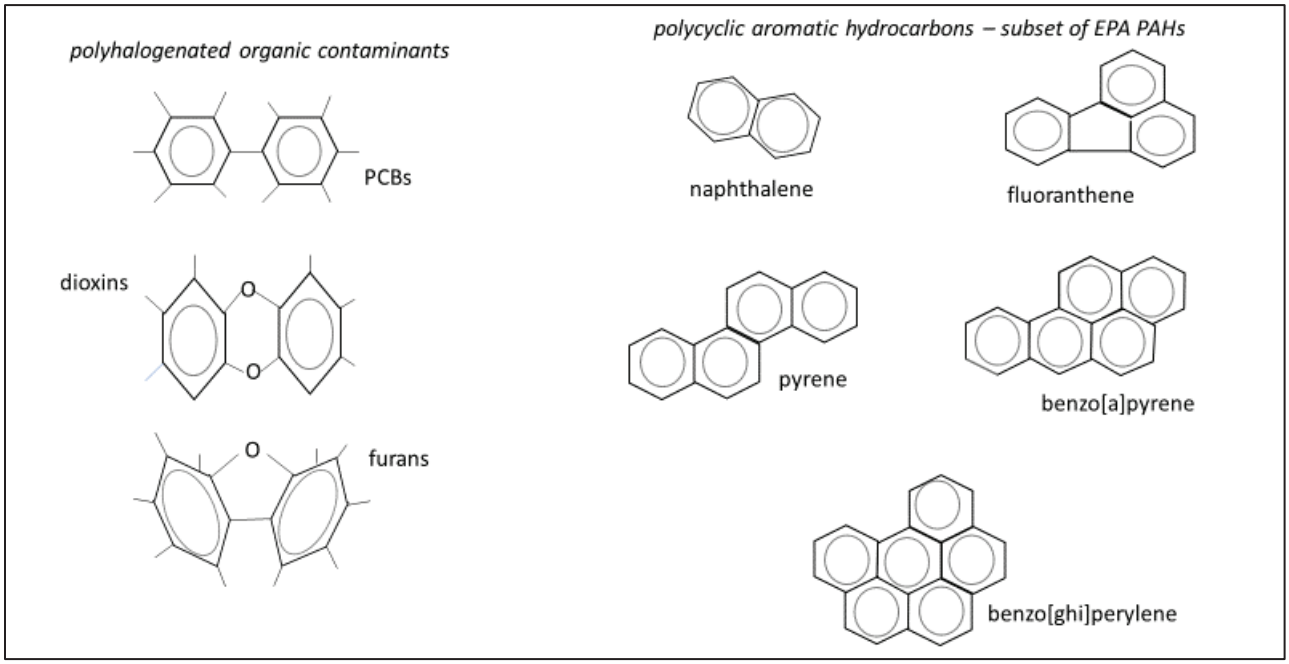

Figure 4. Aromatic chemical structures of several organic contaminant classes including polyhalogenated compounds (PCBs, dioxins and furans) (USFWS, 2007) and several EPA priority pollutant PAHs (Stout et al., 2015). Circle-in-hexagon refers to delocalization of C – C bonds.

The condensed ring structures and fused ring structures of PAHs, PCBs and BC particles are largely responsible for their relative hydrophobic tendencies, resistance to chemical or

physical decay and strong affinity for organic matter (Huntley et al., 1995, Shrestha et al., 2010). The apolar and aromatic surfaces of BC reportedly contribute 1-10% of the total fraction of organic matter in soils and sediments (Shrestha et al., 2010). The sorption of organic solutes to BC during transport and deposition in surface aquatic systems can account for approximately 3 to 38 % of overall TOC mass (Shrestha et al., 2010). Additionally, due to similar formation processes involving either combustion or pyrolysis of carbon-based fuels, BC and PAH particles are often co-located alongside one another and therefore influenced by similar physical and chemical processes (Oen et al*.,* 2006; Emsbo-Mattingly et al., 2001).

Due to advances in the field of environmental forensics over the last half century, there are now vast libraries of chemical signatures or 'fingerprints' of varying organic and inorganic materials, with specific libraries dedicated to petroleum biomarkers (Wang and Stout 2007). Organic contaminants such as PAHs have a strong affinity to BC, especially high molecular weight (3+ring) PAHs (Shrestha et al., 2010). Heavier ring PAHs are more reactive and abundant among pyrolysis byproducts and are responsible for the rapid hydrogen bonding (sorption) with other hydrophobic byproducts, including refractory BC particles (Killops & Killops, 2005; Chen et al., 2019).

PAH origin or 'source classification' is best described as either diagenetic (natural), petrogenic (petroleum-related), or pyrogenic (high temperature burning) (Emsbo-Mattingly, 2001; Uhler et al., 2005). Diagenetic PAHs are created from the rearrangement of natural hydrocarbons as a result of rapid chemical and biological processes (Uhler et al., 2005; Stout et al., 2015). Petrogenic and pyrogenic are both anthropogenic in nature but involve different formation temperatures resulting in chemically different hydrocarbon compounds (Uhler et al.,

2005). Petrogenic PAHs are associated with distillation heating under mild conditions (< 550 ^{o}C) of various petroleum related products, ranging from light fuel oil distillates (i.e., gasoline, kerosene), to 'middle' fuel oil distillates (i.e., diesel, No. 2 heating oil, No.4 fuel oil) and lastly, to heavy fuel oil residuals (i.e., lube oil, No.6 fuel oil) (Uhler et al., 2005). Pyrogenic PAHs are derived from high temperature (> 700 ^{o}C) heating (O_2 is absent) or combustion (O_2 is present) of organic rich materials, including petroleum products (Uhler et al., 2005). Industrial processes are generally related with pyrogenic PAHs due to the relatively high temperatures required for activities such as metal smoldering, coal retorting (for manufactured gas production), or any high temperature conversion of biomass and biofuels (Uhler et al., 2005; Emsbo-Mattingly, 2001; Kruge, 2015).

The simplest explanation regarding pyrogenic and petrogenic source identification involves the degree of alkylation observed. Petrogenic sources signatures are typically dominated by the presence of light, aromatic 2- to 3-ring PAHs with various alkylated benzene and naphthalene derivatives, exhibiting a 'bell-curve' chemical signature (Emsbo-Mattingly et al., 2001; Uhler et al., 2005). Naphthalene (N0 or NAP) for example, which consists of 2 fused benzene rings, and considered a 'priority pollutant' or parent pollutant due its wide industrial use in the manufacturing of various chemicals (i.e., resins) and petroleum (i.e., tar, asphalt) products (Esmbo-Mattingly et al., 2001, ATSDR, 2005) is also the precursor for isomeric alkyl (side chain) compounds such as 1-methylnapthalene (1mN) and 2-methylnpathalene (2mNAP) (Wang and Stout, 2007). NAP's substituted forms (i.e., 2mNAP, and 1mN) are associated with various refined petroleum products (i.e. diesel fuel, crude oil (Wang and Stout, 2007). Car exhausts and industrial discharges are common pathways for NAP, 2mNAP and 1mN (ATSDR, 2005).

Petrogenic sources are dominated by the various isomers of parent compounds due to the incomplete combustion of parent material at relatively mild temperatures (< 550 ºC) (Uhler et al., 2005). Petrogenic source signatures are often more complex to distinguish due to the presence of weathered parent compounds alongside numerous isomer assemblages (Wang and Stout, 2007, Emsbo-Mattingly et al., 2001).

Pyrogenic PAHs are the stronger, more condensed compounds which survived high temperature heating and generally consist of 4- to 6-ring non-alkylated compounds (Emsbo-Mattingly, 2001; Uhler et al., 2005). Pyrogenic sources, which are responsible for both PAH and BC creation, are easily distinguished by their sharply declining PAH profile (Uhler et al., 2005). Pyrogenic PAHs are associated with non-alkylated PAHs due to the relatively high temperatures (> 700 ºC) needed for destruction of alkylated or branched compounds and condensation of highly aromatic compounds (Emsbo-Mattingly et al., 2001). The sharp declining signature of pyrogenic PAHs is directly correlated to increasing formation temperatures (Uhler et al., 2005). Pyrogenic PAHs are associated with various high temperature processes, most notably, coal and gas gasification processes for energy production (i.e., manufactured gas) (Emsbo-Mattingly et al., 2001).

Common sources of pyrogenic PAHs and BC particles include the vapor and particulate emission-phase from the incomplete combustion of diesel and gasoline engines and vegetation during forest fires (Uhler et al., 2005; USFWS, 2005; Hagmann et al., 2020). Another significant source of anthropogenic PAHs and various hydrophobic organic and inorganic pollutants is derived from urban and industrial site run-off and mixing of wastewaters with natural waterways (USFWS, 2007; Emsbo-Mattingly, 2001) and the accidental spilling / leaching of hazardous

waste materials from lagoons or pits (EPA, 2017, Cowan et al., 2015). Characterization of PAHs in urban runoff varies between sites, however, the overall signature of PAH compounds and assemblages associated with urban stormwater runoff and wastewaters typically indicate pyrogenic sources due to the predominance of more reactive and less soluble 3- to 6- ring PAH compounds (Uhler et al., 2005; Kruge, 2015). Petrogenic influences, in the form of engine oil drippings are also associated with urban runoff, however, their overall contribution is not as significant as compared to pyrogenic sources (Emsbo-Mattingly et al., 2001). Weathering processes generally destroy the 'weaker' 2- to 3- ring structures associated with petrogenic or diagenetic PAH sources, as compared to the more reactive and stronger (5- and 6- ring) pyrolytic PAH compounds (Kruge et al., 2018; 2020).

The resistant and aromatic structure of BC particles favors bonding with various hydrophobic particles and because of the relatively stable chemical nature of BC it can also limit certain compounds from further decay as well, locally controlling their fate and transport (Yanju et al., 2009; Shrestha et al., 2010). Ultimately, by investigating the PAH assemblages present and the chemical characteristics of the compounds identified, source determinations (i.e., diagenetic, petrogenic, or pyrogenic) for both PAHs and BC are likely to be revealed (Stout et al., 2015; Kruge, 2018; 2020).

1.2 Previous Black Carbon Studies

Garcia et al. (2013) and Oen et al. (2006) assessed the presence of BC content via the use of thermal and molecular markers, particularly PAH isomers, due to the strong bonding of BC pores to non-polar substances such as PAHs. The CTO-375 (chemothermal oxidation at 375°C) method employed first defined BC, operationally at least, as the remaining 'organic carbon'

(OC) percent following thermal oxidation and volatilization of OC particles with subsequent in situ acidification (Oen et al., 2006; Shrestha et al., 2010). The subsequent PAH to BC ratios investigated by Oen et al. (2006) ultimately confirmed strong correlations between PAH and BC exist, so much so that PAH isomer ratios such as the phenanthrene/ anthracene (PHE/ANT) and fluoranthene/ pyrene (FLA/PYR) have been found to accurately differentiate between pyrogenic and petrogenic sources.

Pyrogenic PAH formation is also responsible for BC formation due to similar formation processes, co-emission and preferential sorption of PAHs to BC (Oen et al., 2006). For example, condensed carbonaceous BC particulates in the form of soot are often created from the rapid heating of organic matter followed by the rapid cooling of incompletely combusted hydrocarbons, resulting in the formation of soot and various 4-, 5- to 6-ring PAHs (i.e. pyrene and benzo-related assemblages) (Emsbo-Mattingly et al., 2001). Therefore, the use of PAH diagnostic ratios, particularly for pyrogenic (i.e., coal combustion or wood burning) assemblages can not only confirm the presence of BC but also provide further insight regarding the physio-chemical properties governing BC accumulation in sediment or soil by manipulating the various co-eluted aromatic (pyrogenic) and aliphatic (petrogenic) compounds present alongside BC compounds. Analytical methods involving gas chromatography mass spectrometry (GC-MS) such as those described by Oen et al. (2006) facilitates screening of both aromatic and aliphatic organic compounds and is the backbone to environmental forensics.

Additionally, Oen et al. (2006) found the highest fraction of PAH mass in the sand fraction of three of the four sediments analyzed and observed a greater correlation between PAHs and BC ($r^2 = 0.85$) than with organic carbon (OC) ($r^2=0.15$) regardless of origin and PAH

contaminant concentrations. Oen et al. (2006) also reported that even in cases where BC to TOC is less than 10 %, approximately 90 % of all PAHs can still be accounted for in the BC fraction due the efficient sorption of PAHs to BC particles.

As explained by Yunker et al. (2002), distinguishing between natural and anthropogenic PAH sources and composition is often done by investigating the principle mass ratios of m/z 178, 202, 228 and 276 parent PAH compounds (see Figure 3 above) and by the PHN/ANT /anthracene and FLA/PYR-alkyl PAH diagnostic ratio series to minimize cofounding physiochemical properties (Yunker et al., 2002). Generally, for mass 178, an ANT/178 ratio of < 0.10 is indicative of petrogenic source inputs while a ratio of > 0.10 indicates a dominance of combustion or pyrogenic source inputs (Yunker et al., 2002). Cross plots of PAH ratios were included in the Yunker et al (2002) study to allow for quick evaluation regarding diagenetic vs petrogenic vs pyrogenic origin sources.

The Bucheli et al. (2004) study investigated the usefulness of PAH isomer ratios and molecular markers for quantifying and determining BC source inputs in rural and urban soils in Switzerland. Specific parent and alky-substituted PAHs and ratios were evaluated as possible tracers of organic matter. PAH ratios such as (MPHN&ANT)/PHN ANT/(ANT&PHN) and FLA/(FLA&PYR) (see Figure 3 above for compound structure reference) studied were successful in distinguishing between combustion sources, providing an even clearer historical snapshot of likely emission sources and transport processes (Bucheli et al. 2004).

The Dai et al. (2008) study also investigated the correlation between PAHs and BC in surface sediments of China's marginal seas. Dai et al. (2008) concluded that there was a strong positive relationship between BC and TOC but not between BC and PAHs in the surface

sediments analyzed due to the differences in biological and chemical processes, as well as weathering processes governing BC and PAH accumulation in study-marine surface sediments.

Agarwal and Bucheli (2011) found TOC was a more useful indicator for PAHs, specifically lighter molecular compounds (i.e., naphthalene), as TOC appears to govern the overall distribution of PAHs in organic-rich background soils. Agarwal and Bucheli (2011) also reported significant BC correlations with mean annual precipitation, iron oxide, aluminum oxide and cation exchange capacity in surficial study soils.

Morphological, textural and mineralogical analysis of amorphous and refractory particles (i.e. BC) using a scanning electron microscope (SEM) equipped with an elemental detector is a common analytical approach employed in soot and BC related studies such as Stoffyn-Egli et al (1997), Niyogi et al. (2012) and Cowan et al. (2015). High temperature urban and industrial related processes (i.e. coal-powered energy use) results in the creation of various waste-related particulates or 'fine particulate matter' (EPA, 2017). The residual carbon by-products often include spherical BC particles alongside various heavy ring (4+ ring PAHs) (Stoffyn-Egli et al., 1997; Esmbo-Mattingly et al., 2001). BC particles are composed mostly of elemental C, with O, H, and S as minor components (Stoffyn-Egli et al., (1997). SEM evaluation is generally difficult for lighter elemental compounds, however, O / C ratios combined with qualitative analysis of surficial and chemical features can reduce charging related issues which may impair analytical use. SEM photomicrographs of BC particles are also incredibly useful for characterization purposes as they can illustrate the various surficial textures of the BC particles themselves, providing additional information regarding the variables influencing dispersion, deposition and accumulation (Kolay, 2014).

1.3 Lower Hackensack River & Estuary

The Hackensack River is approximately 72 km long, commencing from Lake Lucille in New City, Rockland County, New York (+41.184196, -73.995762), where it flows into Newark Bay, New Jersey (+40.709727, -74.116406) (EPA, 2017). The river is classified into two regional zones, the Upper portion and Lower portion. The Upper Hackensack River begins in southeastern New York and continues before impoundment at various northeastern New Jersey Reservoirs scattered throughout Bergen County, New Jersey (EPA, 2017). Generally, the Oradell Reservoir and Dam (+40.956129, -74.029001) is considered to mark the division between the Upper and Lower portions. Primarily as a result of impoundment at the Oradell Dam, only the lower portion is subject to tidal influences (EPA, 2017). Damming of the upper river portion had profound effects on the lower river's hydrology, geomorphology, and chemistry, particularly, salinity, resulting in what was once a freshwater ecosystem, to a more brackish ecosystem (EPA, 2017). Newark Bay and the strong tidal mixing which occurs at the bay/river interface have transformed the entire Lower Hackensack River into a well-mixed, brackish estuarine complex (EPA, 2017).

The United States Environmental Protection Agency (US EPA) classifies the Lower Hackensack River as the "river area between Oradell Dam and its mouth at Newark Bay" and comprises approximately 35 km of tidally influenced waterways. The Lower Hackensack River is further classified by its regulatory EPA ID: NJN000201845. Various technical studies and reports are available through EPA Record Collections regarding the Lower Hackensack River. The 2007 United States Fish & Wildlife Service (USFWS) planning related publication, *The Hackensack Meadowlands Initiative,* also summarizes the various technical studies related to the Lower Hackensack River (USFWS, 2007).

The Lower Hackensack River is bounded by Bergen County to the west and to the east by Hudson County. The lower portion also runs parallel to the Hudson River, approaching within 5 km of the Hudson River along the ridge of the Palisades before widening in a broad meandering tidal estuary, including the New Jersey Meadowlands (EPA, 2017) and as depicted in Figure 5: Regional map of the Lower Hackensack River and study area.

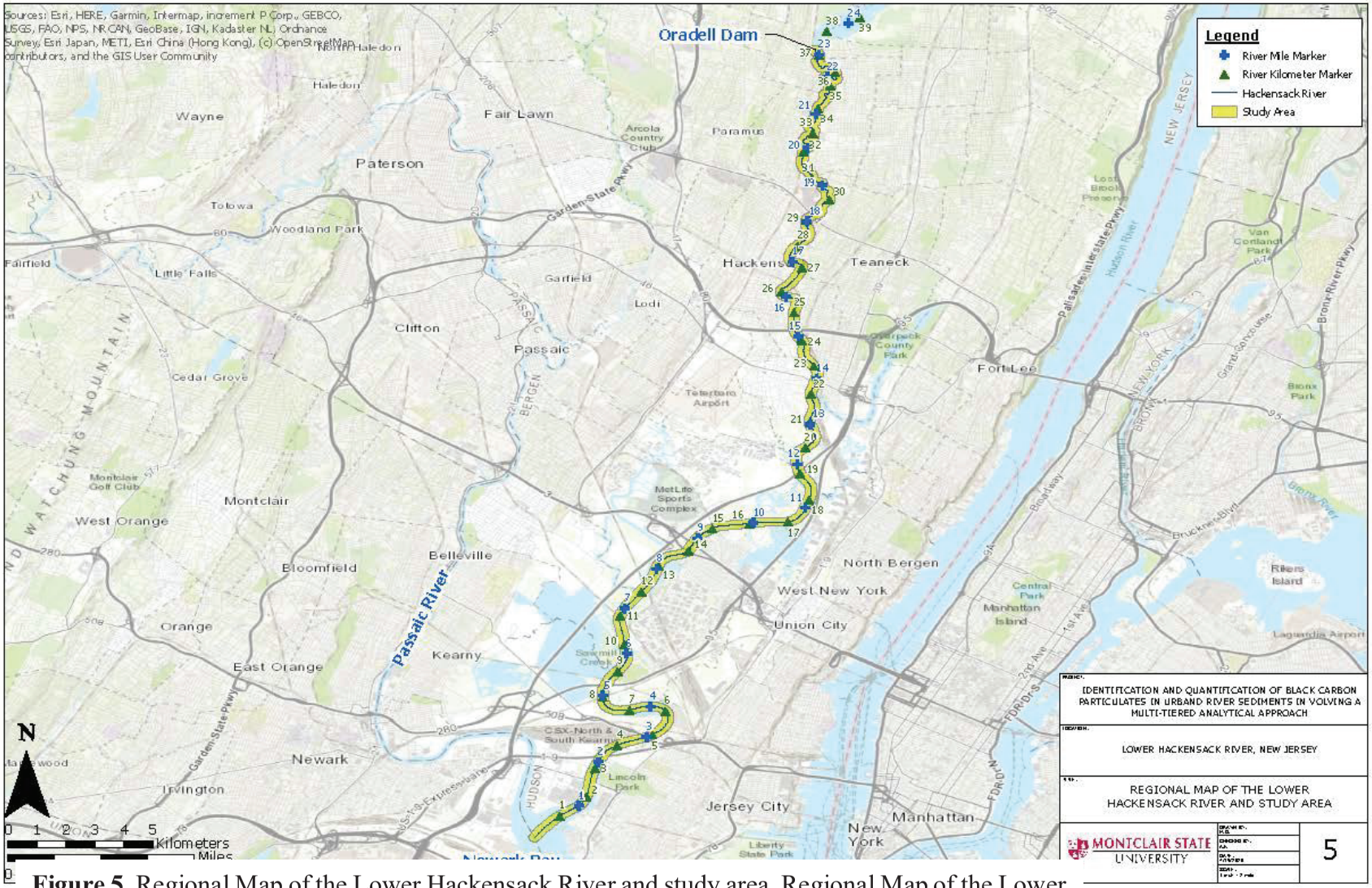

Figure 5. Regional Map of the Lower Hackensack River and study area. Regional Map of the Lower Hackensack River and study area. Blue crosses represent river mile (rm) markers and green triangles represent river kilometer (rkm) markers. Numbering commences at Newark Bay and ceases at Oradell Dam. Study area is shaded in yellow.

The meandering pattern of the lower river has resulted in the formation of extensive side streams and wetlands (EPA, 2017). Various wetlands dominate the middle to lower portions of the river. Figure 6 is a modified figure illustrating the various wetland species dominating the Lower Hackensack River. The lower portion of the Hackensack River is also one component of the overarching Hudson-Raritan Estuary of New York and New Jersey (Murphy et al., 2011).

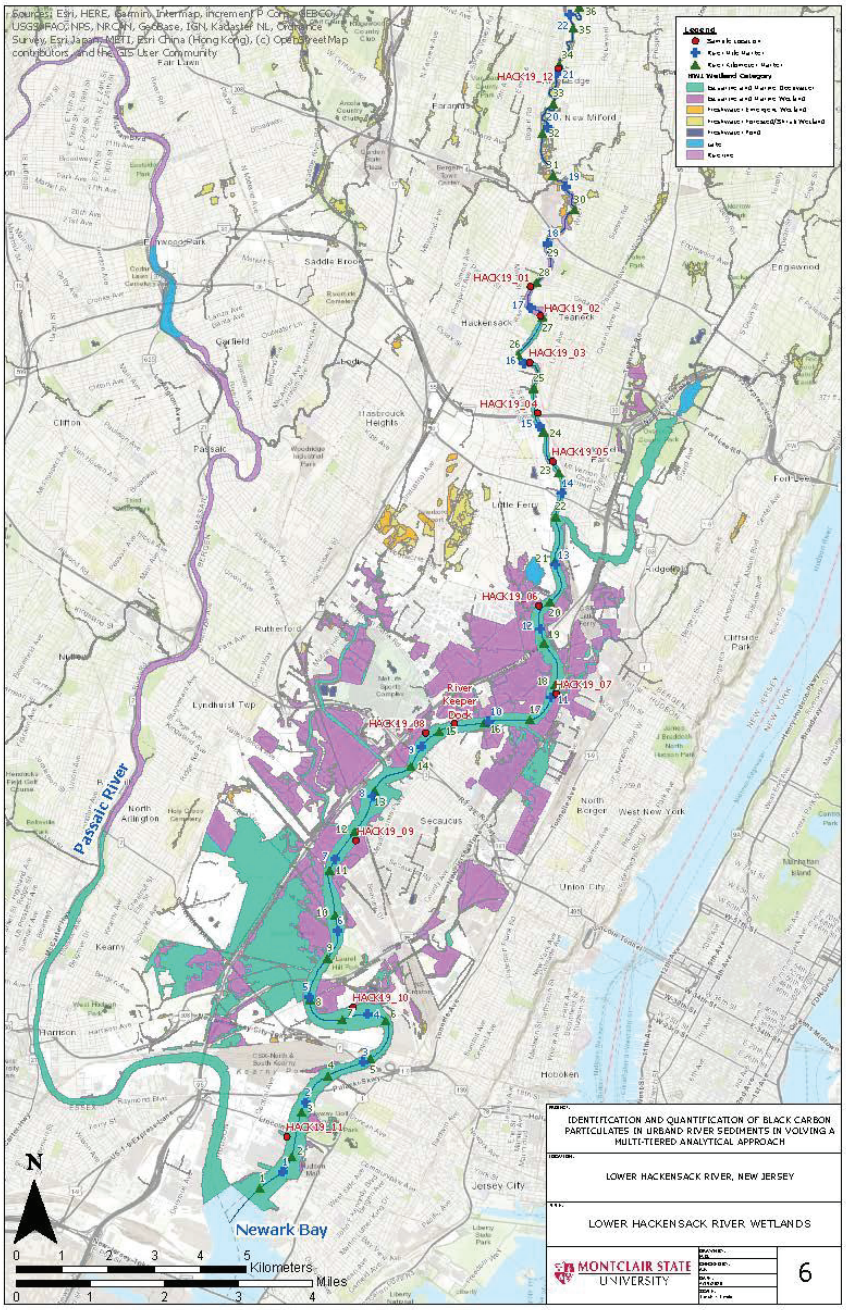

Figure 6. Wetland characterization and distribution type of the Lower Hackensack River. The accompanying legend for Figure 6 is slightly compressed, therefore, the following legend language is repeated for ease of reference. Aqua blue denotes estuarine and marine Deepwater; purple denotes estuarine and marine wetlands; orange denotes freshwater emergent wetlands; yellow denotes freshwater forested/shrub wetlands; navy blue denotes freshwater ponds; blue shading denotes lakes and light purple riverine modified from EPA's 2016 site investigation of the Lower Hackensack River (EPA, 2017).

The New Jersey Meadowlands, hereafter denoted as Meadowlands, designates the approximately 34 km^2 of heavily urbanized and formerly industrialized wetlands in northeastern New Jersey (Konsevick & Bragin, 2010). The Lower Hackensack River is the key waterbody of the Meadowlands, providing hydrologic and ecological support to the various sensitive ecosystem located within (E&E, 2015). The Meadowlands are considered one of the largest brackish estuarine complexes in northeastern United States (EPA, 2017).

Historically, the Meadowlands encompassed a much larger area, with one 1896 New Jersey state survey reporting approximately 111 km^2 of natural, undeveloped wetlands (Marshall, 2004). The shrinkage of such a sensitive natural feature was due to the rapid and systematic urbanization of the area which occurred from the late 19^{th} century through the present, accompanied early on by the general notion that meadows/marshes were unproductive, and utterly "worthless" areas (USFWS, 2007). The Meadowlands and its associated waterbodies were subjected to various forms of anthropogenic intervention, including but not limited to; extraction of natural resources, alteration of water flow, navigational dredging, reclamation/land development often involving contaminated historic fill waste, and lastly, various forms of comingled pollution (USFWS, 2007; E&E, 2015).

1.3.2 Previous Sediment and Environmental Investigations

Sediments in the Hackensack River Estuary and its tidal tributaries (17 total) have been affected by a multitude of legacy contaminants including, but not limited to, various petroleum and aromatic hydrocarbons, heavy metals (i.e., chromium, mercury, beryllium, vanadium, etc.), PCBs, and pesticides (Murphy et al., 2011; Konsevick & Bragin, 2010; EPA, 2017). Additionally, due to its limited inputs of upstream fresh water, large inputs of treated municipal

wastewater discharges, industrial treatment facilities, thermal waste discharges, combined sewer outflows and storm water discharges have also impacted the lower river sediments and its natural hydrodynamic processes, often resulting in the redistribution and resuspension of various sediment matter (Murphy et al., 2011). Further, contaminants associated with Newark Bay and Passaic River sediments have been documented as far north as the Oradell Dam due to the strong tidal flows and mixing of dissolved and suspended particulates (USFWS, 2007).

One example of historic contamination involving the Lower Hackensack River and Estuary is the May 26, 1976 No. 6 industrial oil spill, which resulted in the release of approximately 47,619 barrels or ~7107 tonnes of No. 6 oil along the riverside banks of the former Wellen Oil Company tank farm (Jersey City, NJ/ river km 5.5) (NOAA, 1976). Incident documentation of the historic release details the failure of protective booms, resulting in the upstream dispersion of oil coated shores marshes, creek banks, bulkheads, and protective wildlife management areas (EPA, 2017). Spilled oil was observed as far north as the Route 46 bridge at Ridgefield Park, spanning approximately 12 km of the Lower Hackensack River (NOAA, 1976).

The movement of the spilled No. 6 industrial oil was heavily influenced by the incoming tides and tidal mixing, and winds at the time of the release (EPA, 2017). Ecological incident related documentation stated: “Several dead, oiled birds’ nests containing eggs were found…[D]amage to Salt Marsh Cordgrass was due to smothering by the oil, and not the chemical properties of the oil” (NOAA, 1976). This singular incident resulted in a multitude of sediment and ecological risk assessments and studies. Separate of the historic 1976 No 6. Fuel oil release, there have been countless other spills, releases and/or discharges of various refined petroleum products in the Lower Hackensack River estuary (EPA, 2017; E&E, 2015).

The Lower Hackensack River and its tributaries have been subject to numerous investigations, resulting in a large volume of analytical data (EPA, 2017). The National Oceanic Atmospheric Administration (NOAA) is the primary federal agency responsible for maintaining and compiling all generated analytical data into one centrally located and publicly available database.

Regulatory studies related to the Lower Hackensack River were initiated in 1987 as a result of the formation of the Hackensack Meadowlands Development Commission (HMDC). The objective of the 1987-1989 HMDC study was to "provide an inventory of fishery resources within the boundaries of the Hackensack Meadowlands District". The generated data were used to influence subsequent meadowlands specific policies and interests. In 2001, the HMDC was rebranded as the New Jersey Meadowlands Commission (NJMC) (Konsevick & Bragin, 2010). Under the newly established NJMC, a subsequent fish inventory study was conducted with sampling initiated in 2001 and commencing in 2003. The 2001-2003 fish inventory study expanded on the initial HMDC efforts to include investigation of certain contaminants in fish tissue, as well as a chemical and textural analysis of river bottom sediments (Konsevick & Bragin, 2010). The 21 historic sampling locations from the 1987-1989 HMDC were re-evaluated as part of the 2001-2003 NJMC investigation to allow for elucidation of spatial and 15-year trends involving Lower Hackensack River Sediments. Heavy metal concentrations, grain size distribution and TOC content was determined as a result of the 2001-2003 fishery study. The 2001-2003 study findings ultimately concluded widespread heavy metal contamination of sediments in excess of regulatory concentration limits and reported the observed sulfate/sulfide cycle as being the main mechanism influencing organic matter preservation and sorption capabilities (Konsevick & Bragin, 2010). Following the initial 1987-1989 and subsequent 2001-

2003 study, the USFWS released the following statement: “Virtually, the entire Meadowlands ecosystem is contaminated by mercury, PCBs, pesticides and dioxins.” (EPA, 2017).

In May 2015, under the direct oversight of EPA Region 2, Ecology and the Environment, Inc., (E&E) conducted a Preliminary (Site) Assessment (PA) of the Lower Hackensack River as a result of continuous local and regional pressure to have the river classified as a federally regulated National Priority List (NPL) site in conformance with EPA’s Comprehensive Environmental Response, Compensation, and Liability Act (CERCLA). The 2015 PA was limited in scope and focused on reporting all associated historical operations which may have influenced the river accompanied by review of all available historical data related to the river (E&E, 2015). The 2015 PA was followed by a more comprehensive 2016 Site Investigation (SI) of the Lower Hackensack River spearheaded again by the EPA-Region office in conjunction with the U.S. Army Corps of Engineers (EPA, 2017). Surface and subsurface sediment samples were collected from 189 sampling locations between the Oradell Dam and the mouth of Newark Bay. Surface sediment locations were co-located with subsurface sediment cores which extended up to 305 cm below the sediment surface (EPA, 2017). The collected sediment samples were analyzed for Total Compound List (TCL), Semi-Volatile Organic Compounds (SVOC), PCBs, Target Analyte List (TAL) Metals, mercury, and included routine sediment analyses for TOC and percent moisture. The analytical results for both surface and subsurface sediments revealed elevated concentrations of multiple SVOCs (specifically PAHs), PCBs, and various heavy metals throughout the Lower Hackensack River. Sediment data revealed the highest concentrations of PAHs accumulating along the lower river portion, particularly along the sharp river bend, adjacent to river km 6.

Multiple Lower Hackensack River studies have been conducted separately from the regulatory studies mentioned above. Previous sediment studies such as Miskewitz et al. (2005) and Weis et al. (2005) focused mainly on the influence tidal variations have on local dispersion and accumulation processes for various heavy metal contaminants. The study by Murphy et al. (2011) involved mapping, quantification and characterization of lower riverbed sediments using multibeam bathymetry, side-scan sonar, magnetic field surveys and sub-bottom sediment profiling images down to depths of approximately 30 m. A 2014 conceptual site model of Newark Bay by Shrestha et al., described the significant influence Newark Bay hydrodynamics processes (i.e., cohesive sediment transport) have on the Lower Hackensack River. Newark Bay tides have observed as far north as the Oradell Dam, owing to the well-mixed estuarine environment of the Lower Hackensack River (Shrestha et al., 2014). A 1995 sediment study of Newark Bay reported PAH accumulation in bay sediments occurring at several orders of magnitude higher than source effluents (Huntley et al., 1995). The heavy industrialization and current industrialization of Newark Bay waters is arguably one of the largest non-point pollutant sources impacting the Lower Hackensack River and surrounding meadowlands (EPA, 2017; Murphy et al., 2011; USFWS, 2007).

1.4 Project Aim

While there have been multiple historic and more recent studies conducted related to the Lower Hackensack River, the majority failed to investigate the relationship between TOC, BC and various contaminants of concern. Overall, the studies conducted to date have largely ignored the BC fraction. Therefore, the overall objective of this study was to first quantify TOC and BC amounts using a multifarious analytical approach and secondly, evaluate the distribution of

PAHs and metals throughout the study area to determine whether BC can serve as a predictor of contaminant distribution in a highly urbanized and tidally influenced river ecosystem. The determination of TOC is an essential requirement for most sediment studies due to its ability to serve as an indicator of overall organic matter and potential proxy for various organic and inorganic pollutants due to sorption (Konsevick & Bragin, 2010). The ability and possible formation of infinite C-C linkages is what makes organic compounds, including organic pollutants so prevalent and resistant in urban environments (Killops & Killops, 2005; Stout et al., 2015). The absence or presence of organic carbon (OC) within organic matter can considerably influence sorption/desorption dynamics and a multitude of other critical geochemical processes within the sediment matrix (Killops & Killops, 2005).

In order to accurately describe the observed BC particles, additional elemental and textural analysis was conducted to investigate the surface topography and composition of the BC particles themselves. And lastly, environmental forensics of the Lower Hackensack River sediments was also conducted to assist in the reconstruction of past environmental events (i.e., spills and discharges) using chemical fingerprinting and PAH diagnostic ratios. The use of various biomarkers will provide additional information regarding the physiochemical properties of the observed BC particles.

1.5 Study Area – Overview

The study area encompasses approximately 34 km from south to north of the tidally influenced Hackensack River (see Figure 5). The southern starting point (river kilometer 'rkm' 2.5) coincides with the opening of Port of Newark, while the northern starting point (rkm 28) is in a high-density residential/urban area (River Edge, Bergen County, NJ). As discussed in

section 1.4, the Oradell Dam (rkm 36.5) distinguishes the upper, non-tidal portion from the lower, tidally influenced portion, which is the focus of this study.

The portion of the river investigated covers two municipal counties in New Jersey (Bergen and Hudson), over 17 tributaries (below the Oradell Dam), tidal and non-tidal segments, while also transecting the extensive Hackensack Meadowlands. The tidally influenced Meadowlands are a critical ecological feature and cover over 3000 hectares (ha) (EPA, 2017). The Hackensack Meadowlands are often cited as one of the largest brackish estuarine complexes in the northeastern United States (EPA, 2017). Apart from being one of the largest brackish estuarine systems, the Hackensack Meadowlands were also once considered "one of the three most polluted estuaries" in the United States by the USFWS (EPA, 2017).

Residential land use appears to dominate the northern and mid portions of the study area with varying densities (E&E, 2015). Commercial land use is observed throughout the study area. Mixed land use dominated by commercial and industrial entities appeared to cluster in the mid to lower river portions along the meandering river boundary edges of the following municipalities: South Hackensack, Ridgefield, Carlstadt, Secaucus, Jersey City, and Kearny, New Jersey (E&E, 2015).

Public lands are also located throughout the study area and include several municipal and state parks (i.e., Laurel Hill Park, Secaucus NJ), various wetlands and forested land (E&E, 2015). The various wetlands of the Meadowlands and overarching Raritan/Newark Bay estuary are depicted on Figure 6 (see above).

Previous state and federal environmental studies have generated large volumes of analytical data for the lower 22 km portion of the river (EPA, 2017). Such geographic interest is due the historic relationship between the river the various adjacent industries including,

manufacturing plants, petroleum refineries, energy facilities, and landfills, and its proximity and drainage to the heavily industrialized and polluted Newark Bay (EPA, 2017).

1.5.1 Geologic / Hydrogeologic Setting

The Lower Hackensack River is part of a complex, well-mixed estuarine system, known as the New York/New Jersey Harbor and includes various tributary streams, meadowlands, tidal straits and Newark Bay (Miskewitz et al., 2005). Much of the river consists of water depths of 7 m or less, except for several downstream reaches near the mouth of Newark Bay (EPA, 2017). Murphy et al., (2011) reported the depths of the Lower Hackensack River thalwegs as ranging from 3 to 21 m, with shallow depths observed along the river straights and greater depths in the river bends. The underlying bedrock in the river basin is part of the Newark Group and composed mostly of sedimentary rocks intruded by dikes and sills of diabase of Triassic age (EPA, 2017). Unconsolidated deposits of till, varied silt and clay, alluvium and coarse sand/gravel of Pleistocene and Holocene age overlay most of the bedrock (EPA, 2017).

The boundary edges of the river vary from wide, tidally saturated, silt-dominated marshes/mudflats, to eroded shorelines of former industries, to encroaching wetland-related areas, and to the non-existent shorelines common further downstream (USFWS, 2007, Murphy et al., 2011). Figure 8 (A-F) illustrates the varying shorelines of the Lower Hackensack River.

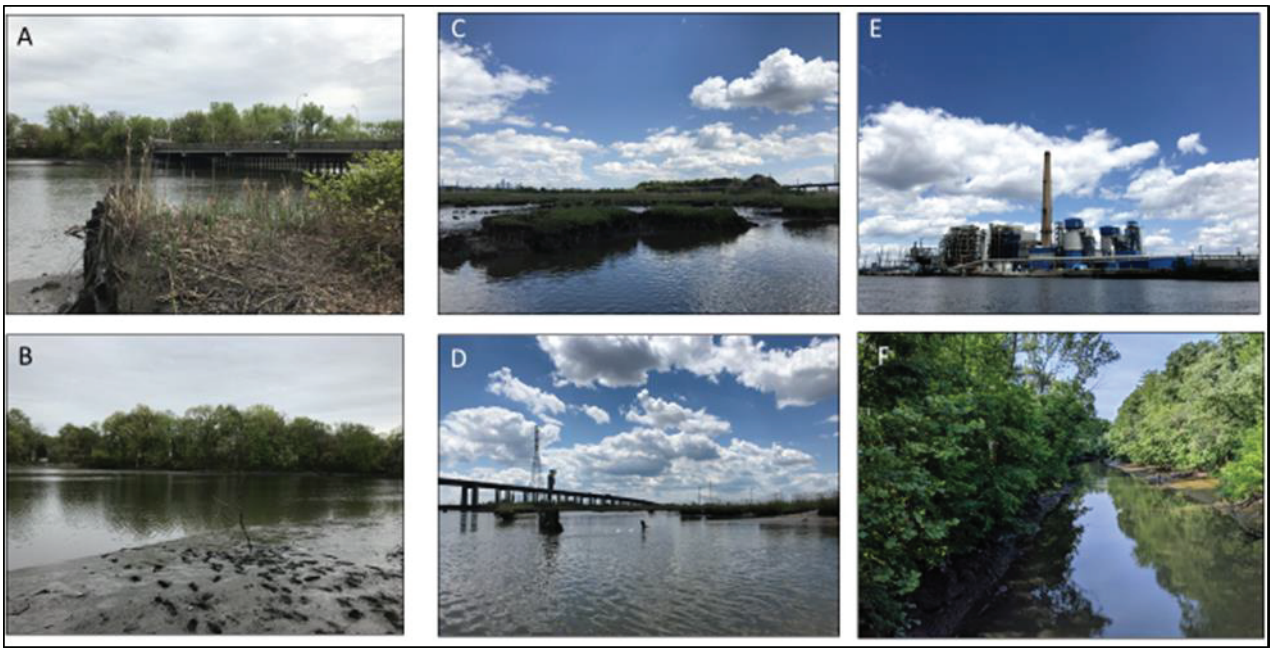

Figure 7 (A-F). The varying shorelines of the Lower Hackensack River include silt-dominated saturated shore-line banks (A & B), to estuarine marshes (C & D), to nearly non-existent or severely eroded shorelines adjacent to former and current industries (E) and organic-rich mudbanks (F).

The edges of the shorelines are intrinsically tied to the geometry of the river and the diurnal tidal currents and sedimentation processes involved (Murphy et al., 2011). Circulation is primarily influenced by the reversing tidal currents (ebb and flood) and mixing of freshwater inflows from the various tributaries and inflows of brackish water from Newark Bay (Murphy et al., 2011; EPA, 2017). The average high ratio of tidal to freshwater flows is ~100:1 for the lower part of the river, resulting in a well-mixed estuarine system suspectable to cohesive sediment transport processes (EPA, 2017; Shrestha et al., 2014).

Shoreline construction and dredging have routinely occurred for more than a century in and around the Lower Hackensack River resulting in varying sedimentation patterns due to lateral confinement along the shoreline (EPA, 2017). Various sedimentation studies involving the Lower Hackensack River and Newark Bay observed prolific scouring of the river bottom

down to the top of Pleistocene sediments, with exposed rocks in the southern flats and accumulation of anthropogenic silt deposits (also referred to as industrial black silt) predominant in the mudflats (EPA, 2017; Murphy et al., 2011).

The combination of highly altered channels, significant freshwater flows from tributaries, and tidal forcing results in subtidal flow patterns with seaward flows of less saline water near the surface and landward flows of saltier water near the bottom (Shrestha et al., 2014). Such tidal flows are also responsible for the dispersion of dissolved and suspended materials, including contaminants of concerns throughout the river. Further, surficial water quality in the lower Hackensack River has been directly impacted by municipal sewage and industrial effluents for the better part of the last century (Image 5-A) (EPA, 2017). Poor recharge from the upper Hackensack River coupled with frequent waste inflows along the mid to lower portions of the river has resulted in a significantly altered Meadowlands and estuary (EPA, 2017).

2. METHODS

Quantifying BC stocks in any depositional environment often involves utilizing an assortment of analytical techniques in order to accurately distinguish BC from other C forms, including IC and thermally unaltered organic carbon (OC). Failure in distinguishing C fractions can result in biased losses of C groups or accidental destruction of BC particles during isolation and extraction procedures (Forbes et al., 2005). Also, without first defining which characteristics determine BC and knowing what methods can facilitate such, it is nearly impossible to quantify BC without over or under shooting total content amounts. Presently, there is no "gold standard" for quantifying BC particles in soil or sediment. This is partially due to the many various environmentally specific or carbon-species specific analytical methods available and their

applicability for distinguishing the full BC spectrum from other C spectrums (Elmquist et al., 2004).

Quantification efforts of BC in this study consisted of a multi-varied analytical approach, including chemical, thermal and selective oxidation analysis. Additional analytical methods were also conducted to investigate the relationship between BC sediment concentrations and other organic pollutants, including various trace and heavy metals and various aromatic hydrocarbons (i.e. PAHs). By investigating the chemical features of the various target aromatic compounds present in the chromatographic sample-specific profile, source determinations (i.e., biomass, petroleum or pyrogenic in origin) can be inferred following cross examination against known chromatographic profiles/signatures of various natural and anthropogenic materials (Kruge, 2015; Uhler et al., 2005). High resolution imagining coupled with elemental analysis of C, O, and trace elements can also assist in identification of BC particles and help distinguish between the various types of BC particles present in a sample matrix (Stoffyn-Egli et al., 1997; Yu et al., 2012).

EPA analytical methods were utilized for both TOC analysis (Kahn, 1988) and PAH analysis (Method 8270) at a NJ commercial laboratory (Integrated Analytical Laboratories) with established QA/QC parameters. PAH identification and quantification and TOC evaluation were also conducted using loss on ignition (LOI) analytical approaches for gravimetric loss calculations and pyrolysis-GS/MS for identification of various pyrolytic compounds including alkylated compounds (*n*-alkanes), petroleum biomarkers and other chromatographic characteristics to further resolve the presence of BC particles (Emsbo-Mattingly, 2001; Kruge, 2015). Scanning electron microscopy (SEM) analysis involved high resolution imaging and

elemental characterization. The results of each analysis were also cross evaluated for the twelve sediment samples and various reference materials analyzed.

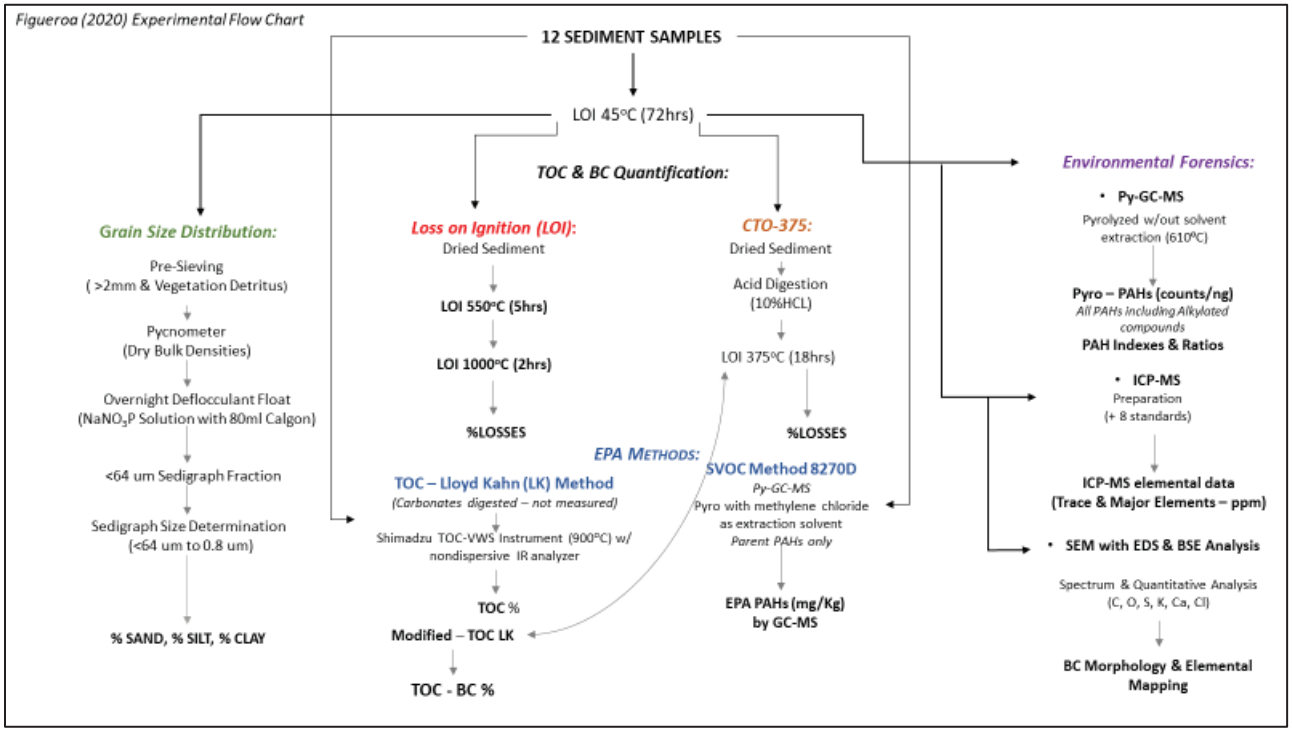

Figure 8. Experimental flow design. A schematic of the different analytical methods involved in quantifying BC particles in the surficial (0 – 15 cm) sediment of the Lower Hackensack River. A modified TOC approach (Kahn, 1988) was designed for this study, with BC determinations further supported by specific chemical signatures and elemental analysis of suspected BC particles.

2.1.2 Study Design

Initial efforts included a comprehensive review of previous environmental, ecological, and investigative studies, publications, and articles related to the Lower Hackensack River. This was followed by a preliminary boat ride down the river to canvass potential sampling sites and develop a better understanding of the complex, meandering study area.

River access was provided by Captain Bill Sheehan of *The Hackensack RiverKeeper,* a non-profit organization dedicated: "defending the Public Trust resources of the Hackensack River Watershed" (Hackensack Riverkeeper, n.d.). The study area was also canvassed on foot to determine feasibility of various sampling equipment and accessibility.

Sampling sites were selected based on several factors, including proximity to known areas of interest, appropriate spatial distribution to other samples, and suitability for sample equipment retrieval. Additionally, sampling of the inner river bend was prioritized due its depositional nature of finer particles and organic-rich material (Konsevick & Bragin, 2010). Examples of the inner bends of the river are included as Figure 9 (A) and Figure 18 (B).

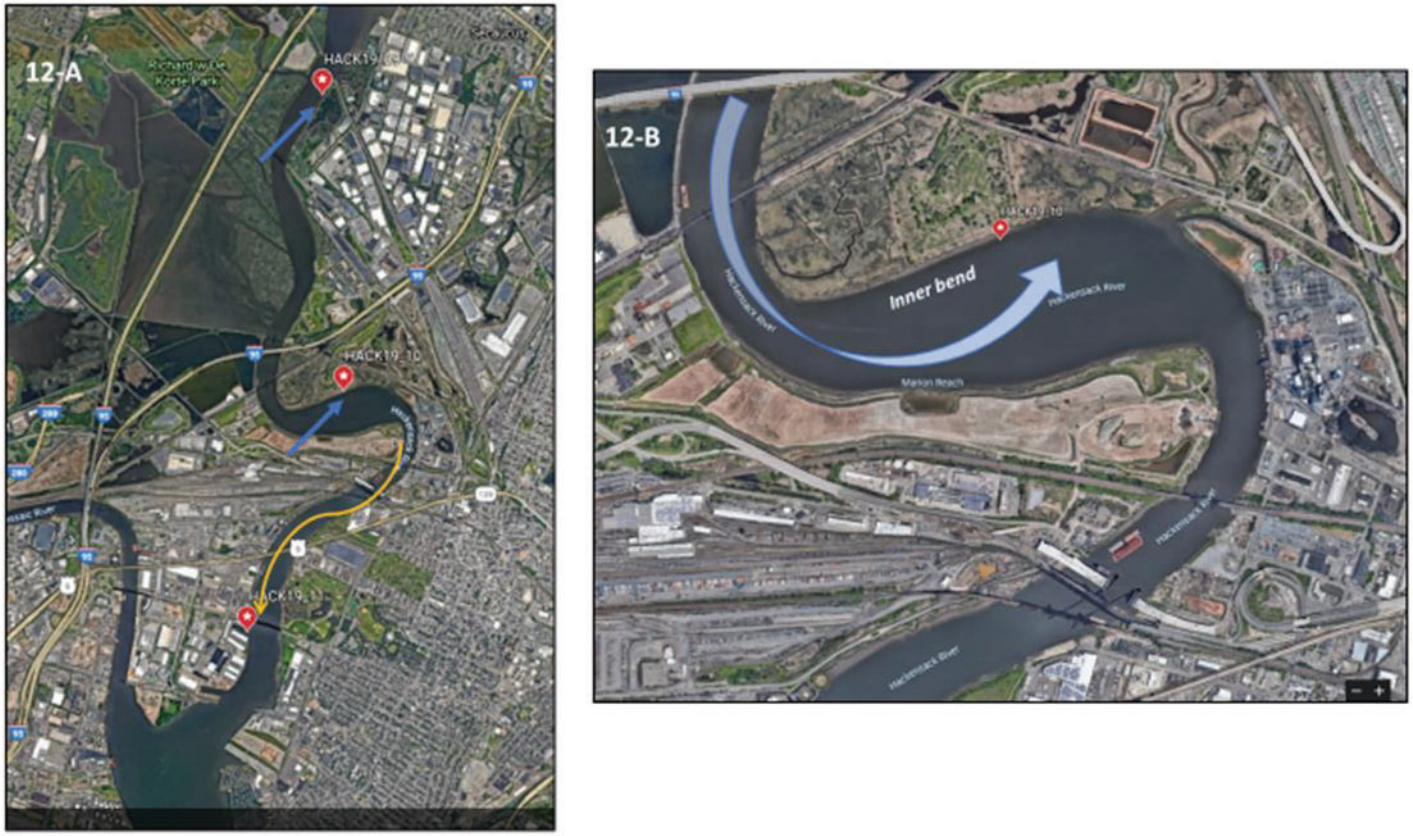

Figure 9 (A-B). Inner and out bends of the Lower Hackensack River. **(A).** Inner bed samples are denoted by the blue areas (HACK19_09 & 10). The yellow snaking arrow marks the outer bend area of HACK19_11. **(B).** Sample HACK19_10 was collected from the inner sharp bend of the lower (downstream) river portion, situated approximately 7 km north of Newark Bay. Malanka Landfill is located to the immediate N, NW of sample HACK19_10. The former fly ash ponds and coal-burning (utilities) structures of the former Hudson Generating Station are located to the NE and E.

Figure 9 (B) shows the location of sample HACK19_10, which was collected from the inner sharp bend of the lower (downstream) river portion, situated approximately 7 km north of Newark Bay. Malanka Landfill is located to the immediate N, NW of sample HACK19_10. The former fly ash ponds and coal-burning (utilities) structures of the former Hudson Generating Station are located to the NE and E. The former Kopper's Coke Company property and Standard Chlorine (Superfund) site are located to the south of HACK19_10, on what is also referred to as some as 'Koppers Coke Peninsula' (EPA, 2016).

Figure 10 illustrates all sample site locations and identifying site feature. Table 1 summarizes sampling locations in relation to river segment (Upper/Mid/Lower) and rkm. The start of the non-tidal portion of the river was attempted, however, due to difficulty regarding access to private and/or protected riverfront areas, the next available location observed was near rkm 34, the location of '*background*' sample, HACK19_12. Figure 10 and Table 1 are included below for reference. A sub-set of sample photologs are also included as Figure 11.

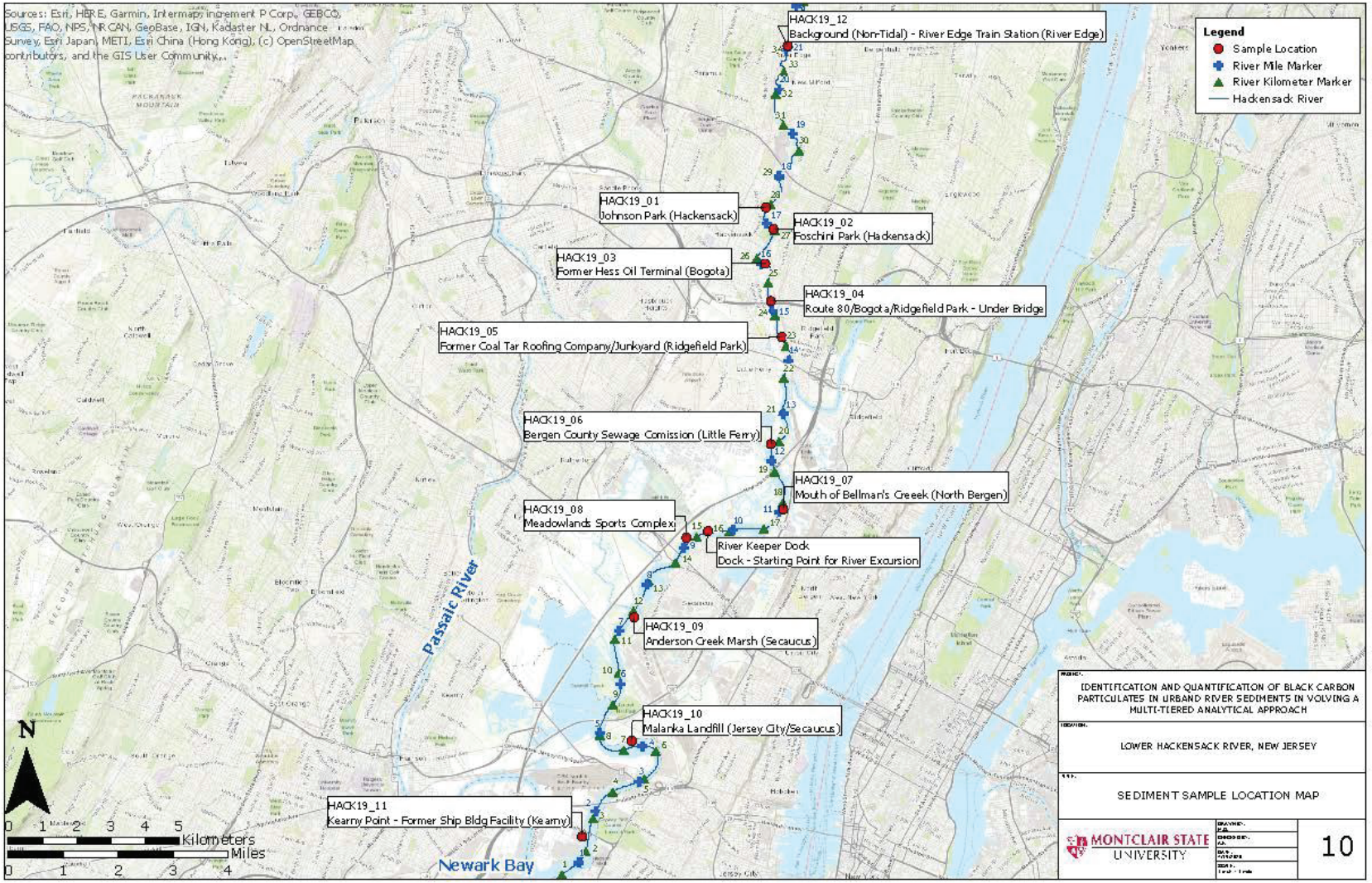

Figure 10. Sample site location map. Sample ID text boxes include specific site features.

Table 1. Study sample location and site description table.

FIELD_ID	X	Y	Lat	Long	River KM	Site Description
Upper River Portion						
HACK19_01	620294	750336.2	40.892408	-74.036385	28	Johnson Park (Hackensack)
HACK19_02	620987	748257.2	40.886692	-74.033918	27	Foschini Park (Hackensack)
HACK19_03	620207.4	744937.8	40.877592	-74.036801	25.5	Former Hess Oil Terminal (Bogota)
HACK19_04	620752	741321.8	40.867658	-74.034901	24.5	Route 80/Bogota/Ridgefield Park - Under Bridge
Middle River Portion						
HACK19_05	621821.5	737848.3	40.858108	-74.031102	23.5	Former Coal Tar Roofing Company/Junkyard (Ridgefield Park)
HACK19_06	620760.5	727562.9	40.829892	-74.035135	20	Bergen County Sewage Comission (Little Ferry)
HACK19_07	621951.7	721278.7	40.812625	-74.030952	18	Mouth of Bellman's Creeek (North Bergen)
HACK19_08	612637.4	718540.9	40.805242	-74.064651	15	Meadowlands Sports Complex (East Rutherford)
Lower River Portion						
HACK19_09	607617.1	710890.2	40.784308	-74.082918	12	Anderson Creek Marsh (Secaucus)
HACK19_10	607350.4	698994.3	40.751658	-74.084085	7	Malanka Landfill (Jersey City/Secaucus)
HACK19_11	602585.5	689779.6	40.726425	-74.101435	2.5	Kearny Point - Former Ship Bldg Facility (Kearny)
Upstream, tidal / non-tidal Interface						
HACK19_12	622372.7689	765893.587	40.93508	-74.028562	34	River Edge Train Station (River Edge, Bergen County NJ)

Figure 11 (A-D). Subset of 2019 sample related photos from the Lower Hackensack River. Fig 11-A depicts the sample area of HACK19_12 (River Edge, NJ). Fig 11-B captures a portion of the Bergen County sewage treatment facility and the approximate area of sample HACK19_06 (Little Ferry, NJ). Fig 11-CC captures the sampling area of HACK19_02 (Foschini Park, Hackensack

NJ). Fig 11-D captures the black, reflective visual characteristics of HACK19_04 (Under Route 80 Bridge, Bogota/ Ridgefield Park, NJ).

2.2 Field Methods

Sediment samples were either collected utilizing a modified Teflon clear 5 cm core tube for hand collection or with a standard 316-stainless steel Ponar grab sampler (sampling area of 0.05 m^2, weight ~22 kg per manufacturing specifications), attached to a 6 m long rope for retrieval (Figure 12 (A-C)). The Ponar grab sampler was often deployed directly from the sampling boat, the *Hackensack Riverkeeper*, however, on occasion was also deployed from overhead structures.

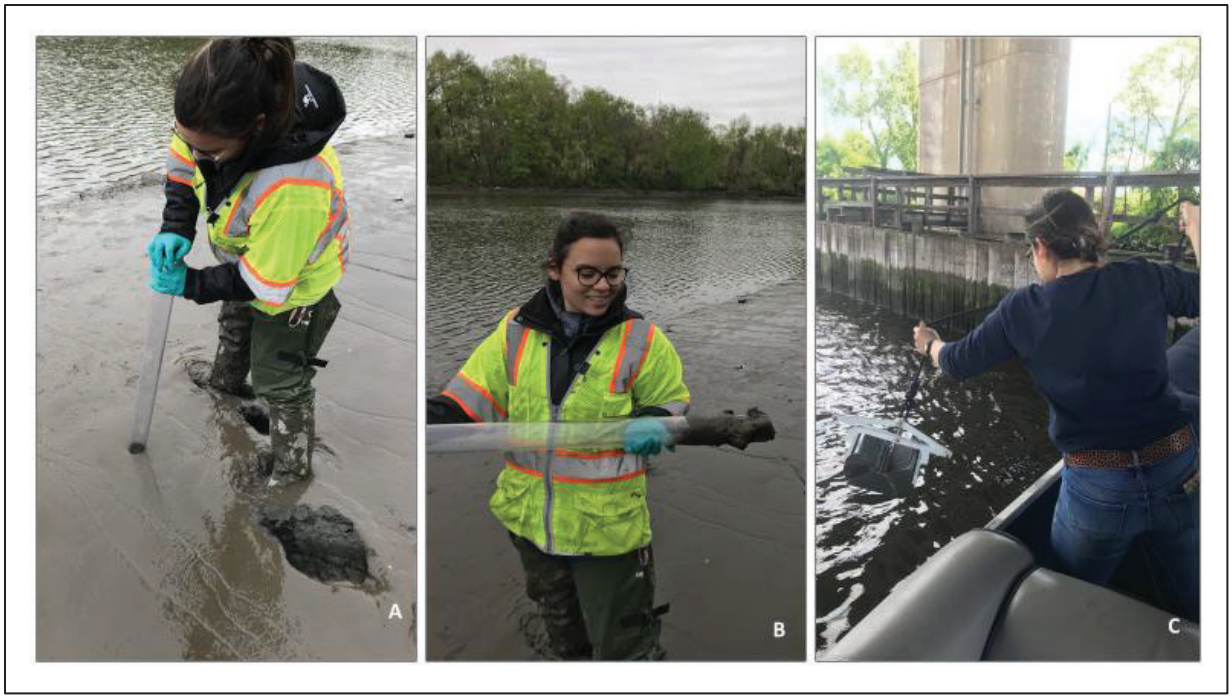

Figure 12 **(A-C).** Study sample collection materials including a modified Teflon clear 5 cm tube (Fig-A & B) and 316 Ponar grab sampler from the sampling boat (Fig 12-C).

Due to the shallow inshore depths (< 2.5 m) in the northern portion of the river, sampling was conducted on foot during low-tide conditions for the first two samples collected. Site IDs HACK19_01 and HACK19_02 were both collected April 28, 2019 using the modified Teflon clean 5 cm core tube. The sample core tub was driven into the mudflat and then spun counterclockwise three times at a 45^{o} angle to capture approximately 15 cm of sediment (Figure 12-A & 12-B). After retrieval the sample was transferred to a single-use aluminum tin for sample homogenization prior to jarring in a laboratory-provided 240 ml glass jar.

On May 16, 2019, river access was once again provided by *The Hackensack Riverkeeper* (Figure 12-C), resulting in the collection of an additional 9 sediment samples. Sampling was initiated approximately 1 km south of sample HACK19_02 and continued downstream, terminating at sample HACK19_11. Water depth was ascertained using the boat's Garmin model Blue Depthfinder. Weather conditions were recorded as clear, sunny skies, mild, with temperatures around 20 ºC.

The Ponar grab was arranged in the open position and dropped directly over the boat edge with force to allow for the Ponar grab to reach the sediment floor and release the closing mechanism (Figure 11-C). The rope line was then tugged to ensure sufficient material was grabbed and then slowly raised up onto the boat for sample retrieval. The Ponar grab was placed into a cleaned plastic tub to allow for the overlying water to slowly decant before being discarded. The Ponar grab was then opened, releasing the sediments into a clean stainless-steel sampling bowl. Any residual material stuck to the inside of the Ponar grab was carefully scooped out using a stainless-steel scoop. The sediment was then homogenized in the same aluminum pan before transfer to clean laboratory-provided 240 mL glass containers. The surficial sediment sampling conducted focused primarily on the first 15 cm of the riverbed. Organic-rich deposits

mixed with black industrial silt and various fragments of historic fill (i.e., industrial waste, construction materials, etc.,) was observed lining the river edges and portions of the river bottom (Images 2-E & 2-F), consistent with previously reported field conditions (EPA, 2017). Samples were stored in a dedicated cooler on ice following collection. Table 2 summarizes the sample pertinent information including location, water depth, appearance and collection.

Table 2. Sediment sampling information. Visual characteristics and water depth are site specific.

Table 2. Sediment Sampling Information					
Site ID	**Sample Date**	**River Location**	**Water depth from Surface**	**Visual Description**	**Additional Notes**
HACK19_01	4/28/2019	Johnson Park, Hackensack NJ	N/A (Mudflat)	Soft dark brown-grey silty mud.	Hand collection via modified teflon sampling tube.
HACK19_02	4/28/2019	Foschini Park, Hackensack NJ	N/A (Mudflat)	Firm dark brown mud with heavy presence of organic fragments.	Hand collection via modified teflon sampling tube.
HACK19_03	5/16/2019	Formerl Hess Terminal, Bogota NJ	11-12'	Soft, saturated, brownish-grey mud.	Grab collection via Ponar Sampler from boat.
HACK19_04	5/16/2019	Below Rt. 80 bridge, Bogota/Ridgefield Park NJ	11-12'	Very soft, saturated, black mud (consistency of mayonnaise).	Slight sheen observed. Grab collection via Ponar Sampler from boat.
HACK19_05	5/16/2019	Former Coal Tar (Roofing) Business, Ridgefield Park NJ	12'	Soft, saturated, black mud with thin brown surface layer, organic & inorganic fragments.	Heavy commercial area (i.e. junkyards, construction-related businesses). Grab collection via Ponar Sampler from boat.
HACK19_06	5/16/2019	Bergen County Sewage Comission, Little Ferry NJ	8'	Soft, saturated, black mud with many phragmites stalks, anerobic odor.	Grab collection via Ponar Sampler from boat.
HACK19_07	5/16/2019	Mouth of Bellmans Creek, North Bergen	5'	Black-brownish-grey peat, some clay, mostly roots.	Grab collection via Ponar Sampler from boat.
HACK19_08	5/16/2019	Meadowlands Sport Complex, East Rutherford NJ	9'	Soft, greyish-brown mud (consistency of mayonnaise).	Grab collection via Ponar Sampler from boat.
HACK19_09	5/16/2019	Anderson Creek Marsh, Secaucus NJ	9'	Soft, brownish black mud, with organic fragments mixed in.	Grab collection via Ponar Sampler from boat.
HACK19_10	5/16/2019	Malanka Landfill (River Bend Marsh), Secaucus NJ	12'	Blackish-brown clay, compact, very gravelly, with HF fragments.	Also, adjacent to the former PSE&G Hudson Generating Coal Plant, Jersey City NJ
HACK19_11	5/16/2019	Former Ship Bldg Facility, now Kearny Point, Kearny NJ	15'	Brownish-black soft mud, also gravely with staining and misc. pieces of HF.	Grab collection via Ponar Sampler from boat.
HACK19_12	7/16/2019	River Edge Train Station, River Edge NJ	2'	Soft, brown mud, anaerobic odor.	Collected in the upstream non-tidal portion of the River. 2 CSO's located in close proximity to sample.

The Ponar grab, 5 cm Teflon sampling tube and miscellaneous sampling tools (i.e., stainless steel bowls and trays) were cleaned using site water and a hard-bristle scrub brush to remove any visible sediment before decontamination using a two-step wash of Alconox-detergent with distilled water rinse.

2.2.1 Sample Preparation

Following sample collection, the sediment samples were transferred to Montclair University Department of Earth and Environmental Studies' Earth Sciences laboratory. The wet sediment samples were stored in a dedicated lab refrigerator set to 4^{o} C. Keeping the samples cooled greatly limits microbial degradation, which if not accounted for could potentially skew quantification of carbon fractions (NJDEP, 2013).

Initial sample preparation consisted of drying the wet sediment in a drying oven set to 45 ^{o}C for 72 ± 2 hours to ensure the complete removal of moisture. Approximately 50 to 150 g were placed in single-use aluminum baking tins (20 X 10 X 6 cm) for drying to accommodate the comprehensive list of analytical methods mentioned. Subsequent to drying, the samples were homogenized using an agate mortar and pestle to produce a finer powder but were not completely pulverized. Visual organic fragments (i.e. twigs, shells, etc.,) and/or any debris were removed by hand prior to sample homogenization.

2.3 Physical Properties of Sediment

To determine the physical properties of the Lower Hackensack River sediments, the analytical efforts focused on sediment water content (percent moisture), bulk density, organic matter (OM) content and particle size distribution (or sediment texture). Evaluating the physical properties of sediments allows for crucial insight into the hydrodynamic processes involved and provides additional insight regarding the molecular composition of sediments.

2.3.1 Grain Size Distribution

A Micromeritics Sedigraph 5100 Particle Size Analyzer was utilized to determine the grain size fractions of the study sediments. Particle size determination focused on a size range of

.80 to 70 µm, also known as the 'fine fraction' for sediments (Oen *et al*. 2005). Particle size results are reported as 'percent-finer-than'.

Initial sample preparation involved sifting dried sample sediment through a 63 µm sleeve to remove coarser particles per instrument specification. Several grams of each sample were then transferred to Columbia University's Lamont-Doherty Earth Observatory (LDEO) geochemistry laboratory (Palisades, NY). Approximately 2 g of sample were weighed and then transferred to a Micromeritics Pycnometer for dry sample density determinations. Once sample densities were recorded, approximately 1.5-2.0 g of sample were weighed and measured into pre-labeled sedigraph cups. A solution of sodium metaphosphate and distilled water (DI) was created and used as sample deflocculant. Approximately 70 mL of deflocculant was added to the sample cups to ensure a 2-3% sample concentration. The samples were then stirred and left overnight in the deflocculant solution to encourage settling.

Following an overnight solution bath, the samples were then placed in a sonicator bath for 30 minutes before Sedigraph analysis. The basic principles of Sedigraph analysis are centered on sedimentation rates governed by Stokes' law. Samples results were then transferred from the LDEO Sedigraph computer, with post-analytical modification and querying of sample data/reports conducted remotely.

Grain size fractions were based on specific size ranges, consistent with USDA Texture Classification limits and are as follows:

- Fine Sand (62 µm-70 µm);
- Silt (4 µm- 62 µm); and
- Clay (<4 µm).

Moisture content or percent moisture (%M) is a routine environmental measurement which determines the amount of water present in moist solids, such as soil and sediment following drying of the sample material (IAL, 2019). %M was reported as a percent of the total sample and was determined using the following equation:

$$\% M = 100^* (\text{Wet Weight} - \text{Dried Weight})/\text{Wet Weight}$$

2.3.2 Total Organic Carbon – Lloyd Kahn

TOC amounts can be measured directly or can be determined using gravimetric analysis so long as both total carbon (TC) and inorganic carbon (IC) amounts are accounted for prior (Heiri et al., 2001). In this study, TOC analysis was conducted following the EPA/industry standard known as the Lloyd Kahn (LK) Method for TOC determination (Kahn, 1988). The LK Method analysis for TOC determination was performed at Integrated Analytical Laboratories (IAL) located in Randolph, NJ.

The samples were analyzed for TOC on a Shimadzu TOC-VWS Analyzer with an SSM-5000A Solid Sample Module. The sample procedure followed the guidance provided by the National Environmental Index (NEMI) for TOC analysis. Initial analytical steps involve acid treatment to remove IC from carbonates and bicarbonates. However, IC is not measured as part of the LK Method.

Dried sample sediment was homogenized and diluted as necessary before a small micro-portion was injected into a heated reaction chamber packed with an oxidative catalyst. Samples were heated isothermally at 900 ºC in combustion boats. The water within the sample matrix eventually vaporized, resulting in the oxidation of IC and OC to CO_2 and H_2O. The CO_2 was then transported in the carrier-gas stream and measured by a nondispersive IR analyzer at IAL. TOC

data were reported in mg/kg on a dry weight basis. The minimum reporting value for TOC was 100 mg/kg (0.01 %).

2.4 Black Carbon Quantification

In order to accurately quantify and characterize BC particles several analytical methods were undertaken. Methods included focused on gravimetric losses, elemental analysis, chemo-thermal oxidation, and elemental mapping. Additionally, BC particle morphology was also included to assist in differentiating BC particles from other carbonaceous particles (Stoffyn-Egli et al., 1997; Niyogi et al., 2011).

2.4.1 Loss on Ignition (LOI) Analysis

Loss on ignition (LOI) was performed for all twelve sediment samples and for several reference materials, including calcium carbonate [A], powdered graphite [B], methylcellulose powder [C], commercially available activated black carbon [D] and refined industry coal [E]. High carbon content reference materials were selected for comparison purposes and to provide insight into how different carbon forms respond to timed, sequential temperature ramps of 550 ^{o}C and 1000 ^{o}C. The LOI procedures employed herein followed the standard operations of procedures (SOP) outlined by Rosenmeier & Abbott (2015), which is ultimately a modification of that described by Heiri *et al*. (2001). Table 3 summarizes the LOI analytical steps undertaken.

Table 3. Sequential Loss on Ignition (LOI) analytical methods table.

Sample #	#
Drying Temp. (C)	45
Exposure Time (h)	72
1st LOI Temp. (C)	550
Exposure Time (h)	4
2nd LOI Temp. (C)	1000
Exposure Time (h)	2

Approximately 2g of homogenized dried (45 ºC/72 h) sediment were transferred into clean, dried ceramic crucibles. The sample-filled crucibles were then weighed and recorded on an analytical balance to the 0.0001 gram prior to placement inside a muffle furnace preheated to 550 ºC for approximately 4 hours. To avoid overheating, sample-filled crucibles were transferred to the furnace only after a constant temperature was achieved. Following exactly 4 hours of ignition at a steady 550 ºC, the sample-filled crucibles were then removed and transferred to a drying oven set to 60 ºC for approximately 1 hour to allow for safe handling. Following 1 hour of cooling in the drying oven, the samples were then immediately weighed to avoid atmospheric moisture adsorption by the samples. Upon recording all post-550ºC sample-filled crucible weights, the samples were returned to the muffle furnace for a 2-hour ignition at 1000ºC.

Following the 2-hour ignition at 1000 ºC, the sample-filled crucibles were again, transferred to a cooling oven for safe handling. Following adequate cooling, the sample-filled crucibles were immediately weighed, with the final dry weights recorded. Differences in weight loss following combustion at 550 ºC and 1000 ºC were used to calculate percent losses (% losses) and to estimate %IC as described by Rosenmeier and Abbott (2015) and Heiri et al. (2001). % IC involved duplicate method calculations routinely used in LOI determinations, to account for the varying molecular weight of carbonates and bicarbonates and for method comparison.

2.4.2 CTO-375 Analysis

Multiple BC sediment studies, such as Oen et al. (2006) and Agarwal and Bucheli (2010), have demonstrated the effectiveness of using a multi-step chemothermal oxidation (CTO) method such as CTO-375 for quantification of BC particles. The traditional approach to CTO-

375 involves thermal oxidation at 375 ºC for 24 hours with active oven airflow to ensure complete combustion of organic matter, followed by micro-acidification of carbonates in Ag capsules before quantification of residual carbon as BC using elemental analysis (Agarwal & Bucheli, 2011; Oen et al., 2006).

For this study a modified CTO-375 approach was applied and conducted at Montclair State University. Approximately 1g of dried (45ºC/72hrs) sample material was finely homogenized using an agate mortar and pestle. Initial sample weights were recorded prior to digestion with 5 mL of 10% hydrochloric acid (HCl) for carbonates (including bicarbonates) removal. Following in situ acidification (18hrs) and a triplicate deionization rinse for efficient removal of carbonates, the samples were then transferred to clean ceramic crucibles and dried at 60 ºC in a drying oven overnight and milled to a fine powder by using an agate pestle and mortar.

The digested and dried samples were then transferred to a pre-heated muffle furnace set to 375 ºC and heated for approximately 18 hours. To reduce charring potential caused by oven temperature overshooting and relative atmospheric humidity, samples were only moved once a steady temperature of 375ºC was maintained (Heiri et al., 2001). Upon adequate cooling, the post-375ºC sediment samples were weighed, with final weights used to determine percent losses. The post-375ºC residue-aggregates were then carefully broken and homogenized with a mortar and pestle once again. The post-375ºC residues were then carefully transported to IAL Laboratories for final quantitative BC analysis involving a Shimadzu elemental analyzer.
In this study, BC is defined as the residual carbon which survived pre-treatment acidification and sequential thermal stress (375ºC and 900ºC) and oxidation. The sum of all residual carbon

captured by the elemental analyzer involving the modified Kahn (1988) approach described below is characterized as BC.

2.4.3 Modified Lloyd Kahn for BC Analysis

Quantification of BC content was ultimately achieved utilizing a Shimadzu TOC-VWS Instrument outfitted with an SSM-5000A Solid Sample Module. Carbon analysis of the post-375°C residues (Section 2.4.2) followed the same steps as described in the Lloyd Kahn Method for TOC analysis (*Section 2.4.1*) separate of the pre-treatment with acid for carbonates removal.

Dried sample sediment was homogenized and diluted as necessary before a small micro-portion was injected into a heated reaction chamber packed with an oxidative catalyst. Samples were heated isothermally at 900 ºC in combustion boats. The water within the sample matrix eventually vaporized, resulting in the oxidation of IC and OC to CO_2 and H_2O. The CO_2 was then transported in the carrier-gas stream and measured by a nondispersive IR analyzer at IAL. BC results were initially reported in mg/kg (dry weight basis). The BC results were compared to the percent losses derived from the LOI and CTO-375 analyses, TOC concentrations and lastly, PAH quantification results.

2.4.4 EPA Method 8270 – Pollutant PAHs

EPA Priority Pollutants, which consist of 16 parent (non-alkylated) compounds are often quantified in sediment investigations. Raw sediment samples were provided to IAL for PAH analysis in addition to TOC-related analyses. PAH analysis followed the guidelines provided under USA EPA Method 8270 for semi-volatile organic compounds (SVOCs or PAHs) by GC/MS (Stout et al., 2015). Method 8270 is a routine and accepted environmental measurement

for EPA PAHs, comparing identified and quantified PAH compounds against known standards which are often displayed as the larger compound peaks near smaller parent PAH peaks.

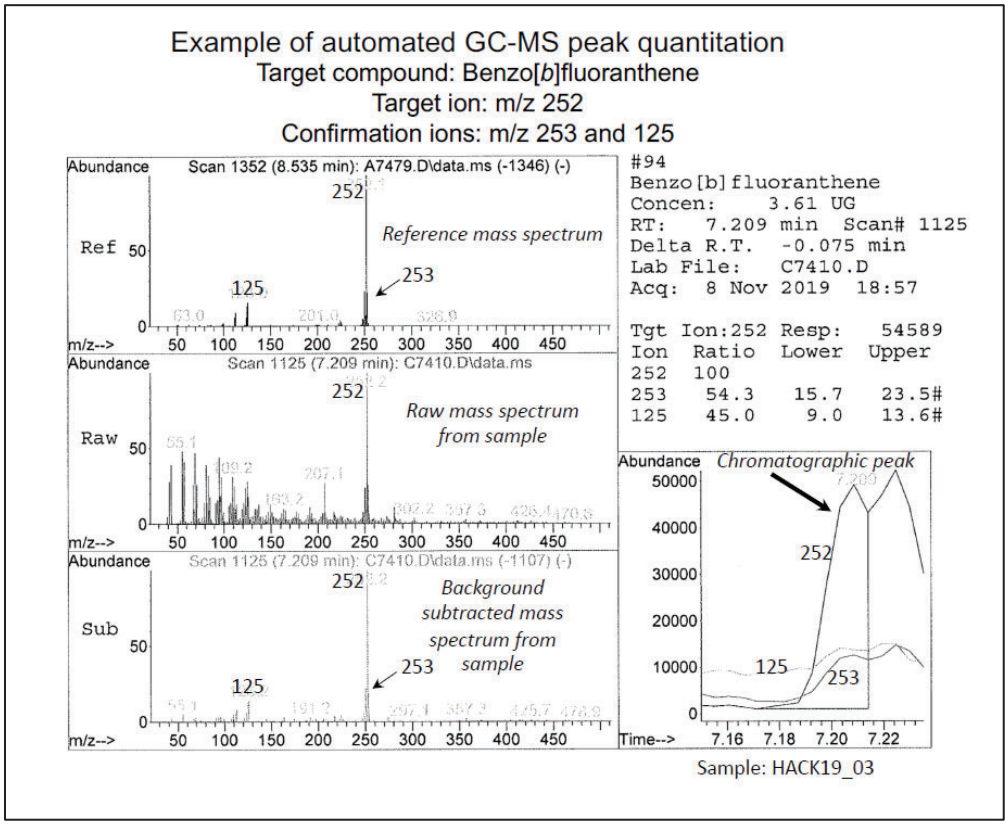

Figure 13. Example of automated GC-MS peak quantitation using USEPA Method 8270 of target PAH compound, benzo[*b*]fluoranthene (5+ ring structure) for sample HACK19_03. The bolded black arrow of the lower-right image denotes the m/z 252 chromatographic peak identified. Examples of the reference mass spectrum, raw mass spectrum from sample and adjusted spectrum are shown on the right.

Sample preparation involved an ultrasonic extraction procedure using CH_2Cl_2 as the extraction solvent. The sediments were then dried with sodium sulfate and serially extracted with CH_2Cl_2. The extract was then concentrated down prior to GC/MS analysis. PAH compounds were then separated by GC with the mass spectrometer subsequently obtaining a mass spectrum of each compound. The positively identified compounds were then compared against an internal

set of standards and known spectral library and quantified in mg/kg (Figure 13, Kruge, 2015; Stout et al., 2015; IAL, 2020).

2.4.5 Pyrolysis-Gas Chromatography-Mass Spectrometry (Py-GC-MS)

Py-GC-MS was included in this study to also facilitate the detection of organic contamination in river sediments but primarily, to account for a fuller suite of hydrocarbons present, not just the 16 parent (non-alkylated) EPA Priority Pollutants. The other primary objectives of Py-GC-MS analysis included evaluation of general chromatographic patterns/fingerprints, PAH compositions, diagnostic ratio analyses and spatial patterns (Stout et al., 2015; Emsbo-Mattingly et al., 2001). Py-GC-MS analysis is an alternative analytical method associated with forensic chemistry studies due to its wide applicability for rapid identification of various organic assemblages (Kruge et al., 2018; 2020; Lara-Gonzalo et al., 2015, Hagmann et al., 2019). Py-GC-MS analysis was performed at Montclair State University.

The initial Py-GC-MS analysis was accomplished using a CDS 5150 Pyroprobe (CDS Analytical Inc., Oxford, PA) coupled to a Thermo Finnigan Focus DSQ GC/MS (Thermo Electron Corporation, Madison, WI) equipped with an Agilent DB-1MS column (30 m × 0.25 mm i.d. × 0.25 μm film thickness). The GC oven temperature was programmed from 50 °C to 300 °C (at 5 °C min^{-1}), with an initial hold of 5 min at 50 °C and a final hold of 15 min at 300 °C. Pyrolysis was performed for 20 s at 610 °C. The MS was operated in full scan mode (50-500 Da, 1.08 scans s^{-1}). The MS was calibrated by autotuning with PFTBA and blanks were run each day before samples were analyzed. Compounds were identified using the W8N08 mass spectral library (John Wiley and Sons, Inc., New York, NY), the online NIST Standard Reference Database Number 69 (webbook.nist.gov/chemistry/), and by reference to the literature (Hagman et al., 2020). Selected compounds of interest were quantitated using the GC-MS software. Mass

spectral response factors, previously calculated from acquired and library mass spectra, were applied to correct the raw peak area counts. The data are reported as corrected area counts per nanogram of dry sample (counts/ng sample) and were normalized using toluene. These data are only semi-quantitative since standards were not employed.

2.4.6 Inductively Coupled Plasma Mass Spectrometry (ICP-MS)

ICP-MS was conducted to investigate the distribution of metal concentrations throughout the river and to investigate whether any correlations exist between metals and BC fractions. A total twelve (12) sediment samples, eight (8) standards and three (3) blanks were analyzed in triplicate runs as part of this ICP-MS analysis.

ICP preparation followed the Marine Sediment SOP *(n.d.)* developed by Dr. Stefanie Brachfeld and Dr. Matthew Gorring (Montclair State University, NJ). Sample preparation commenced with adding approximately 400 mg of lithium metaborate ($LiBO_2$) flux to approximately 100 mg of dried sample with the goal of 0.5% tolerance for both masses. Following careful homogenization of the two materials, the samples were then funneled into clean graphite crucibles prior to analytical pyrolysis in a muffle furnace maintained at 1025 ^oC for 35 minutes. At the 35-minute mark the crucibles were carefully removed from the furnace with laboratory tongs, with crucible contents (i.e. molten glass bead) carefully and quickly poured into Telfon beakers containing 50 mL of trace metal grade 7% HNO_3. Once the glass beads were thoroughly incorporated into the HNO_3 solution, the beakers were then moved onto stir plates for approximately 20 minutes. Magnetic stir bars were also added to the beakers to facilitate thorough sample agitation. Following complete dissolution, the sample-solution was then filtered through 100 mm filter paper directly into 60 mL (or '500x') Nalgene™ sample bottles. To analyze the sample a dilution factor of 10,000x was required and achieved by

pipetting 500x solution and 9.5 mL of 2% HNO_3 into 15 mL tubes. The samples (n=12), blanks (n=3) and USGS and NIST calibration standards (n=8) were then arranged in an auto sampler rack prior to sample analysis.

As part of the QA/QC for this method, three blanks consisting solely of HNO_3 and $LiBO_2$, and eight US Geological Survey (USGS) and/or National Institute of Standards and Technology (NIST) geochemical standards (Table 4) followed the procedural steps described above. The standards were used for instrumental calibration and post-processing calibration curves (Flood, 2019).

Table 4. USGS and NIST geochemical reference standards included in ICP-MS analysis. Geochemical code, medium type, and extraction location are included for quick reference.

Standard Code	Type	Location
BHVO-2	Basalt	Hawaii
GSP-2	Granodiorite	Colorado
G-2	Granite	Rhode Island
RGM-1	Rhyolite	California
W-2	Diabese	Virginia
QLO-1	Quartz Latite	Oregon
DNC-1	Dolerite	North Carolina
BIR-1	Basalt	Icelandic

Trace, majors, and rare earth (REE) analysis was achieved using MSU's Thermo Scientific™ ICAP Q ICP-MS with ASX-560 auto sampler with argon gas as the carrier gas. All samples, apart from HACK19_09 through HACK19_12, were analyzed in triplicate runs with drift solutions measured every fifth sample during the instrument run. Samples HACK19_09 through HACK19_12 were analyzed in double runs, with the third run sacrificed due to lack of rack availability and timing.

The ICP-MS data generated was then transferred into a pre-formatted Microsoft Excel 2017™ spreadsheet allowing for the conversion of raw data in counts per second (CPS) to parts per million (ppm) for all reported elemental amounts. Major elements were reported as oxides with reporting as normalized weight percent (wt%). Trace and rare earth elemental data were reported in normalized ppm amounts. Metals of concern (e.g., vanadium (V), nickel (Ni), cobalt (Co), chromium (Cr), and lead (Pb) were specifically targeted to determine whether any spatial correlations exist between BC and common anthropogenic metals based on BC sorption properties..

2.4.7 Scanning Electron Microscopy (SEM)

Sample preparation for SEM was relatively straightforward, dried homogenized sediment material was mounted to SEM sample stubs using either carbon or copper adhesive tape or placed directly on the stub. The samples were then observed by the Hitachi S-3400N SEM and with Buker -AKS EDS (energy dispersive x-ray spectroscopy) detector. Analyzed sediments were not coated to avoid potential charging damage. Due to the elusive nature of BC particles, visual identification focused on dark, amorphous particles involving backscatter compositional imaging. With the understanding that lighter elements such as C and O appear 'darker', in contrast to heavy elements with high atomic numbers which backscatter electrons more strongly and appear 'lighter' (Stoffyn-Egli et al. 1997). Confirmation of BC presence was ultimately concluded with SEM-EDS via elemental mapping of C and O accompanied by spectrum analysis for chemical characterization of BC particles. Generally, suspected BC particles were confirmed by having C amounts in excess of 65%, with total C amounts closer to 90% or greater (Shrestha et al., 2010). Observed BC morphology was also compared to the findings of several fly ash

studies, including Cowan et al. (2015 & 2017), Stoffyn-Egli et al. (1997), Cowan et al., (2015) and Niyogi et al., (2011).

3.0 Analytical Results

3.1 Physical Properties of Sediment

3.1.1 Grain Size Distribution

Grain size distribution focused on very fine sand (70 µm) down to clay (≤ 4 µm). Overall the findings were generally consistent across the samples, with silty-clay conditions dominating the surficial-river sediment matrix as shown in Figure 14.

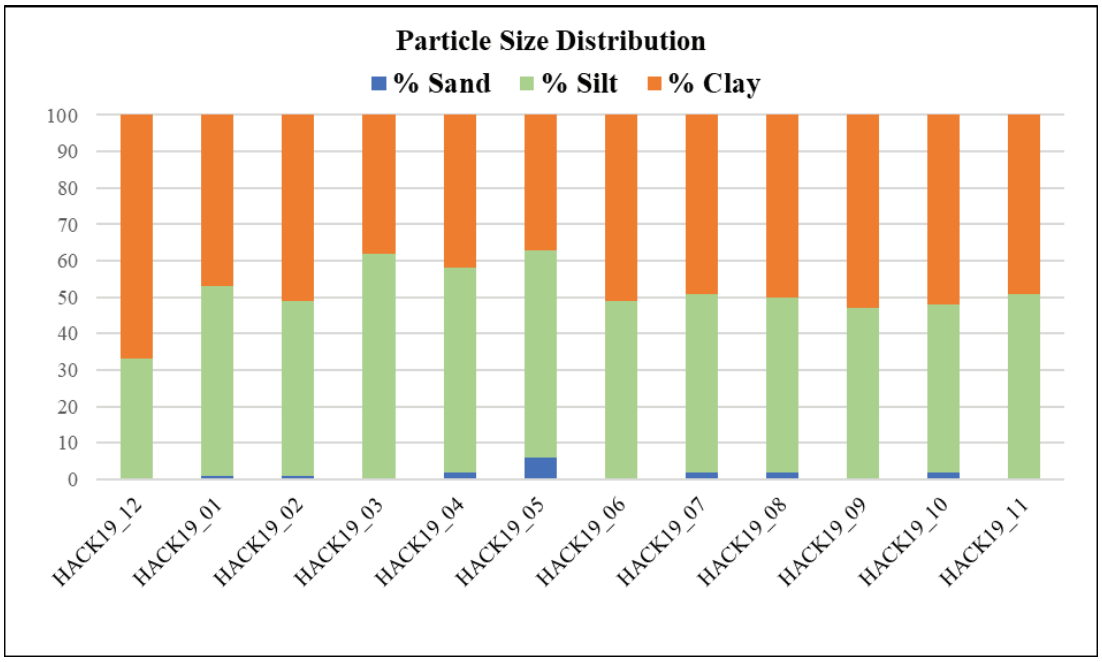

Figure 14. Grain Size Distribution Results by % Sand (62-70 µm), % Silt (4-62 µm), and % Clay (<4 µm). Higher silt concentrations observed in the mid river sediments. The highest % of clay was observed in the non-tidal sample, HACK19_12. % Sand is low throughout, without its highest % total reported at 6% in HACK19_05.

During sample collection the samples appeared to vary in visual appearance from what is best described as ‘black mayonnaise’ in appearance and texture to darker grey-brown silty, saturated muck, to brown organic clay dominated by the presence of various fragments of wetland-related vegetation. Figure 15 (A-D) includes examples of such varying sample appearances.

Figure 15 (A-D). Varying textural characteristics of study samples. Black mayonnaise best describes the visual characteristics of the sediment from sample HACK19_04 (Fig 15-A). Sediment of HACK19_10 appears more compressed and stratified with varying silt deposits (Fig 15-B). HACK19_02 (SS02 in image) consisted mostly of fresh, decaying organic inputs (Fig 15-C). HACK19_05 appeared stained black and more stratified than HACK19_04. Fresh brown silt deposits appear smeared atop the sample (Fig 15-D).

3.1.2 Total Organic Carbon – Lloyd Kahn Results

TOC concentrations were initially reported in mg/kg and then subsequently converted to percent TOC (% TOC) to allow for convenience of evaluation against the other analytical results which were predominantly reported as percent of total sample. TOC analysis involves the combustion of organic matter (and organic carbon) to CO_2 which is then measured by an elemental analyzer for quantification purposes (Kahn, 1988).

TOC concentrations ranged from 2.82% (HACK19_10) to 7.13% (HACK19_05). For this study, carbon-rich sediments were distinguished as having % TOC in excess of 5% based on similar BC-and organic carbon related sediment studies such as Li et al. (2010), Agarwal and Bucheli (2011) and EPA (2017). Table 5 lists the average physical properties of sediment including % fines (silt & clay fractions), % TOC and % moisture (M). Figure 16 illustrates the spatial distribution of % TOC against rkm.

Table 5. Average physical properties of the study sediment samples including % Fines (silt and clay fractions), % total organic carbon (TOC) and % moisture (M).

Sample ID	% Fines	% TOC	% M
HACK19_12	~ 100	4	39
HACK19_01	~ 99	4	37
HACK19_02	~ 99	4	40
HACK19_03	~ 100	6	69
HACK19_04	~ 98	6	66
HACK19_05	~ 94	7	69
HACK19_06	~ 100	4	61
HACK19_07	~ 98	3	54
HACK19_08	~ 98	4	57
HACK19_09	~ 100	4	48
HACK19_10	~ 98	3	42
HACK19_11	~ 100	4	64

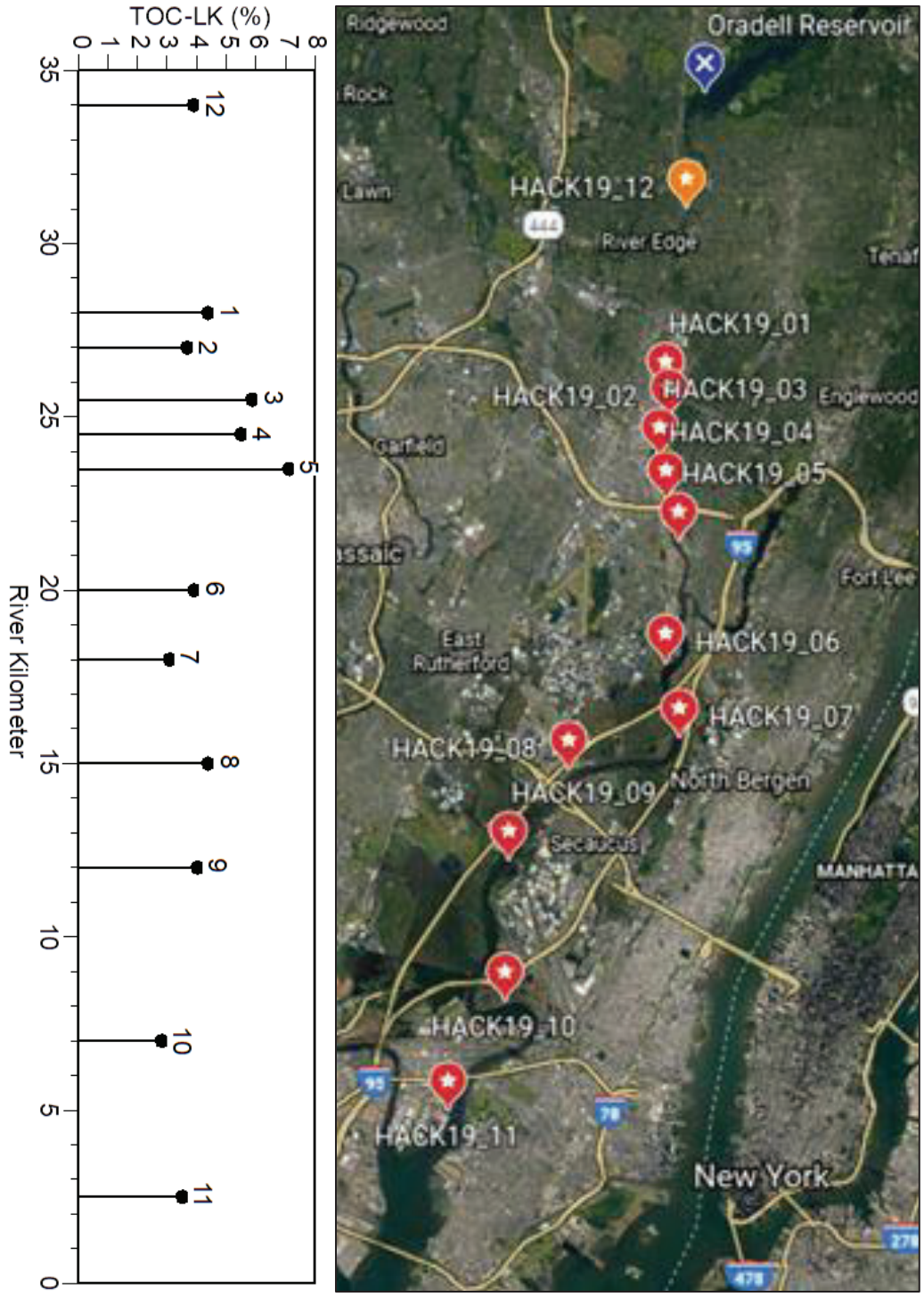

Figure 16. Spatial distribution of TOC % plotted against river km. The Google image on the right provides reference to the river sample numbers displayed on the left. HACK19_12, the upstream background sample is reflected as an orange point instead of the red-star points shown for sample-site locations. The Oradell Reservoir/Dam (non-tidal) is reflected as a blue point.

3.2 Black Carbon Quantification Results

3.2.1 Loss on Ignition (LOI) Results

LOI is a common analytical method used for estimating soil/sediment organic carbon. No universal protocol exists for LOI analysis, however. The degree of customization relating to furnace type, sample mass, duration, temperature, etc., and relative low cost and lab equipment lends to the LOI's attractiveness for analytical quantification, however, it is also those same variable which are responsible for LOI's varying reporting style, owing to its use as an estimation parameter verse quantification parameter.

LOI results were calculated as percent losses relative to combustion temperature. LOI calculations and assumptions are as follows:

% LOSS 550 ^{o}C = 100 X (Loss @ 550 ^{o}C (g) / Initial sample wt. (g))

% LOSS 1000 ^{o}C = 100 X (Loss @ 1000 ^{o}C (g) / Initial sample wt. (g))

% Carbonates or 'IC – LOI' = 100 X 2.274 X (Loss 1000 ^{o}C (g)/ Initial sample wt. (g))
Where 2.274 =equals the molecular weight of $CaCO_3$ / molecular weight of CO_2

Duplicate % IC (Heiri et al. 2001) = 100 X 1.36 (Loss 1000 ^{o}C (g)/ Initial sample wt. (g))
Where 1.36 = constant to determine approximate wt. of IC in original sample

LOI results are tabulated in Table 6. Figure 17 shows the positive but weak linear relationship between the % losses at 550 ^{o}C and 1000 ^{o}C. Overall, majority of burning of organic matter occurred during the 550 ^{o}C (4 hrs) heating which is consist with previous studies such as Heiri et al., (2001).

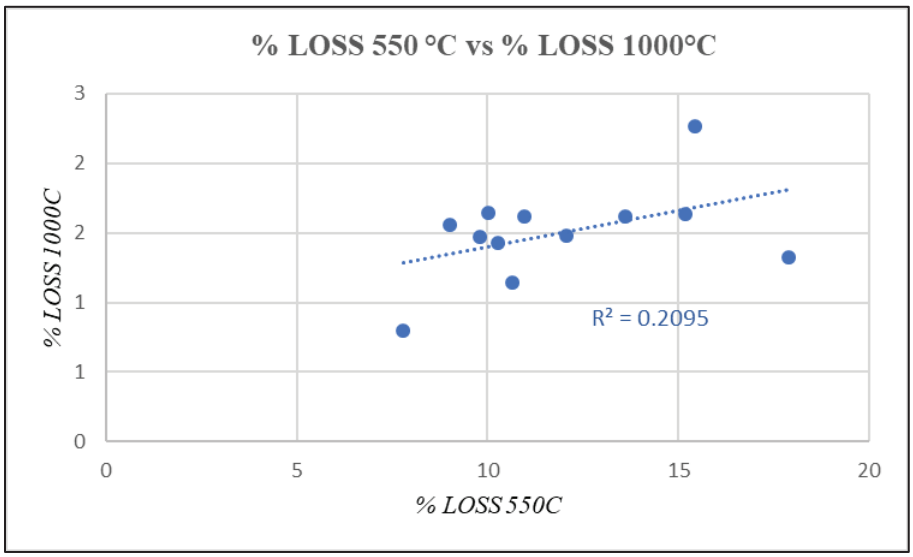

Figure 17. LOI scatterplot showing % LOSS 1000 ºC vs % LOSS 550 ºC. Relationship appears positive, however, not significant as supported by the low R^2 value of 0.2095.

Table 6. Sequential LOI results (550 ºC and 1000 ºC) for site samples and reference materials. The Heiri et al. (2001) title in Table 6 refers to the duplicate method comparison for determining % IC. Both % IC methods are routinely used in LOI determinations.

Table 6. Loss on Ignition Results (550C & 1000C)				
Sample ID	**% LOSS 550°C**	**% LOSS 1000°C**	**% IC - LOI**	**% IC-LOI (Heiri et al. 2001)**
HACK19_01	10.65	1.15	2.61	1.56
HACK19_02	17.91	1.32	3.01	1.80
HACK19_03	15.19	1.63	3.72	2.22
HACK19_04	12.06	1.48	3.37	2.01
HACK19_05	15.45	2.26	5.14	3.08
HACK19_06	10.03	1.64	3.74	2.24
HACK19_07	9.79	1.47	3.35	2.00
HACK19_08	10.26	1.43	3.24	1.94
HACK19_09	10.96	1.62	3.68	2.20
HACK19_10	9.01	1.55	3.53	2.11
HACK19_11	13.62	1.62	3.68	2.20
HACK19_12	7.79	0.80	1.82	1.09
Reference Materials:				
[A] - Calcium Carbonate (Supplement)	0.34	41.62	94.65	56.61
[B] - Powdered Graphite	58.51	24.22	55.07	32.93
[C] - Methyl Cellulose Powder	99.23	0.17	0.40	0.24
[D] - Commercial activated carbon	91.16	0.40	0.91	0.54
[E] - Refined Industrial Brown Coal	12.97	*	*	*
Footnotes:				
% IC - LOI is calculated using a multiplier of 1.36 to account for carbonates in the form as CaCO3.				
% IC - LOI (Hieri et al. 1999) was calculated using the multiplier of 2.274 to account for carbonates				
* = Not Applicable, sample-filled crucible was damaged following ignition at 1000C				

LOI results by themselves are not strong substitutes for quantitative analyses such as Kahn (1988), as heating at 550 ºC can not effectively quantify TOC amounts without the use of an elemental analyzer equipped with a nondispersive IR analyzer for quantification of oxidized OC in the form of CO_2. The presence of clay minerals and metal oxides can interfere with structural alterations of water during heating, leading to possible over-estimations (Heiri et al., 2001). Figure 18 illustrates the weak positive linear relationship observed for the % LOSS at 550 ºC versus % TOC – LK results. Table 7 summarizes LOI results at 375 ºC, 550 ºC and % TOC via Kahn (1988).

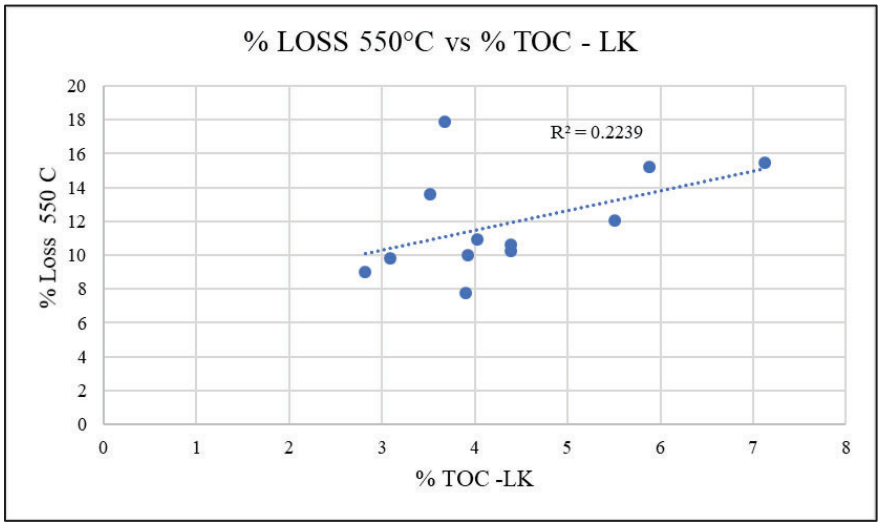

Figure 18. Scatterplot of % LOSS at 550 ºC and % TOC via Kahn (1988). A weak linear relationship exists as shown by the positive trendline and R^2 value of 0.2239.

Table 7. LOI (375 °C & 550 °C) vs % TOC-LK.

Sample ID	% Loss 375°C	% Loss 550°C	% TOC - LK
HACK19_12	6.28	7.79	3.90
HACK19_01	13.82	10.65	4.39
HACK19_02	12.30	17.91	3.68
HACK19_03	11.89	15.19	5.88
HACK19_04	11.92	12.06	5.51
HACK19_05	11.08	15.45	7.13
HACK19_06	7.99	10.03	3.92
HACK19_07	7.63	9.79	3.09
HACK19_08	6.17	10.26	4.39
HACK19_09	7.20	10.96	4.03
HACK19_10	7.38	9.01	2.82
HACK19_11	8.73	13.62	3.52

Samples HACK19_02 and HACK19_11 showed the greatest variability. Generally, LOI calculations appeared to over-estimate the presence of TOC present.

Further, as much as 5% error is expected when determining % IC with strictly LOI results, as the burning of carbonates, including bicarbonates is not 100% efficient at heating of 1000 °C with no pre-treatment (Heiri et al., 2001; Ashworth, 1997). Considerations regarding oven size, sample positions within the oven, ambient temperature and moisture, and the presence of various organic minerals (i.e., clay minerals or metal oxides) or inorganic particles (i.e., crushed shells) are several examples of the unaccounted variables frequently associated with LOI analysis and quantification. While LOI is useful for evaluating the thermal evolution of sediment or soil and is a quick and low-cost approach for determining the gravimetric losses associated with specific combustion temperatures, its potential drawbacks regarding accuracy and reproducibility are still significant.

3.2.2 CTO-375 Results

CTO-375 data is tabulated in Table 8. '*Percent loss at 375 ºC'* includes the OC fraction, with the '*% Residues Post-375 ºC'* including the BC fraction. Lastly, the *'Acid Soluble Fraction'* represents the IC fraction. Initial CTO-375 efforts, including % loss determinations were conducted in support of the more advanced analytical BC measurements using element analysis.

Overall, following combustion at 375 ºC did not result in significant losses of total organic matter as supported by the relatively low '% LOSS 375 ºC' amounts (<15 %) summarized in Table 8. The main purpose of CTO-375 however, was for subsequent sample preparation using a modified Kahn (1988) TOC analysis for BC quantification.

Table 8. CTO-375 % losses results. Carbonates were dissolved during acid-treatment. The organic material combusted at 375 ºC also includes organic carbon particles. The post-375 ºC residues include black carbon particles which were ultimately quantified using an element analyzer.

	Including IC	*Including OCP*	*Including BCP*
Sample ID	**Acid Soluble Fraction (%)**	**% LOSS 375°C**	**% Residues Post-375°C**
HACK19_12	5.61	6.28	88.11
HACK19_01	2.22	13.82	83.96
HACK19_02	0.30	12.30	87.40
HACK19_03	7.79	11.89	80.32
HACK19_04	5.50	11.92	82.58
HACK19_05	5.90	11.08	83.02
HACK19_06	5.57	7.99	86.44
HACK19_07	3.50	7.63	88.86
HACK19_08	5.33	6.17	88.50
HACK19_09	5.13	7.20	87.66
HACK19_10	4.93	7.38	87.69
HACK19_11	7.83	8.73	83.44

The residual C remaining in the post-375 ºC residues, including BC particles were likely intermixed due to the varying presence of other organic and inorganic particles in the sediment

resulting in complex C-related mixtures following the incomplete combustion of the relatively wet sediments. Figure 19 shows the thermal evolution from 375 ºC to 1000 ºC. The greatest losses occurred consistently at 550 ºC. Losses at 1000 ºC were relatively low throughout except for a brief spike in HACK19_05. The greatest observed loss at 375 ºC appears in HACK19_12. Losses at 375 ºC appears to follow a similar trend compared to the losses at 550 ºC. Samples HACK19_10, HACK19_07 and HACK19_12 are the least affected in terms of % losses.

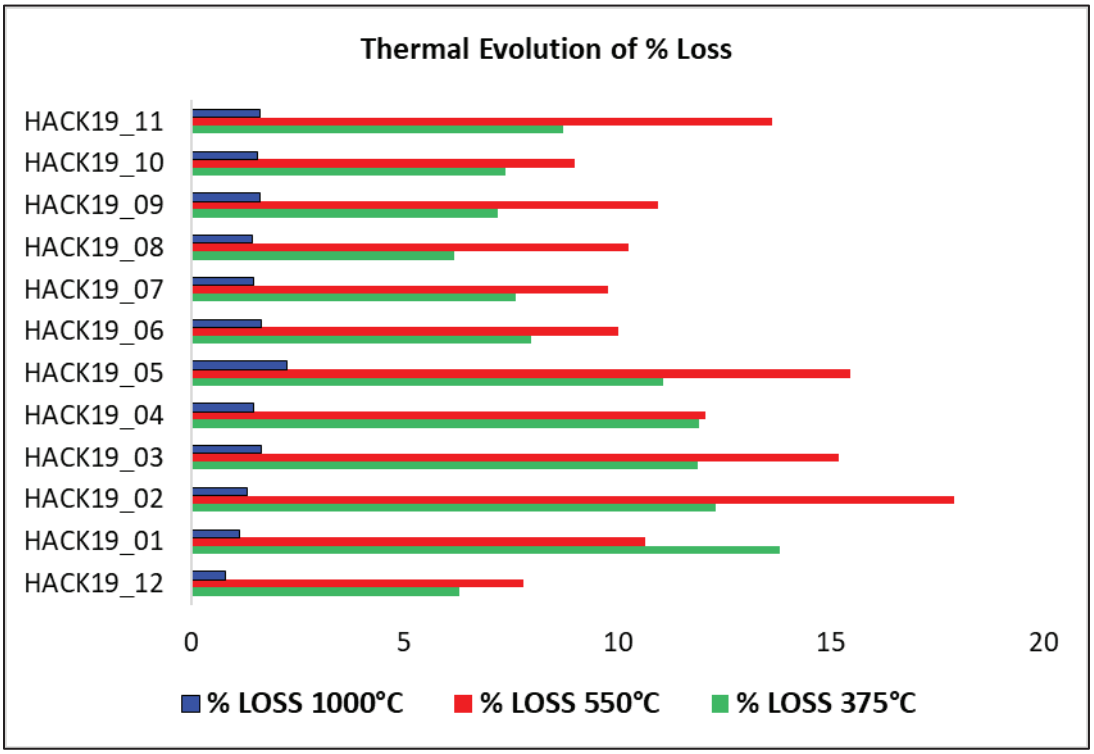

Figure 19. Thermal evolution of % losses at 375 ºC, 550 ºC, and 1000 ºC. Samples are arranged from downstream to upstream. The greatest % of loss occurred at 550 ºC for 4 hours denoted in red. Heating at 375 ºC for 18 hours then followed as denoted by the green graph bars. Lastly, minimal loss (< 2%) is observed at heating of 1000 ºC for 2 hours as observed by the blue graph bars.

3.2.3 Modified Lloyd Kahn BC Results

BC determination via the modified LK method previously described, also originally reported BC concentrations as mg/kg. BC concentrations were below the detection limit in

several samples and are shown as “ND” in the results table. No method detection specifically exists for BC in this application as it was a modified approach and ‘unusual’ request compared to the routine analytical requests associated with environmental testing laboratories such as IAL. The method detection limit for TOC is 1,000 mg/kg (0.01 %) (IAL, 2020). Therefore, it was assumed a similar detection limit of 1,000 mg/kg (0.01 %) would be applicable for ‘ND’ BC concentrations (i.e. HACK19_12). Table 9 summarizes the analytical results of % TOC and % BC using the Kahn (1988) Method and study modification process, denoted as ‘%BC-LK’.

Table 9. % TOC and % BC results using the Kahn (1988) Method for TOC analysis and modified TOC-analysis (% BC-LK). Samples HACK19_05 and HACK19_10 are bolded and shaded to denote the highest reported values of either % TOC (7.13 % - HACK19_05) and % BC (1.56 % - HACK19_10).

Sample ID	% TOC	% BC-LK
HACK19_12	3.90	0.10
HACK19_01	4.39	0.10
HACK19_02	3.68	0.13
HACK19_03	5.88	0.14
HACK19_04	5.51	0.23
HACK19_05	**7.13**	**0.18**
HACK19_06	3.92	0.18
HACK19_07	3.09	0.10
HACK19_08	4.39	0.11
HACK19_09	4.03	0.23
HACK19_10	**2.82**	**1.56**
HACK19_11	3.52	0.13

The outlier is clearly sample HACK19_10 which reported % BC at 1.56 %, a concentration significantly higher than the rest of the samples analyzed. HACK19_10 reported % TOC at 2.82 %, only slighter high then the % BC amount. Sample HACK19_05 instead reported the highest TOC amount at 7.13 % with an accompany BC amount of 0.18 %. The physiochemical

properties of the environment where these samples were located are likely responsible for the relative concentration mentioned.

The TOC and BC results are displayed alongside one another in Figure 20. TOC and BC concentrations appear to follow a similar relative trend of overall distribution, with the reference table bar increasing and slightly retreating as it continues downstream towards rkm 0. HACK19_10 is the main outlier in this data set and is associated with the graph break included on Figure 20 (B).

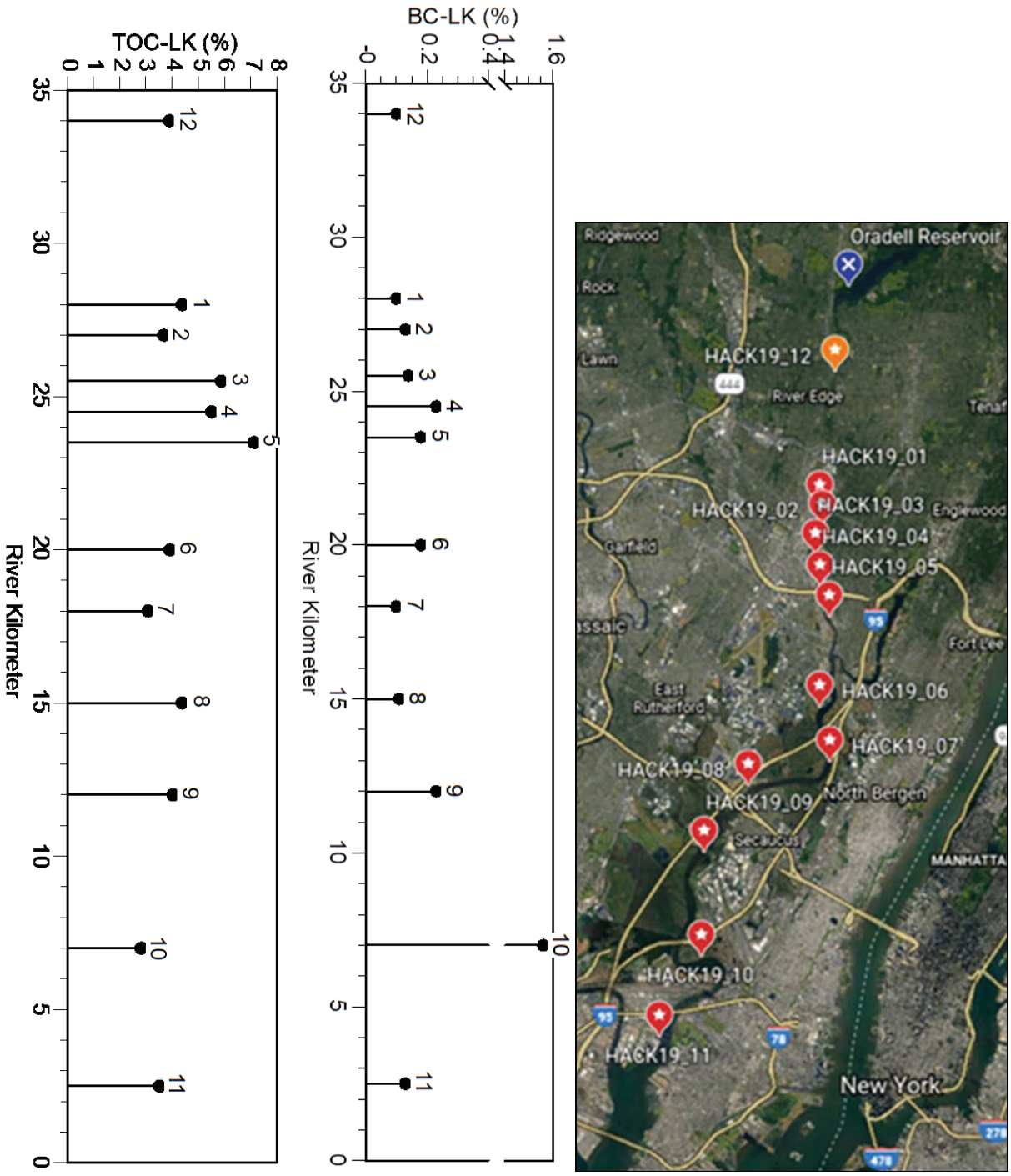

Figure 20. TOC-LK (%) and BC-LK (%) plotted against rkm. HACK19_10 reported the highest BC % at nearly 2 % compared to the other BC amounts of 0.10 % to 0.25 %, thus acting as a bit of an outlier in the sample set. HACK19_10 was collected from the eastern, inner-river bend of the lower industrialized river portion adjacent to the former coal-powered Hudson Generating Station and across the shores of the former Standard Chlorine and Kopper's Coke industries.

3.2.4 EPA PAHs

The PAH results by EPA Method 8270 reported the standard 16 PAH compounds plus one associated with TCL/PAH analysis (Figure 21, Table 10). TCL stands for 'Target Analyte List' and that is exactly what Method 8270 is, a targeted analysis of strictly parent (non-alkylated) PAHs (Emsbo-Mattingly et al., 2001). However, exceptions are made for compounds such as 2-methylnapthalene (2mN). 2mN is often included in regulatory evaluations of EPA PAHs due to its association with refined petroleum products, particularly light distillates (i.e., diesel) for fuel use and energy consumption (e.g., No. 2. Fuel oil for residential/commercial heating) (Stout et al., 2015). 2mN is also a contingent analysis for the evaluation of contaminated soils or groundwater by No.2 fuel oil per NJDEP regulations (NJDEP, 2013).

'Total Target Compounds' is the summation of all individual PAH compounds and is shown below the priority pollutant compounds. Results are reported as mg/kg (dry basis). Non-detects (ND) were reported for several PAH compounds in various samples. The fully analytical report prepared by IAL regarding the results of EPA Method 8270 including full chromatographic profiles and QA/QC procedures is included as Appendix B to this paper.

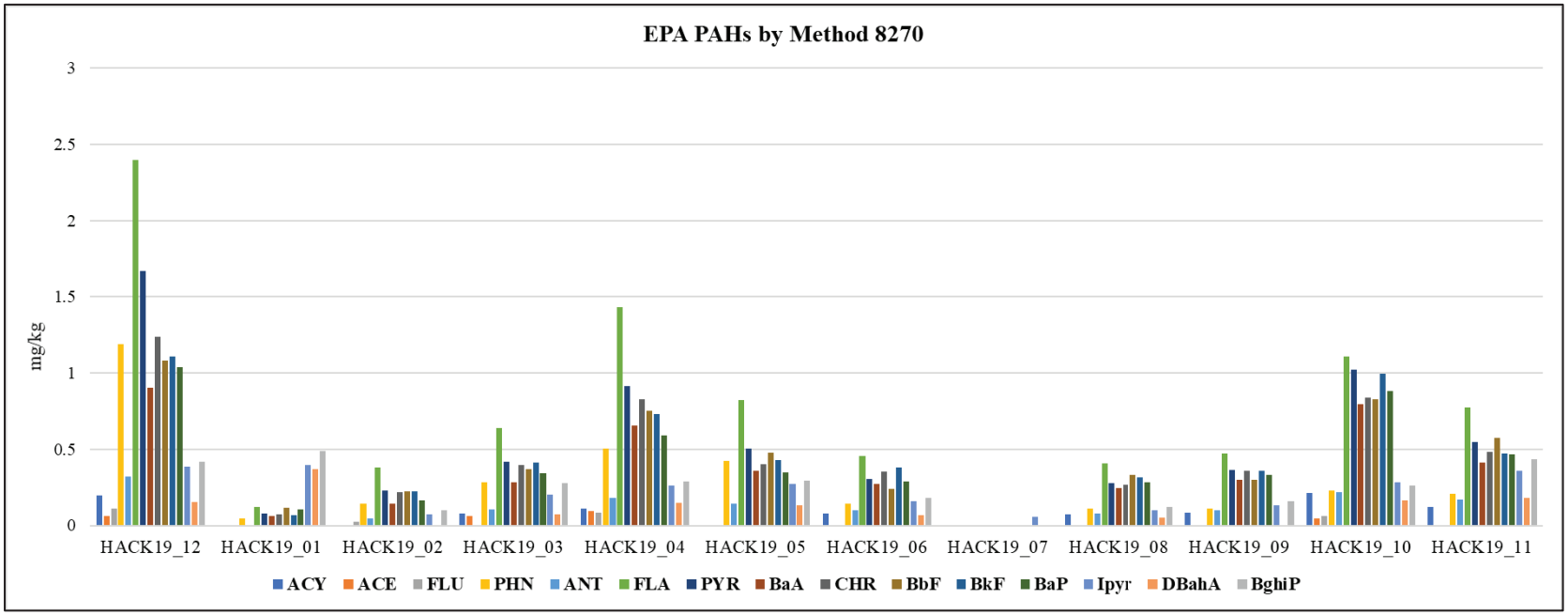

Figure 21. Bar graph distribution of EPA PAHs concentrations (mg/kg) by Method 8270. To avoid skewing the bar graph, lighter PAH compounds (i.e., NAP, 2mNAP) are not included due to their relatively low to ND concentrations. Sample HACK19_12 showed the highest concentrations for EPA PAJs. HACK19_07 barely reported any parent PAHs.

Ring #	EPA - PAHs (mg/kg)	HACK19_01	HACK19_02 (*)	HACK19_03	HACK19_04	HACK19_05	HACK19_06	HACK19_07	HACK19_08	HACK19_09	HACK19_10	HACK19_11	HACK19_12
2	Napthalene (N0) or NAP	ND	ND	ND	ND	ND	ND	ND	0.054	0.056	0.158	0.113	0.056
2*	2-Methylnapthalene (2mN)	ND	ND	ND	ND	ND	ND	ND	ND	ND	0.036	ND	ND
3	Acenaphthylene(ACY)	ND	ND	0.08	0.111	ND	0.08	ND	0.071	0.084	0.214	0.122	0.197
3	Acenaphthene (ACE)	ND	ND	0.063	0.096	ND	ND	ND	ND	ND	0.048	ND	0.064
4	Fluorene (FLU)	ND	0.022	ND	0.081	ND	ND	ND	ND	ND	0.064	ND	0.108
3	Phenanthrene (PHN)	0.045	0.142	0.285	0.502	0.425	0.144	ND	0.108	0.109	0.231	0.208	1.19
3	Anthracene (ANT)	ND	0.048	0.107	0.182	0.141	0.098	ND	0.078	0.098	0.216	0.171	0.322
4	Fluoranthene (FLA)	0.124	0.38	0.641	1.43	0.822	0.457	ND	0.409	0.472	1.11	0.772	2.4
4	Pyrene (PYR)	0.078	0.23	0.42	0.917	0.504	0.306	ND	0.279	0.365	1.02	0.549	1.67
5	Benzo[a]anthracene (BaA)	0.06	0.141	0.284	0.655	0.359	0.274	ND	0.247	0.302	0.793	0.414	0.902
4	Chrysene (CHR)	0.073	0.217	0.399	0.828	0.404	0.353	ND	0.266	0.359	0.839	0.481	1.24
5	Benzo[b]fluoranthene (BbF)	0.114	0.226	0.368	0.752	0.479	0.241	ND	0.334	0.299	0.827	0.572	1.08
5	Benzo[k]fluoranthene (BkF)	0.065	0.226	0.414	0.732	0.428	0.382	ND	0.318	0.357	0.996	0.471	1.11
5	Benzo[a]pyrene (BaP)	0.103	0.162	0.342	0.591	0.348	0.287	ND	0.281	0.331	0.881	0.465	1.04
6	Indeno[1,2,3-cd]pyrene (Ipyr)	0.394	0.074	0.203	0.264	0.275	0.158	0.059	0.102	0.133	0.284	0.361	0.384
5	Dibenz[a,h]anthracene (DBahA)	0.367	ND	0.071	0.15	0.131	0.067	ND	0.052	ND	0.164	0.179	0.153
6	Benzo[g,h,i]perylene (BghiP)	0.488	0.1	0.28	0.287	0.296	0.183	ND	0.119	0.161	0.259	0.434	0.419
	Total Target Compounds (17)	1.91	1.97	3.96	7.58	4.61	3.03	0.059	2.72	3.13	8.14	5.31	12.3
	NAP+2mNAP	0	0	0	0	0	0	0	0.054	0.056	0.194	0.113	0.056
	PHN+ANT+FLA+PYR	0.247	0.8	1.453	3.031	1.892	1.005	0	0.874	1.044	2.577	1.7	5.582

Table 10. EPA PAHs by EPA Method 8270. Quantification of 16 Priority Pollutant PAHs and sum of Total Target Compounds. Associated ring # is included on the left hand-side for reference. The asterisk (*) refers to branched / alkylated structures. Yellow highlighting denotes the highest concentration (mg/kg) for the specific EPA PAH compound. Yellow shading is particularly evident in HACK19_12 for 3+ PAHs. Sum of lighter PAH compounds (i.e., NAP, 2mNAP) and heavier (3+ ring) PAHs are also included.

Sample HACK10_12 reported the highest concentrations of overall EPA PAHs. HACK19_12 was collected in the transitional (freshwater non-tidal to brackish water) upstream area of the river, directly below the River Edge road traffic bridge and adjacent to the River Edge Train Station. HACK19_12 reported the highest concentrations of 3 and 4 ring PAHs (i.e. ACE, PYR, CHR) and several 5 ring PAHs (BbF, BaP). FLA, PYR, BbF and BaP are all useful indicators of pyrogenic source (Uhler et el., 2005). HACK19_12 also reported the highest sum of 3+ ring PAHs or 'ΣPAH'. The highest TIC total was also reported in HACK_12 at 12.3 mg/kg.

HACK19_07 reported the most NDs. The ND concentration does not mean there is zero presence of that specific compound, rather it is too low to be detected by the instrument. Lighter PAH compounds (i.e., NAP and 2mN) had the highest concentration totals in HACK19_10. The highest ANT (3-ring) concentration was also reported in HACK10.

Sample HACK19_01 reported the highest concentrations of pyrogenic 5 and 6 ring PAHs (i.e., Ipyr, DBahA). HACK19_01 also reported ND's for all 2-4 ring PAH compounds. HACK19_04 reported the highest concentrations of PHN and FLA. PHN and its substituted alkyl series (i.e., 1-methylphenanthrene) are abundant in petroleum products and are useful biomarkers for forensic fingerprinting (Olsen, 2014; Wang & Stout, 2007).

The overall distribution of ΣPAHs was investigated against RKM (Figure 22) to investigate the spatial distribution of contaminants and allow for comparison of other compounds of concern. Lighter PAH compounds (i.e., NAP and 2mN) were excluded due to their higher solubility and relatively low concentrations.

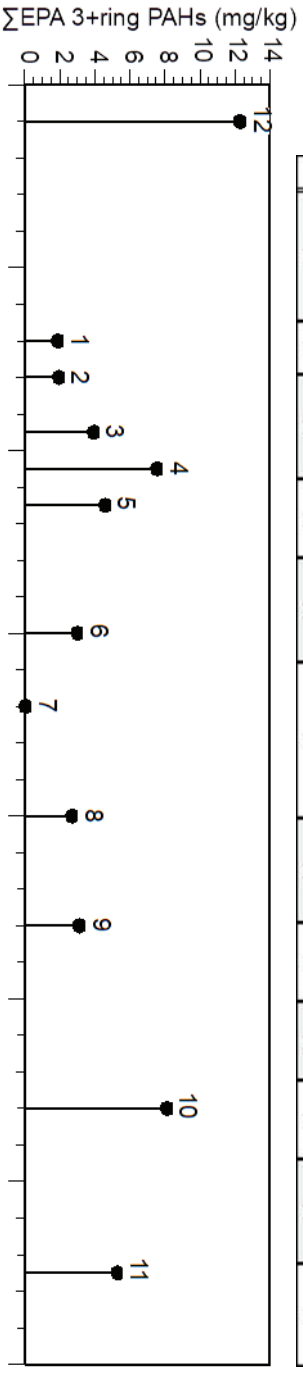

Site ID	River Location	Water depth	Visual Description	Additional Notes
HACK19_12	River Edge Train Station, River Edge NJ	2'	›rown mud, anaerobic	Collected in the upstream non-tidal portion of the River. 2 CSO's located in close proximity to sample.
HACK19_01	Johnson Park, Hackensack NJ	Mudflat	Soft dark brown-grey silty mud.	Hand collection via modified hand auger.
HACK19_02	Foschini Park, Hackensack NJ	Mudflat	Firm dark brown mud with heavy presence of organic fragments.	Hand collection via modified hand auger.
HACK19_03	Formerl Hess Terminal, Bogota NJ	11-12'	Soft, saturated, brownish-grey mud.	Grab collection via Ponar Sampler from boat.
HACK19_04	Below Rt. 80 bridge, Bogota/Ridgefield Park NJ	11-12'	Very soft, saturated, black mud (consistency of mayonnaise).	Slight sheen observed. Grab collection via Ponar Sampler from boat.
HACK19_05	Former Coal Tar (Roofing) Business, Ridgefield Park NJ	12'	Soft, saturated, black mud with thin brown surface layer, organic & inorganic fragments.	Heavy commercial area (i.e. junkyards, construction-related businesses). Grab collection via Ponar Sampler from boat.
HACK19_06	Bergen County Sewage Comission, Little Ferry NJ	8'	Soft, saturated, black mud with many phragmites stalks, anerobic odor.	Grab collection via Ponar Sampler from boat.
HACK19_07	Mouth of Bellmans Creek, North Bergen	5'	Black-brownish-grey peat, some clay, mostly roots.	Grab collection via Ponar Sampler from boat.
HACK19_08	Meadowlands Sport Complex, East Rutherford NJ	9'	Soft, greyish-brown mud (consistency of mayonnaise).	Grab collection via Ponar Sampler from boat.
HACK19_09	Anderson Creek Marsh, Secaucus NJ	9'	Soft, brownish black mud, with organic fragments mixed in.	Grab collection via Ponar Sampler from boat.
HACK19_10	Malanka Landfill (River Bend Marsh), Secaucus NJ	12'	Blackish-brown clay, compact, very gravelly, with HF fragments.	Also, adjacent to the former PSE&G Hudson Generating Coal Plant, Jersey City NJ
HACK19_11	Former Ship Bldg Facility, now Kearny Point, Kearny NJ	15'	Brownish-black soft mud, also gravely with staining and misc. pieces of HF.	Grab collection via Ponar Sampler from boat.

Figure 22. ΣPAH (mg/kg) study site distribution. Sample summary table is included for site specifics.

The use of alkylated isomer compounds in forensic fingerprinting is due to the relative strength of the compounds against biodegradation and other physical processes compared to their parent compound. However, the limited focus on Method 8270 on parent compounds, excluding other compound groups (i.e., petroleum biomarkers) can arguably be outweighed by the increased instrument sensitivity associated with analytical method 8270. Figure 22 is an example of internal IAL calibration peaks and extractable compounds identified for HACK19_03.

INTEGRATED ANALYTICAL LABORATORIES, LLC

Quantitation Report (QT Reviewed)

Data Path : C:\msdchem\1\data\19-11-08C\
Data File : C7410.D
Acq On : 8 Nov 2019 18:57
Operator : EDM
Sample : HACK_19-,E19-07990-005,Xs,15.1g,67.5,0.5
Misc : 191106-01,11/06/19,10/28/19,1
ALS Vial : 32 Sample Multiplier: 1

Quant Time: Nov 11 11:16:17 2019
Quant Method : C:\MSDCHEM\1\METHODS\CS2919.M
Quant Title : BNA CALIBRATION METHOD
QLast Update : Fri Nov 08 08:29:50 2019
Response via : Initial Calibration

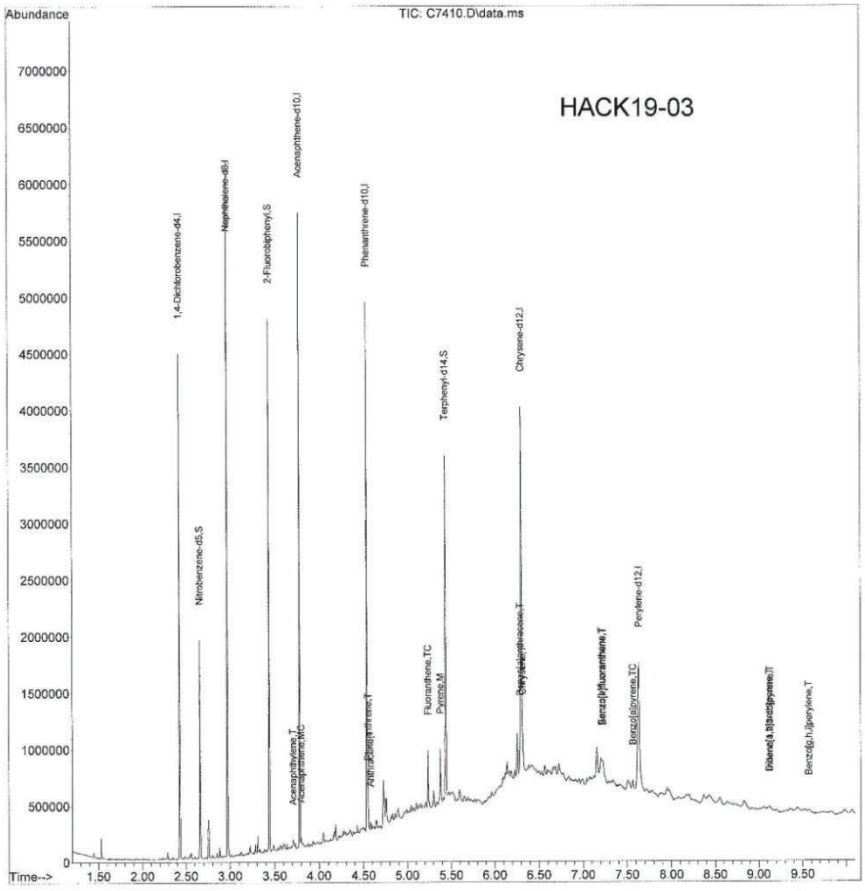

CS2919.M Mon Dec 02 14:25:42 2019 MSDC Page: 2

Figure 23. EPA Method 8270 example of IAL's internal calibration peaks for sample HACK19_03. Standards are labeled adjacent to their associated peaks. Target PAH compounds appear as the smaller peaks. All other compounds are excluded from characterization.

3.2.5 Pyrolysis PAHs

A single analytical Py-GC-MS run at high temperature heating (e.g., 610 ºC) allowed for closer inspection and characterization of individual carbon compounds and different isomer assemblages of various pyrolysis artifacts in conjunction with EPA Method 8270 (Lara-Gonzalo et al., 2015; Kruge et al., 2015; 2018; 2020; Hagmann et al., 2019). Pyrolysis PAH (pyro-PAHs) results were normalized using pyrolytic toluene raw counts and reported as corrected peak area counts / ng dry sediment.

Py-GC-MS study results include quantification of PAHs beyond the standard EPA PAHs (n = 16), including identification and relative abundance of alkylated PAH homologues associated with various biogenic, petrogenic and pyrogenic origin sources (Emsbo-Mattingly et al., 2001; Kruge et al., 2008). Information regarding alkylated homologues and other biomarkers can be qualitatively and quantitatively investigated by first examining the chromatic signatures present and their relative abundance.

Raw pyrolytic data is displayed in the form of a chromatographic profile (Figure 24) to allow for quick identification of certain known assemblages. Initial quantification efforts focused on interpretation of detected compounds and followed by comparison against library mass spectra of known compounds (Section 2.5.4).

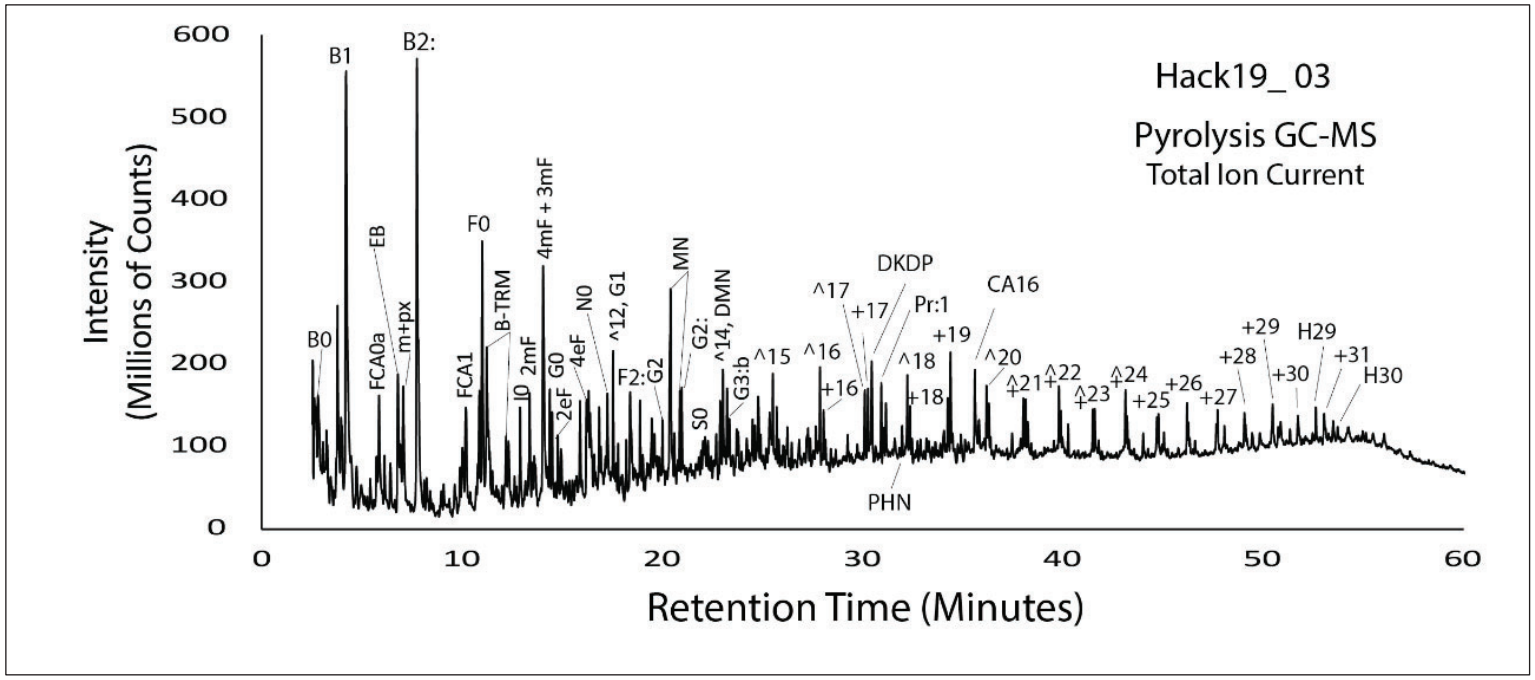

Figure 24. Py-GC-MS total ion current chromatograph for HACK19_03. Structural information can be determined by utilizing associated MS software to screen and display fingerprints of forensically useful compounds such as petroleum biomarkers or terrestrial plant biomarkers (Kruge, 2015). Peak identification of compounds shown is included in Appendix A. Each target compound was monitored for its parent and alkyl homologue (Uhler et al., 2005).

Figure 24 in contrast to Figure 23 includes the identification of numerous more compounds including aliphatic, aromatic, diagenetic and petroleum-related biomarkers. Most of these were entirely excluded from classification in Figure 23.

Py-GC-MS analysis also included quantification of identifiable EPA PAHs summarized in Table 11.

Pyro- PAHs	HACK19_12	HACK19_01	HACK19_02	HACK19_03	HACK19_04	HACK19_05	HACK19_06	HACK19_07	HACK19_08	HACK19_09	HACK19_10	HACK19_11
NAP	327.5	238.8	375.2	652.9	559.5	741.7	146.3	199.8	327.8	354.7	391.6	392.6
2mNAP	311.4	215.7	382.6	660.8	567.6	703.2	432.4	197.7	283.2	332.5	235.6	384.7
1mN	293.2	156.6	331.2	711.8	541.1	690.5	541.2	157.2	258.0	294.0	144.5	325.0
PHN	143.8	40.0	79.1	160.0	160.4	129.4	92.0	33.0	56.1	78.3	42.5	77.5
ANT	89.6	10.9	42.6	72.3	67.4	60.8	54.6	9.3	34.6	40.3	13.1	51.6
FLA	176.1	11.2	71.1	111.7	157.1	109.4	86.5	6.3	65.2	82.4	110.2	83.0
PYR	127.6	7.5	48.2	84.2	99.1	67.9	58.4	5.7	39.3	54.3	142.0	59.1
RET	62.6	3.5	24.6	186.7	108.2	134.2	122.3	80.8	53.5	49.8	24.9	98.0
NAP+2mNAP	638.9	454.5	757.8	1313.7	1127.2	1444.9	578.7	397.5	611.0	687.3	627.2	777.3
PHN+ANT+FLA+PYR	537.0	69.6	241.0	428.2	484.0	367.4	291.5	54.3	195.2	255.3	307.8	271.1

Table 11. Py-GC-MS results for parent PAHs. Results were determined as corrected peak area counts / ng dry sediment. Red shading signifies the highest concentration amounts for compounds identified. Sum of lighter PAH compounds and heavier ring PAH compounds are included.

Lighter PAH compounds (e.g., NAP and 2mNAP) were reported at the highest concentrations in sample HACK19_05. These compounds were reported as ND for EPA PAH methods results (Table 10). ANT and FLA (pyrogenic indicators) reported the highest amounts in HACK19_12, consistent with the EPA PAH results for HACK19_12. HACK_10 reported the highest PYR (pyrogenic indicator) amount, contrasting that of EPA PAH results which reported the highest PYR in sample HACK19_12. Retene (RET) a wood smoke indicator detected the highest total in HACK19_03. PHN (petroleum indicator) compounds were greatest in HACK19_04, consistent with EPA PAH results.

The quickest way to interpret and analysis pyro-PAH results is either via the sample-specific chromatograms or histograms of specific compounds and associated isomers. Bar graphs are also applicable for quick visual interpretation of overall PAH distribution. Figure 25 illustrates the overall distribution of lighter pyro-PAHs (Fig 25-A) and heavier pyro-PAHs (Fig 25-B).

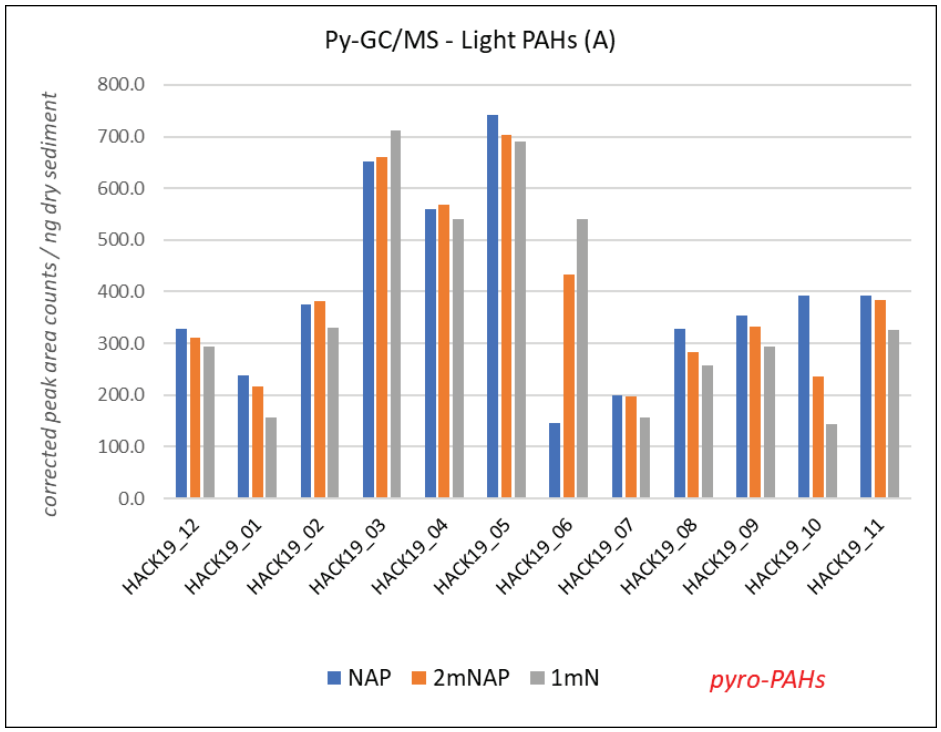

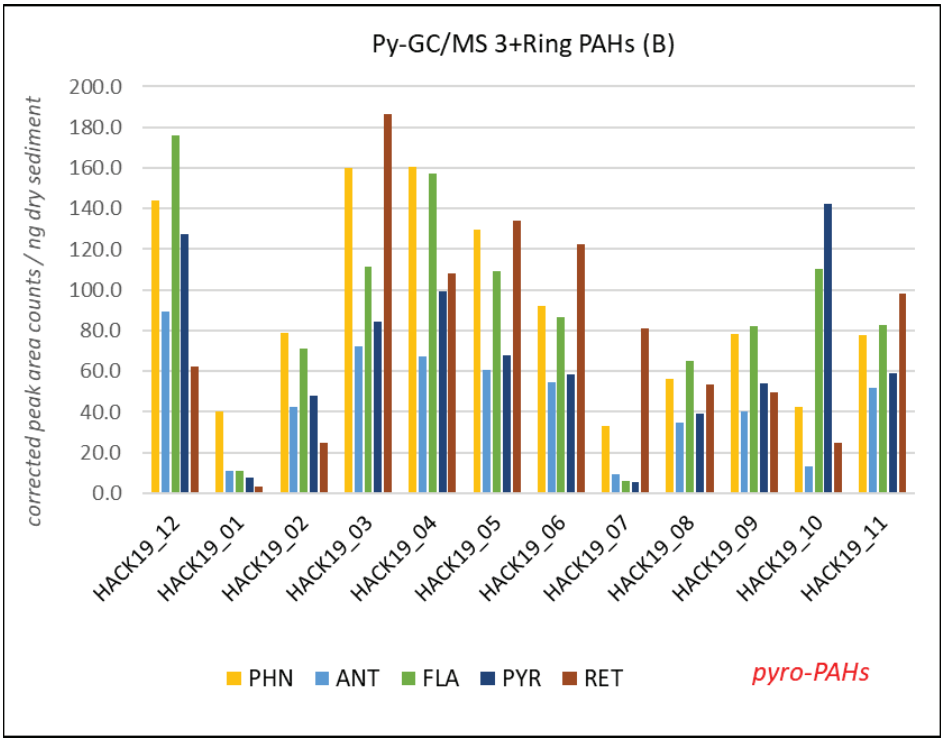

Figure 25. Bar-graph distributions of light (2 ring) PAHs (A) and heavy (3+ ring) PAHs (B) using Py-GC-MS. Lighter PAHs were concentrated in the upper to middle river sample sites (e.g.,

HACK19_03, -04, and -05), dropping off at HACK19_07 before rising in downstream sample HACK19_11.

Characterization of all liberated and detectable hydrocarbon compounds combined with the quick interpretation time demonstrate the advantages of using Py-GC-MS in sediment characterization studies. The disadvantages include the potential creation of additional pyrolytic compounds which are typically excluded from detection in Method 8270. TOC is a known indicator of certain pollutants (i.e., heavy metals & PAHs) (Agarwal and Bucheli (2011); Konsevick and Bragin (2010). TOC results were evaluated again pyrolytic toluene concentrations and revealed a moderately strong ($R^2 = 0.592$) positive linear relationship (Figure 26).

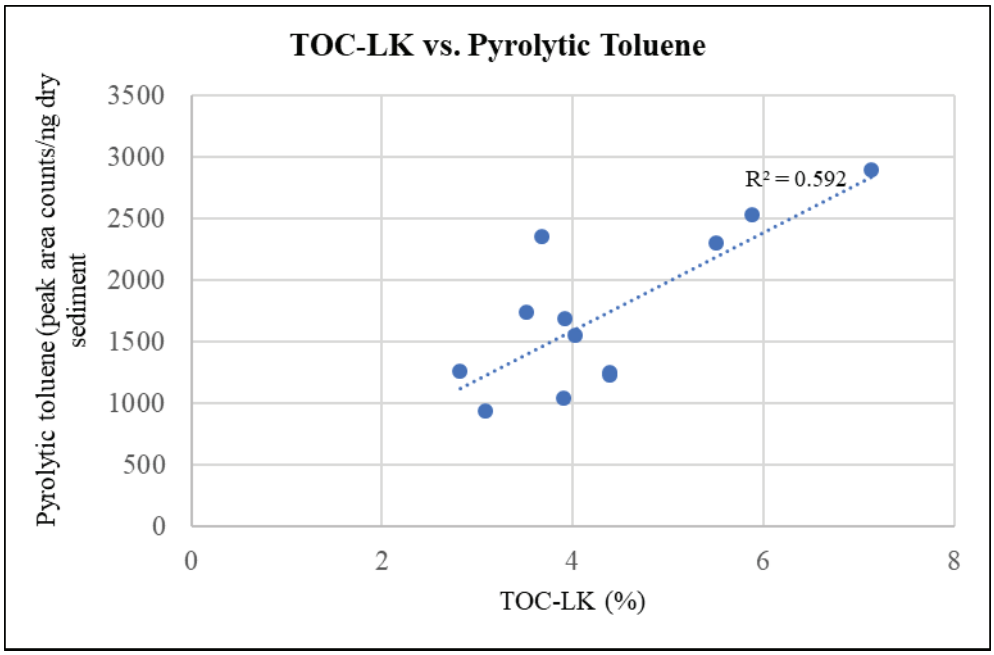

Figure 26. TOC-LK (%) vs Pyrolytic Toluene. Moderately strong, positive linear relationship exists between TOC and pyrolytic toluene results.

EPA PAH and Py-GC-MS ΣPAH and NAP+ 2mNAP results were also compared against one another for method evaluation purposes (Figure 27).

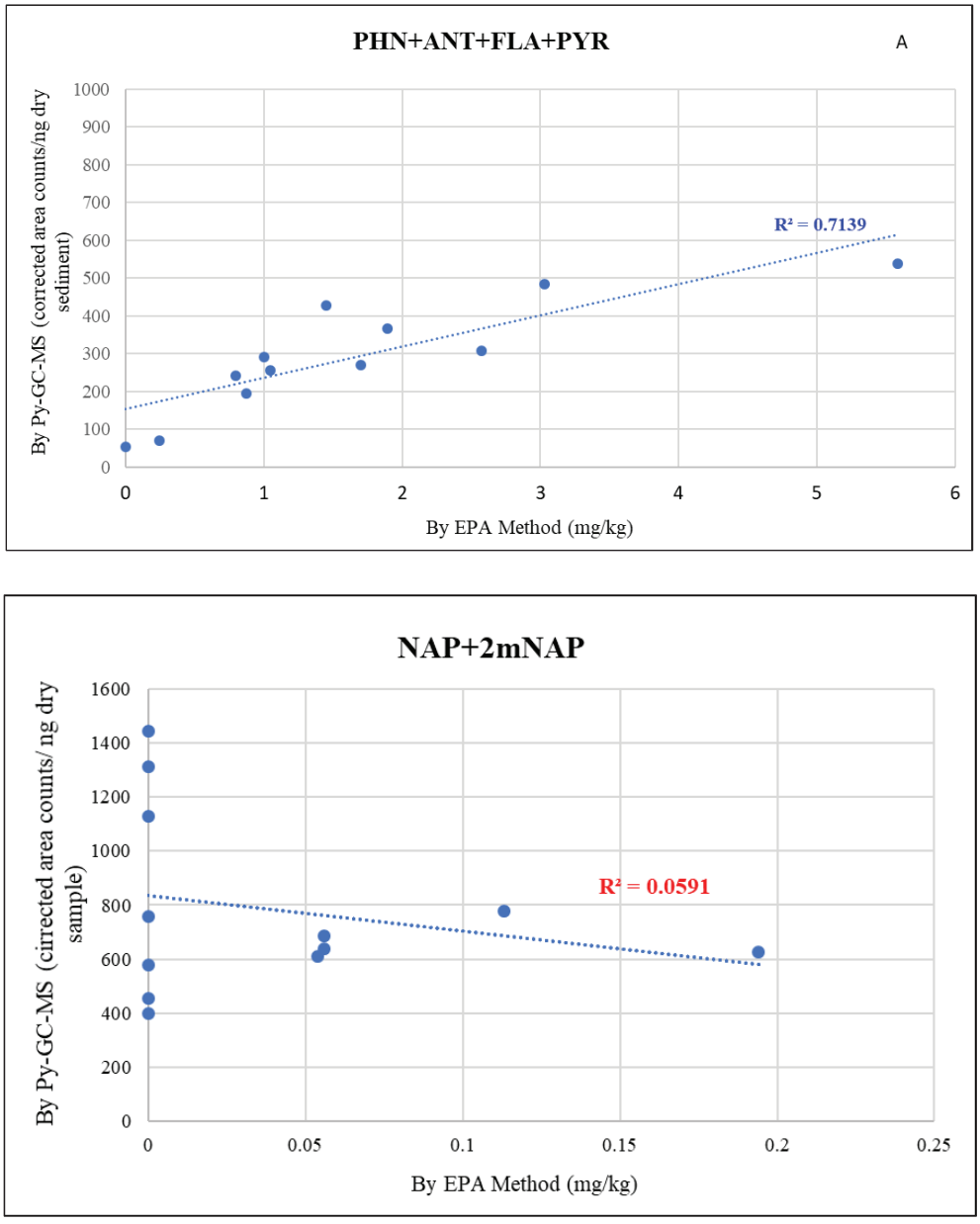

Figure 27. Priority PAH method results comparison using Py-GC-MS and EPA Methods. Fig.27-A shows the strong linear positive relationship observed for ΣPAH compounds. Fig. 27-B shows the weak negative relationship for lighter NAP and 2mNAP compounds.

Py-GC-MS and EPA 8270 results showed a strong positive linear relationship for 3+ ring PAH compounds as shown by the R^2 value of 0.7319. No significant relationship was observed for lighter PAH compounds however as reflected by the R^2 value of 0.0591. Similar results were also observed in a sediment characterization study involving the Passaic River by Olsen (2014) and Bujalski (2010).

3.2.6 Biomarkers & Chemical Signatures – Investigation Results

Parent or 'EPA PAH' compounds and various hydrocarbon assemblages were evaluated to distinguish between the various low-level pyrolytic extractable peaks emitted during Py-GC-MS analysis and assist with diagnostic ratios and source analyses (Kruge, 2015). Various carbon compounds, from aliphatic hydrocarbons (normal alkanes) to isoprenoid hydrocarbons (biomass markers), to hopanes (petroleum biomarkers), to various phenols (lignin pyrolysis markers) and so on were evaluated. Figure 28 shows the chromatographic profile of petroleum biomarkers (i.e., tricyclic terpanes and hopanes for sample HACK19_03. Complete pyro-chromatograms for all study samples are included as Appendix A to this paper.

Pyrogenic and petrogenic source determinations were ultimately determined via the use of PHN series (parent and alkyl-substitutions) results (Figure 29). PHN series results were also used for diagnostic source evaluation involving a simple ratio of series components (Figure 30). PHN is associated with both petrogenic and pyrogenic sources, thus acting as a 'mixed-source' (Emsbo-Mattingly et a., 2001). By assigning values to the ratio one can differentiate between the likely petro or pyro influence. The sum of all dimethylphenanthrenes is denoted as PHN2. PHN denotes the parent phenanthrene. The index ratio was calculated using the following ratio:

PHN2/ (PHN+PHN2). Petrogenic influence is classified as > 0.6 and pyrogenic < 0.6 (Kruge et al., 2018).

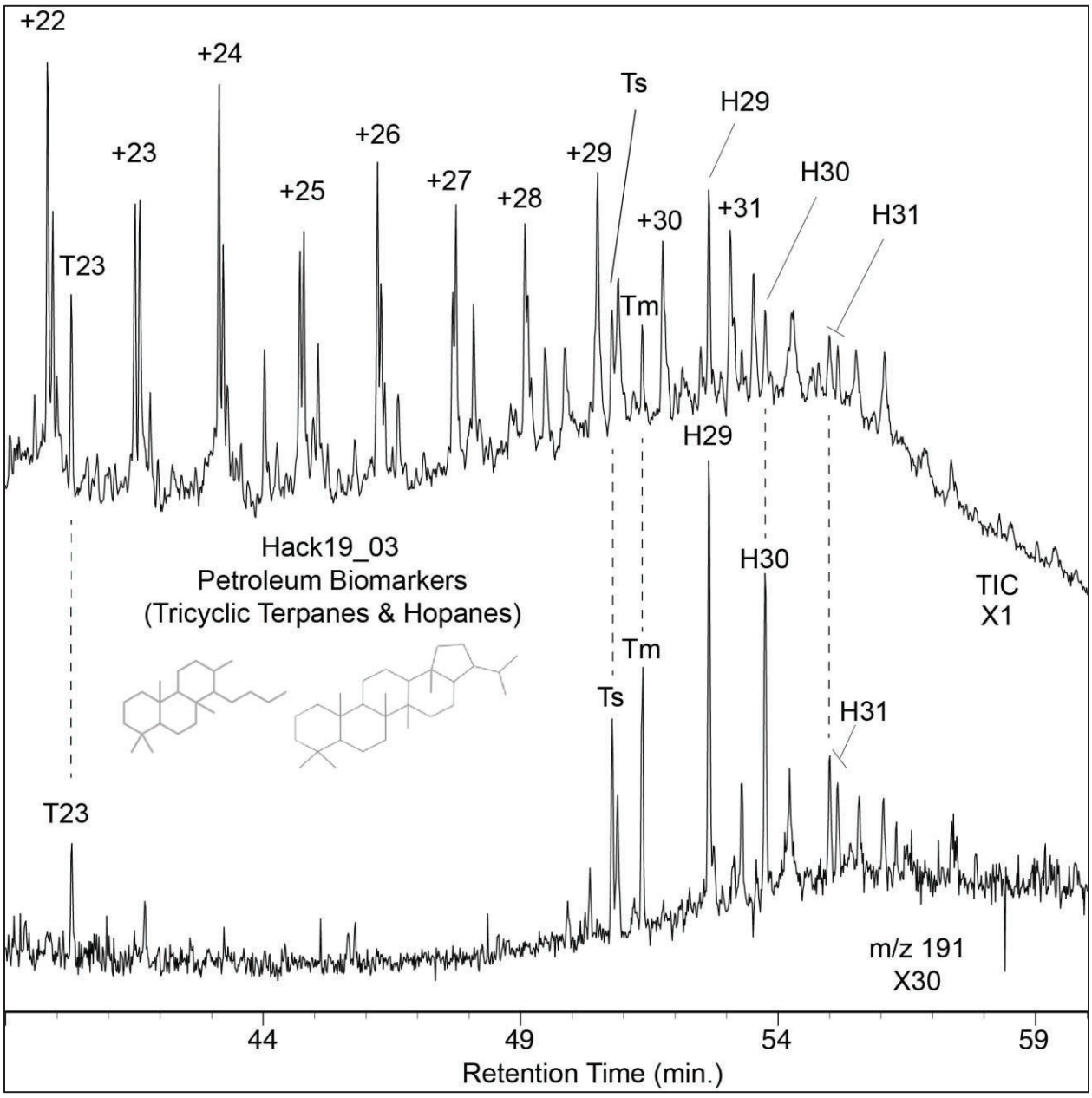

Figure 28. Chromatographic reference of petroleum biomarkers in HACK19_03. Forensically useful compounds such as tricyclic terpanes and hopanes (aka petroleum biomarkers) were evaluated as part of the environmental forensics of study samples.

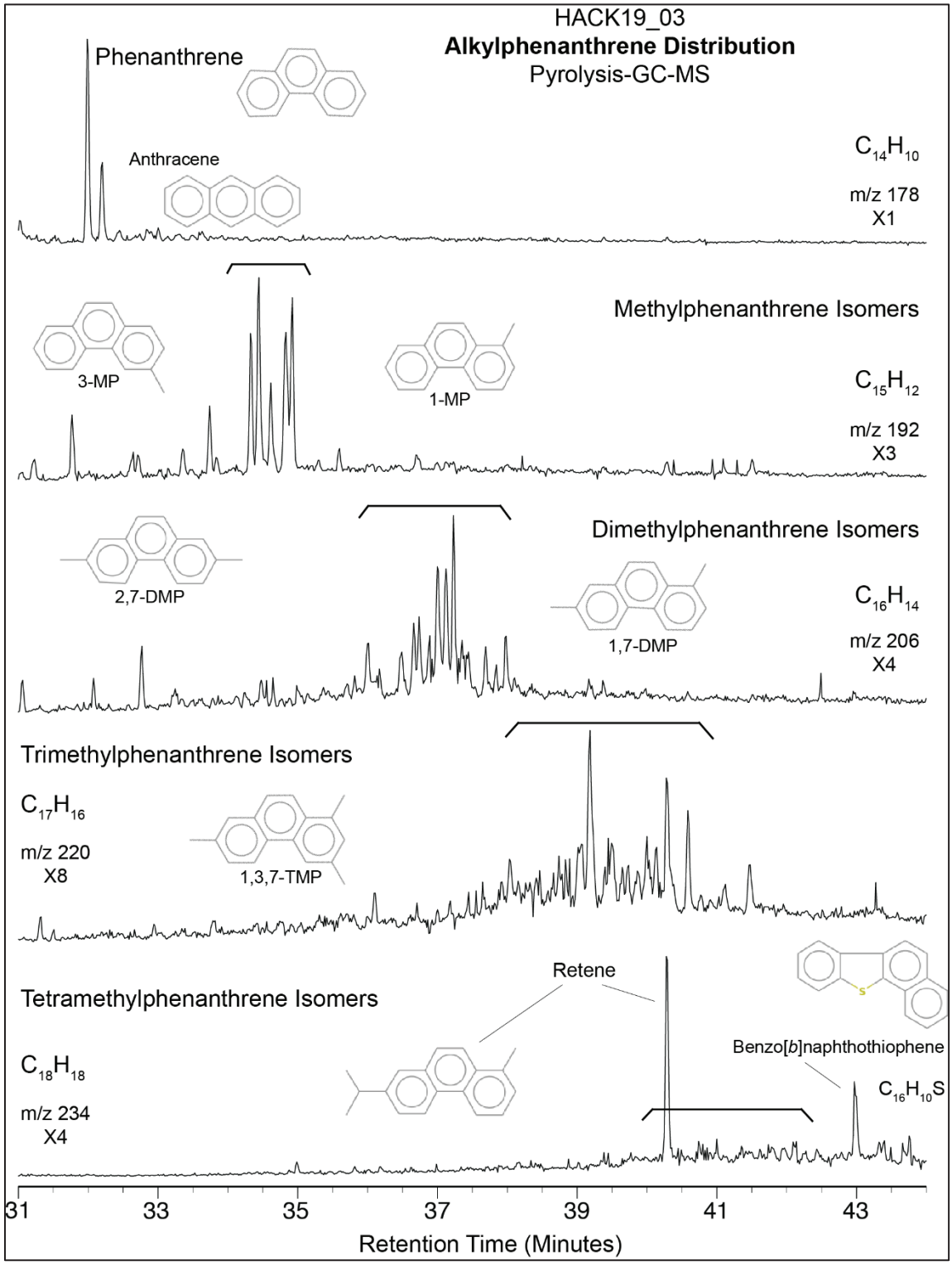

Figure 29. Py-GC-MS Alkylphenanthrene distribution (petroleum biomarkers).

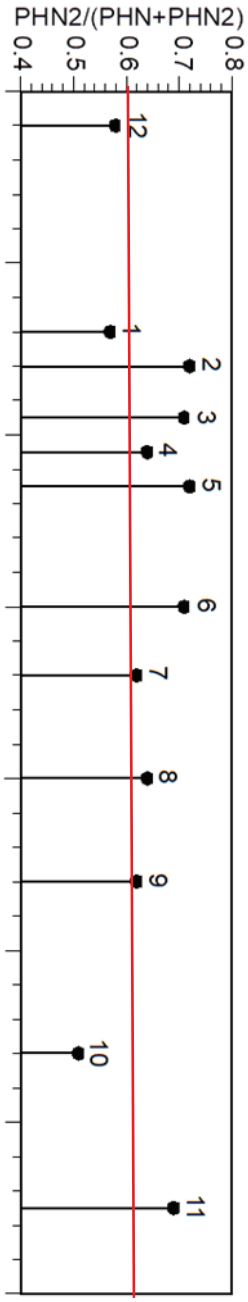

Site ID	River Location	Water depth	Visual Description	Additional Notes
HACK19_12	River Edge Train Station, River Edge NJ	2'	›rown mud, anaerobic	Collected in the upstream non-tidal portion of the River. 2 CSO's located in close proximity to sample.
HACK19_01	Johnson Park, Hackensack NJ	Mudflat	Soft dark brown-grey silty mud.	Hand collection via modified hand auger.
HACK19_02	Foschini Park, Hackensack NJ	Mudflat	Firm dark brown mud with heavy presence of organic fragments.	Hand collection via modified hand auger.
HACK19_03	Formerl Hess Terminal, Bogota NJ	11-12'	Soft, saturated, brownish-grey mud.	Grab collection via Ponar Sampler from boat.
HACK19_04	Below Rt. 80 bridge, Bogota/Ridgefield Park NJ	11-12'	Very soft, saturated, black mud (consistency of mayonnaise).	Slight sheen observed. Grab collection via Ponar Sampler from boat.
HACK19_05	Former Coal Tar (Roofing) Business, Ridgefield Park NJ	12'	Soft, saturated, black mud with thin brown surface layer, organic & inorganic fragments.	Heavy commercial area (i.e. junkyards, construction-related businesses). Grab collection via Ponar Sampler from boat.
HACK19_06	Bergen County Sewage Comission, Little Ferry NJ	8'	Soft, saturated, black mud with many phragmites stalks, anerobic odor.	Grab collection via Ponar Sampler from boat.
HACK19_07	Mouth of Bellmans Creek, North Bergen	5'	Black-brownish-grey peat, some clay, mostly roots.	Grab collection via Ponar Sampler from boat.
HACK19_08	Meadowlands Sport Complex, East Rutherford NJ	9'	Soft, greyish-brown mud (consistency of mayonnaise).	Grab collection via Ponar Sampler from boat.
HACK19_09	Anderson Creek Marsh, Secaucus NJ	9'	Soft, brownish black mud, with organic fragments mixed in.	Grab collection via Ponar Sampler from boat.
HACK19_10	Malanka Landfill (River Bend Marsh), Secaucus NJ	12'	Blackish-brown clay, compact, very gravelly, with HF fragments.	Also, adjacent to the former PSE&G Hudson Generating Coal Plant, Jersey City NJ
HACK19_11	Former Ship Bldg Facility, now Kearny Point, Kearny NJ	15'	Brownish-black soft mud, also gravely with staining and misc. pieces of HF.	Grab collection via Ponar Sampler from boat.

Figure 30. PHN diagnostic source ratio (PHN2/(PHN+PHN2) for petrogenic (< 0.6) and pyrogenic (> 0.6) source identification. Ratio calculations are plotted against rkm with sample specific information include to the right. The red line is placed at the 0.6 mark for reference. Samples HACK19_12, HACK19_01 and HACK 19_10 are indicative of pyrogenic origins.

The results of the PHN/(PHN+PN2) ratio showed a predominance of petrogenic influences. However, the results also pointed to pyrogenic sources in three of the samples (HACK_12, HACK19_01 and HACK19_10. HACK19_07 is marginally over the threshold of 0.6, as is HACK19_09.

The PHN series is often included in diagnostic source ratios due to its relative thermal stability and because PHN is a gas-phase PAH, it is suitable for investigations regarding atmospheric deposition of various fine particulates (i.e., sooty BC) (Tobiszewski et al., 2012). Sample HACK19_10 reported the lowest series ratio value, just marginally above 0.5, as compared to the HACK19_12 and HACK19_01 values which are closer to 0.6. HACK19_10 was collected along the inner shores of regulated landfill (Malanka Landfill) and former coal burning power station (Hudson Generating Station). HACK19_12 was collected in the upstream non-tidal / tidal interface area, adjacent to a commuter train station and in proximity to several combined sewer outflows. Lastly, HACK19_01 was collected from the inner mud banks adjacent to public parks.

Petrogenic source values are most obvious in upper-to-middle-river portions (i.e., HACK19_02, HACK19_03 and HACK19_05). Petrogenic source values then drop at HACK19_07, hovering just over 0.6 threshold before dropping to HACK19_10 and then sharply increasing in HACK19_11. HACK19_11 was collected from the shores of a former boat manufacturing facility now known as ‘Kearny Point’. A noticeable drop was also observed in sample HACK19_04 which was collected from underneath the route 80 bridge. HACK19_03 and HACK19_04 were collected along the shores of former petroleum related industries (i.e., former tank terminals).

Plant and marine biomarkers were also included as part of the environmental forensics of this study. The Vinylguaiacol Indole Index, commonly referred to as the 'VGII Index' or 'Veggie Index', is a recent analytical forensics parameter employing Py-GC/MS data to differentiate between the various organic forms and the processes in which lead to their deposition (Kruge, 2015). VG is a lignin marker and I is often used to represent microalgae.

The VGI Index is calculated as the ratio of vinylguaiacol (VG) to the sum VG plus indole (I) (i.e.VG/(VG+I)) using the m/z 117 and m/z 150 counts only (Kruge, 2015).

The VGII index assess the relative contributions of terrestrial and aquatic matter to sediments on a scale of 0 to 1(Kruge, 2015). Organic inputs from microbes are synonymous with very low VGII values (i.e., 0.01), while terrestrial organic inputs are more indicative of values in excess of 0.5 (Kruge, 2015). A previous Newark Bay sediments study (Kruge, 2015) revealed predominance of aquatic organic inputs with VGII values of 0.34, while a terrestrial organic predominance was observed several km upstream in a Passaic riverbank sample. The Passaic River runs parallel to the Lower Hackensack River. The two rivers join at the mouth of Newark Bay.

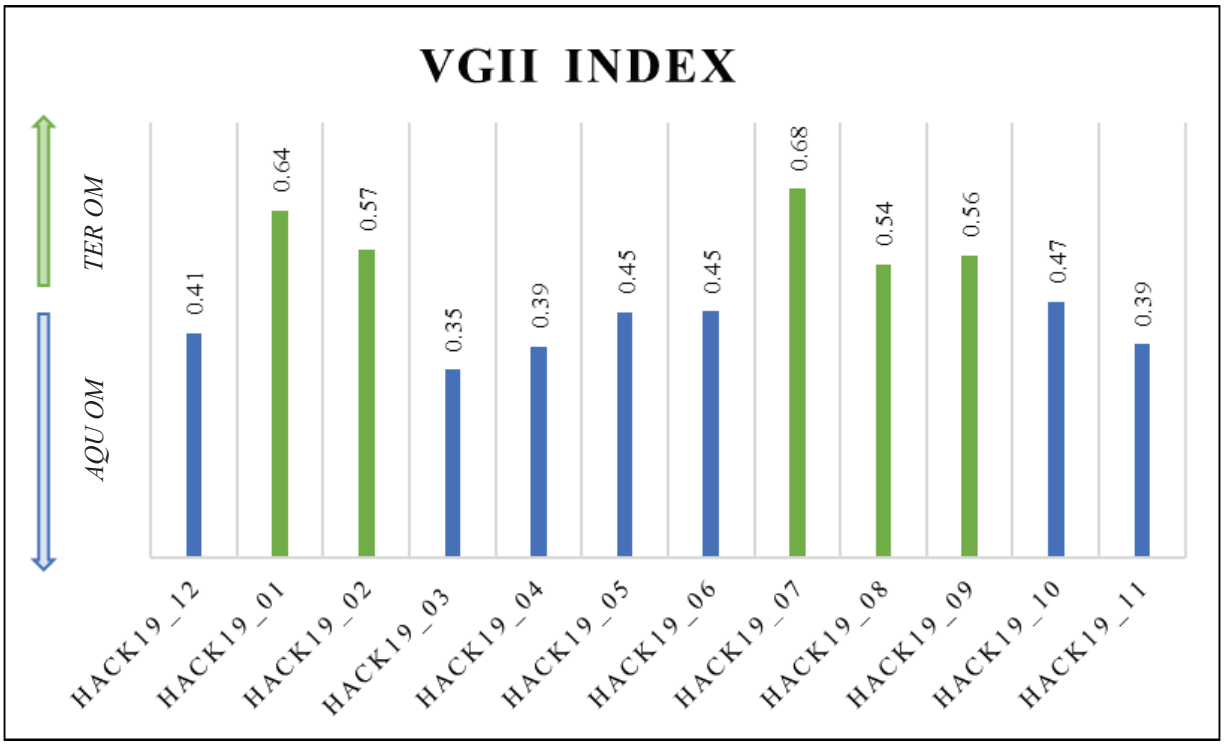

Figure 31. VGII Index for Sediments. The VGI Index is calculated as the ratio of vinylguaiacol (VG) to the sum VG plus indole (I) (i.e.VG/(VG+I)) using the m/z 117 and m/z 150 counts only (Kruge, 2015). The ratio is based on a scale of 0 to 1, with 0.5 being the common threshold limit (Kruge, 2015). Blue shading indicated aquatic carbon preference and green shading to signify terrestrial source inputs.

Samples HACK19_08 and HACK19_09 both have VGII values in excess of 0.5, at 0.54 and 0.56, lending to higher terrestrial organic input. Additionally, both samples were collected at the interface of the mid-to-lower river portions (Table 1), with HACK19_08 collected approximately 15 km north of the mouth of Newark Bay (Figure 10). VGI values began to drop after HACK19_09, with the furthest downstream sample (HACK19_11) revealing a VGII value of 0.39. HACK19_07 revealed the highest VGII value at 0.68, which was fairly expected as the sample was collected at the mouth of Bellman's Creek in North Bergen (rkm 18). The sediment collected for HACK19_07 had various pieces of vegetation intermixed the saturated, silty material. Further, a thin brown silty-sand layer was observed atop the underlying anoxic grey

organic layer. HACK19_03 revealed the lowest VGII value at 0.35, indicative a predominance of aquatic organic material (Kruge, 2015). HACK19_03 was collected adjacent to the former Hess Oil Terminal in Bogota.

Further evaluation regarding likely carbon inputs was also accomplished through environmental fingerprinting of Py-GC-MS data. For example, characterization regarding natural biogenic carbon sources was accomplished by evaluating the overall distribution of normal hydrocarbons or 'alkanes' (Uhler et al., 2005). Odd over even carbon predominance (OEP) usually points to biogenic sources in the form of plant waxes (Uhler et al., 2005). Figure 32 illustrates the OEP observed in HACK19_03 near C22-C35.

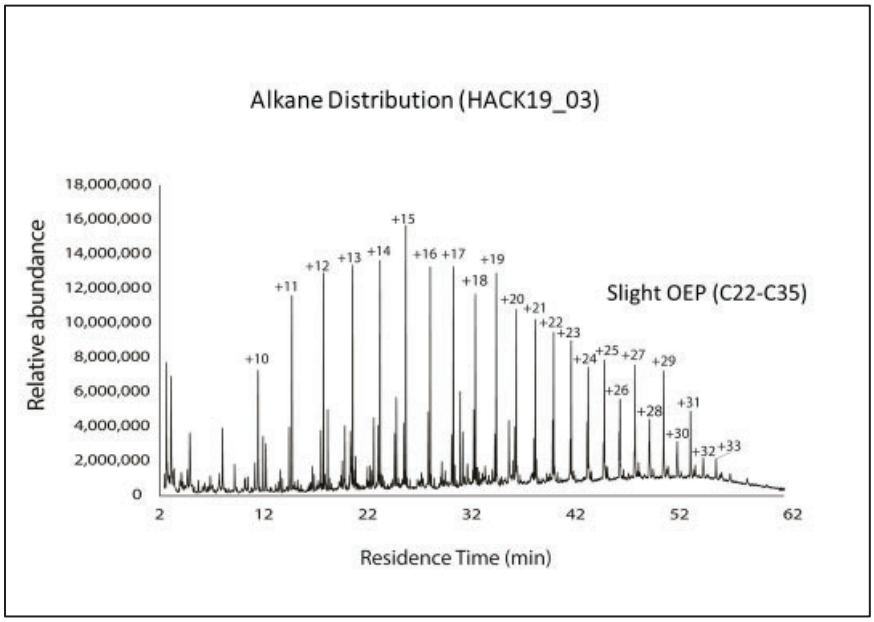

Figure 32. Alkane distribution (m/z 91) for HACK19_03. Slight OEP observed in the C22-C35 range.

3.3 ICP-MS Metals Results

3.3.1 Major Elemental Oxides

ICP-MS analysis for major elements (Si, Al, Fe, K, Na, Mg, Ca, Ti, P and Mn) are reported as normalized percentages of their oxides. SiO_2 is the main major elemental oxide reported, with totals consistently reported in excess of 65 %. Al_2O_3 and FeO_3 are observed as the second and third most prevalent major elemental oxide measured. Table 11 summarizes the full ICP-MS results for major elemental oxides. Cells shaded in light green are to signify concentrations of interest. For example, background sample HACK19_12, reported the highest concentration for MnO and lowest concentration of Fe_2O_3, likely due to the overall organic-rich matrix of the sample site. Sample HACK19_04 reported the highest concentration of CaO.

Table 12. ICP-MS, Major Elements (%'s). Total amounts are reported as normalized percentages of their respective oxides. Triplicate runs were averaged to determine sample averages.

ICP-MS - MAJOR	01 Avg.	02 Avg.	03 Avg.	04 Avg.	05 Avg.	06 Avg.	07 Avg.	08 Avg.	09 Avg.	10 Avg.	11 Avg.	12 Avg.
SiO2	72.57	71.88	67.72	71.22	67.95	72.93	70.29	70.64	70.41	67.12	66.60	77.16
Al2O3	14.31	14.08	15.35	13.38	15.53	12.60	15.19	14.47	14.48	17.18	15.19	11.92
Fe2O3	5.24	6.25	7.18	5.33	7.42	5.87	6.27	6.18	6.28	7.14	7.63	4.23
K2O	2.40	2.29	2.48	2.15	2.50	2.59	2.77	2.54	2.55	2.52	2.87	1.87
Na2O	1.72	1.70	1.72	1.93	1.79	1.76	1.77	1.90	2.01	1.76	2.33	1.53
MgO	1.63	1.56	2.03	1.77	2.01	1.68	1.84	1.86	1.83	1.59	2.44	1.02
CaO	1.05	1.05	1.65	3.02	1.32	1.28	0.76	1.15	1.21	1.36	1.39	1.10
TiO2	0.83	0.81	0.85	0.72	0.86	0.78	0.87	0.86	0.85	1.01	0.88	0.63
P2O5	0.20	0.32	0.90	0.41	0.53	0.44	0.17	0.33	0.32	0.27	0.55	0.42
MnO	0.06	0.06	0.12	0.07	0.08	0.07	0.06	0.07	0.07	0.06	0.11	0.12

3.3.2 ICP-MS Trace Elements (Metals of Concern)

A sub-set of ICP-MS trace elements were evaluated for characterization purposes including vanadium (V), chromium (Cr), cobalt (Co), nickel (Ni) and lead (Pb). These metals were chosen based on previous sediment studies such as Konsevick & Bragin (2010), Weis et al.

(2005), Miskewitz et al. (2005), and the 2016 final expanded site investigation of the Lower Hackensack River (EPA, 2017) and due to their relative association with various industrial processes and wastes.

Ni and V are common metal pollutants, occurring in petroleum (Killops & Killops, 2005) and possibly in industrial products. Chromium (Cr) contamination is ubiquitous throughout Hudson County, New Jersey, due to the various industrial uses of chromium waste for wetland filling and general backfilling (EPA, 2017). Various chromium related manufacturers once occupied the edges of the Lower Hackensack River (E&E, 2015). Lead (Pb) and cobalt (Co) are additional examples of common trace metals associated with refinement of various hydrocarbon compounds for various petroleum and chemical products and are common automotive pollutants. Table 13 summarizes the results of the targeted metals of concern analysis using ICP-MS.

Table 13. ICP-MS Metals of Concern. Concentrations are reported in mg/k. Blue shading reflects the highest concentration of specific trace compounds.

ICP-MS Trace	V	Cr	Co	Ni	Pb
HACK19_12	53	113	8	25	18
HACK19_01	82	65	13	31	18
HACK19_02	86	92	16	30	17
HACK19_03	87	225	13	42	18
HACK19_04	75	142	10	34	18
HACK19_05	84	207	13	37	18
HACK19_06	74	260	12	42	17
HACK19_07	107	73	15	37	16
HACK19_08	91	196	13	39	18
HACK19_09	46	88	7	20	9
HACK19_10	128	252	20	59	18
HACK19_11	123	172	16	47	20

Cr concentrations appeared to vary the most in terms of concentrations. The highest Cr concentration was revealed in HACK19_06 at 260 mg/kg, followed by HACK19_10 at 252 mg/kg, with the lowest Cr concentration reported at 65 mg/kg. The highest V concentration was revealed in sample HACK19_10 at 128 mg/kg. In general, HACK19_10 revealed the greatest concentrations of metals of concern (i.e., V, Co, & Ni). Interpretation and analysis of ICP-MS trace elements also included the use of diagnostic ratios for V and Ni as (V/(V+Ni), additional evaluation of Cr and V anomalies and review of the overall distribution of metals. Cr and V anomalies were investigated using the ratio of the observed value (mg/kg) divided by the NJ urban Piedmont average (mg/kg) from Sanders (2003). There are no associated units with the results as they cancel out during the calculation. Results greater than one (>1) mean value observed is above the ambient concentration of extractable metals (Sanders, 2003).

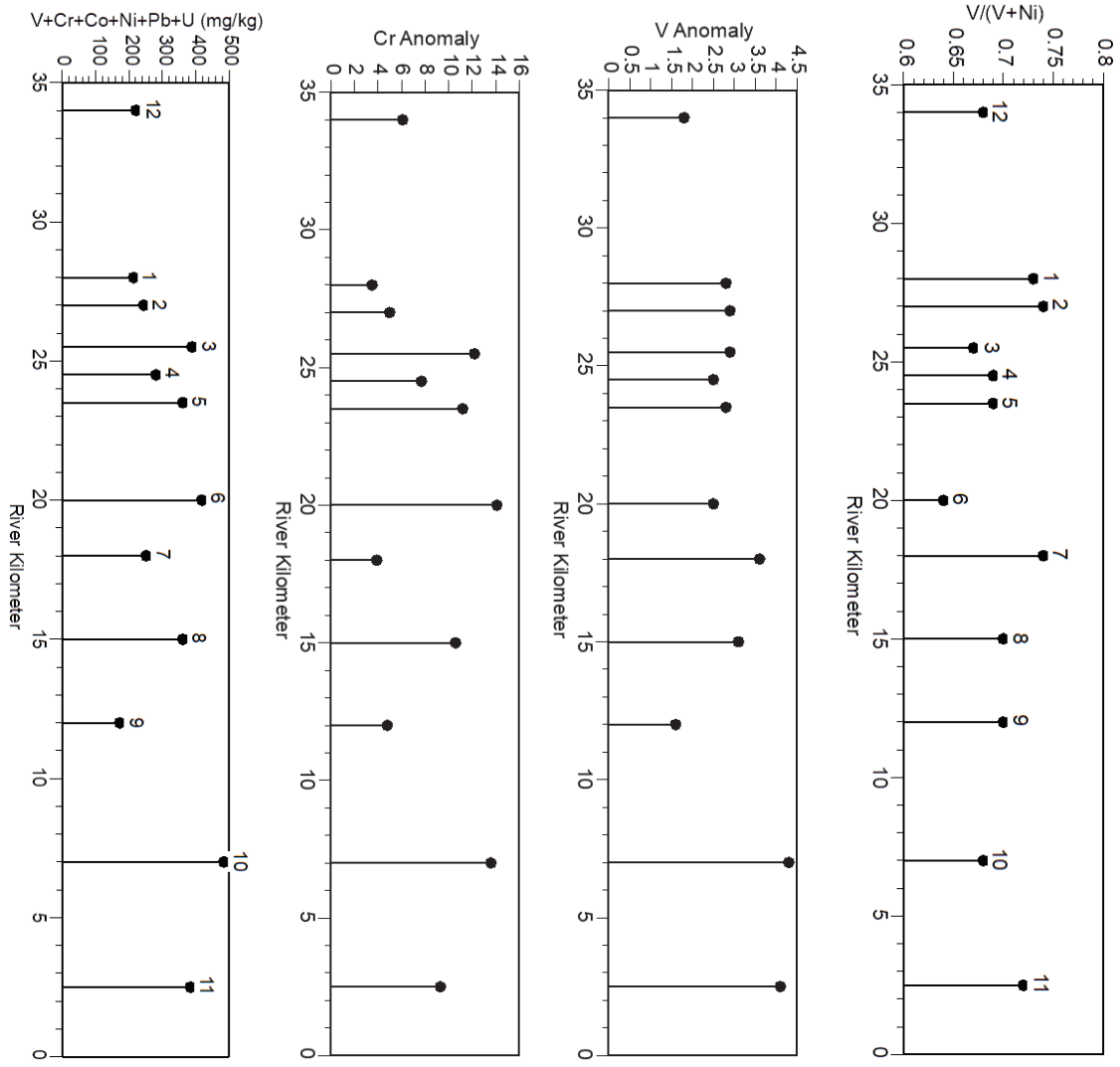

Figure 33. Spatial variation of ICP-MS metals of concern. Sample-site specific characteristics are included for evaluation purposes.

Concentrations of metals of concern fluctuated moving downstream. This is observed in Figure 33 and is possibly due to the tidal variations influencing local hydrodynamics of the various sampling sites as described by Miskewitz et al., (2005). The ratio of (V/V+Ni) is actually an oil fingerprinting index (Killops and Killops, 2013; Petres et al., 2005; Tissot and Welte. 1984). The overall fluctuation could point to various spills from various sources. Overall, the findings are

consistent with previously reported metal concentrations apart from Pb concentrations. Pb concentrations were consistently reported lower than anticipated (≤ 20 mg/kg). The 2016 Pb surface sediment results from the extensive SI sampling of the entire Lower Hackensack River by the EPA revealed a Pb concentration range of 10 mg/kg to 121 mg/kg. Great variability in Pb and all metals of concern was observed in the hundreds of surficial and subsurface sediment samples analyzed (EPA, 2017. Therefore, based on the Pb results of this study and the low and similar concentration of Pb totals, it is highly likely instrumental, or laboratory error occurred. Therefore, for the purpose of this study the generated Pb results will be discounted. Qualitative evaluation regarding overall distribution and abundance of contaminants of concern was supplemented using the 2016 EPA analytical SI results data.

3.4 SEM-BSE and SEM-EDS Results

The SEM efforts in this study are complimentary to the findings reported by Oen et al. (2006), Stoffyn-Elgi et al. (1997) and Cowan et al. (2015)). Varying degrees of biogenic silica (i.e. diatoms), biogenic-wastes, terrigenous sediments (i.e., sand) (Figure 34), and various organic and inorganic particles (Figure 35) were observed dominating the sediment matrix. Table 14 details the absence (or presence) of key characteristics observed throughout the subset of samples evaluated via SEM-BSE and SEM-EDS.

Table 14. SEM surface characteristics absence/presence table for the subset of samples analyzed via SEM-EDS and SEM-EDS analyses. Subset of samples included HACK19_04, HACK19_09, HACK19_10, HACK19_11 and HACK19_12. Grey shading relates to commonly associated BC morphology. Spherical smooth particles are shaded lighter grey due to the specific chemical and structure characteristics associated with such particles. **Boldface X** noticeably more present.

Surface Characteristics (SEM)	***Sample #***				
	4	**9**	**10**	**11**	**12**
biogenic silica (i.e., diatoms)	**X**	X	X		**X**
biogenic wastes			X		**X**
terrigenous sediments	**X**	X	X	X	X
organic particles (i.e., organic matter)		X			X
inorganic particles (i.e. shells)	X	X		X	X
amorphous structures	X	**X**	**X**	X	X
spherical smooth particles		**X**	**X**		
round porous particles		X			
round to irregular particles with rough surfaces		**X**	**X**	X	

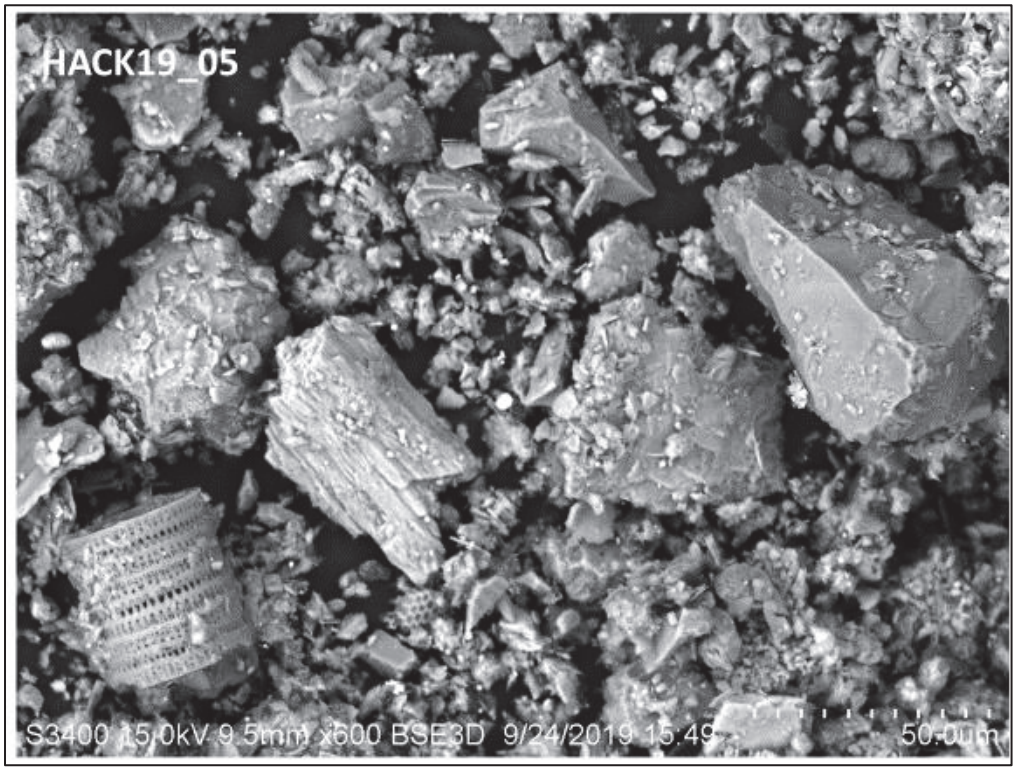

Figure 34. SEM secondary electron image of HACK19_05 the presence of diatoms, terrigenous particles and amorphous structures.

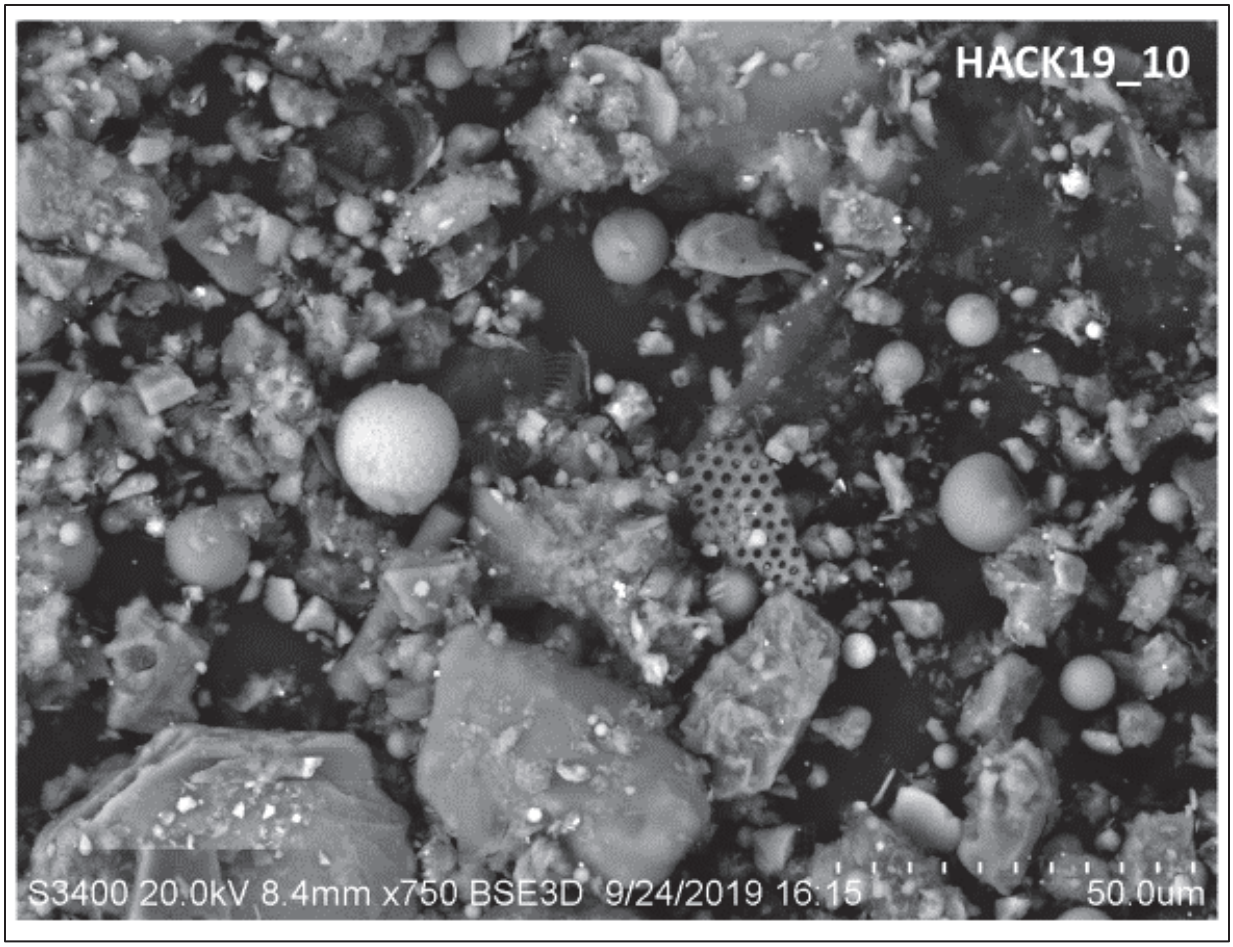

Figure 35. SEM secondary electron image of HACK19_10. Smooth spherical particles of varying sizes are seen dominating the surface of HACK19_10. Diatoms and amorphous particles are also present. Spot-analysis with SEM-EDS was performed for the large 'white' spherical particle observed above.

Perfectly to near perfectly smooth particles of varying sizes appeared to litter the lower river sediment samples, particularly in sample HACK19_10. HACK19_10 was collected along the inner bend of the sharp lower bend along the shores of Malanka Landfill (Secaucus / Jersey City, NJ) and near the northern shores of the former Hudson Generating Station (Jersey City, NJ).

EDS spectrum spot analysis revealed low C peaks with very high O peaks for the varying ‘white’ smooth spherical particles observed, not necessarily indicative of BC particles, but possibly of molten glass beads.

Ultimately, identification of BC particles was accomplished with SEM-BSE, with characterization of elemental compounds and elemental image mapping of O and C compounds achieved with SEM-EDS. The clearest evidence of BC particles was observed in samples HACK19_04 and HACK19_09, with C and O masses dominating the elemental composition, illustrated by red C and green O overlays (Figure 36). Further, several black areas of interest from both samples revealed C percent masses in excess of 60% and upwards of 95% or greater, with O percent masses ranging from 4% to upwards of 30%.

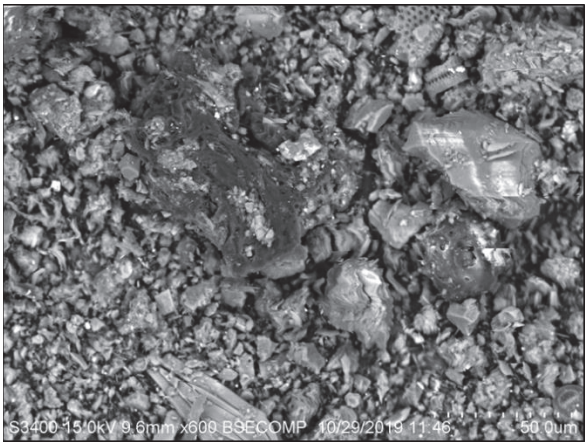

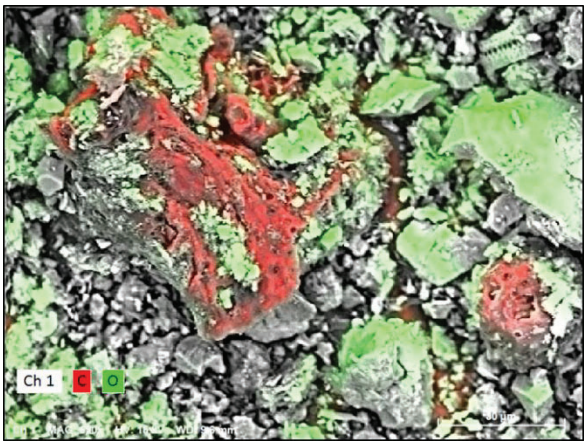

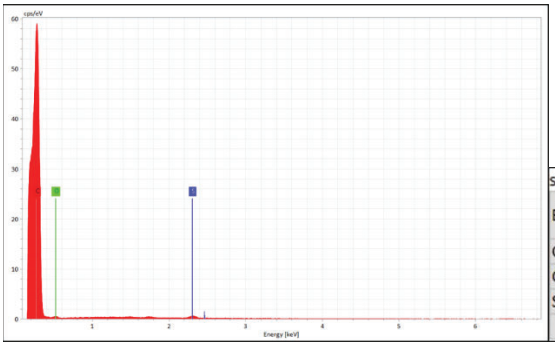

sample 90-black area 3 eds.spx

Element	At. No.	Netto	Mass [%]	Mass Norm. [%]	Atom [%]	abs. error [%] (1 sigma)	rel. error [%] (1 sigma)
Carbon	6	214674	95.15	95.15	96.50	3.78	3.97
Oxygen	8	2607	4.35	4.35	3.31	0.25	5.67
Sulfur	16	2657	0.50	0.50	0.19	0.04	7.48
		Sum	100.00	100.00	100.00		

Figure 36. SEM secondary electron image of suspected BC particle based on its amorphous textural appearance. SEM-EDS elemental image of C (red) and O (green). EDS spectrum results for BC particle showing the significant C peak are included in the far left. BC particle characterization of C, O and S compounds is also included.

Initial SEM efforts can be described as 'trial and error'. Initial challenges arose due the varying possible characteristics associated with BC particles and determining how to properly account for all possibilities. Preliminary evaluation involved switching between standard SEM and variable-pressure (VP) vacuum mode SEM for samples HACK19_09, HACK19_10, HACK19_11 and HACK19_12 (example shown in Figure 37). Charging related issues were initially encountered due the samples not being coated and instead being directly affixed to mounting stubs with either C or Co tape or no tape at all, making them less conductive to the electron beam. VP-SEM mode appeared to have the most minimal charging interference, however the images captured appeared blurry and in low contrast.

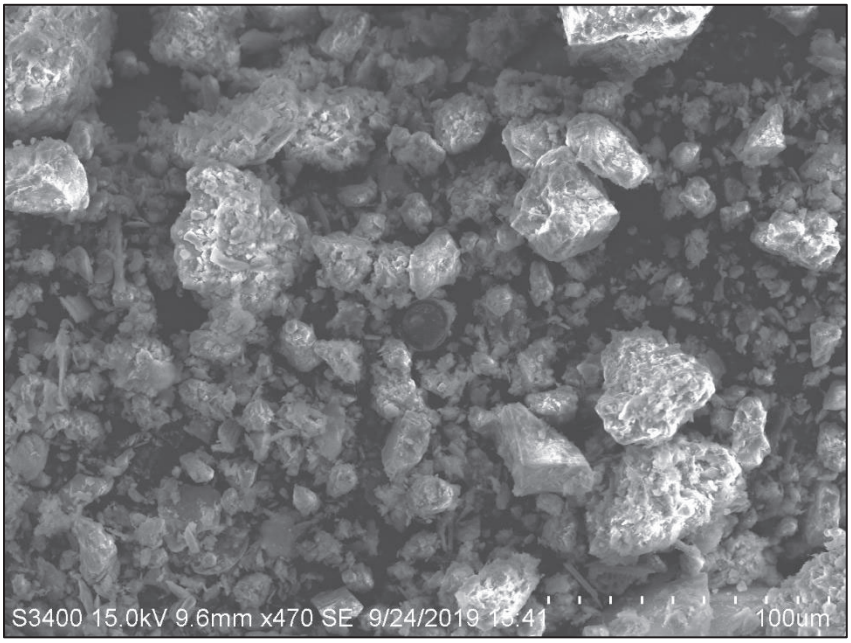

Figure 37. SEM-VP image showing the blurry and poor contrast conditions encountered (sample HACK19_09).

Since the focus of this study involves light elemental compounds (C, O, H), there was concern in the overall practicability of EDS quantification. Therefore, it is important to note that the identification of BC particles was based on visual identification followed by chemical confirmation and elemental mapping of O and C. This methodological approach is time-consuming and not practical for studies with large sample-sets. Yet, it is often large sample sets (n = 100+) which provide the clearest snapshot for understanding the various physical, chemical and hydrological processes influencing BC deposition, transport and accumulation. It is still a beneficial tool for evaluating BC, however, it should be conducted in conjunction with quantification methods such as the modified TOC approach included in this study and Py-GC-MS for identification and understanding of possible chemical signatures present.

4.0 Discussion

4.1 Organic Carbon and BC Deposition

Vascular plant and hydrophytic plant debris are pervasive in highly vegetated transitional estuaries, like the Hackensack Meadowlands, often collocated in the presence of various anthropogenic contamination, discharge refuse and urban river runoff (Wang and Stout, 2007; Emsbo-Mattingly et al., 2001). Similar conditions were observed in the transitional (non-tidal to tidal) area of background sample HACK19_12 which was collected only several rkm downstream of Oradell Reservoir and Dam.

Due to flocculation of fine particles such as clays and silts along the shallow riverbanks, the occurrence of organic-rich mud is common (Laughlin et al., 2014). Tidally influenced anoxic conditions also slow the decomposition of organic-rich matter (Miskewitz et al., 2001). The presence of organic-rich environments in waterways (i.e., marshes) can be described as potentially huge sponges for various hydrophobic contaminants (i.e., BC and PAHs).

TOC analysis is often included in any sediment or ecological risk assessment, as TOC has been found to normalize organic pollutants so ecological risk receptors can be determined (NJDEP, 2013). TOC determination allows for further understanding regarding the mechanisms governing distribution, transport and accumulation of fine organic particulates including various hydrocarbons, metals and BC particles (Konsevick & Bragin, 2010). Depositional zones are characteristically associated with higher TOC amounts (≥ 2 %) (Killops & Killops, 2005) and higher percentages of fine-grained (≤ 0.0625 mm) particles (Konsevick & Bragin, 2010).

Anthropogenic organic pollution is ubiquitous throughout the Lower Hackensack River and is often described as “black silt”. Murphy et al. (2011) defined black silt as compromising of

“approximately 50% silt particles, 25% water, and 25% hydrocarbons with trace amounts of metals”. The presence of black silt was encountered in nearly every sampling location, separate of HACK19_12, HACK19_01, and HACK19_02. Lighter brown silty sand deposits were sometimes observed smeared atop the black silt, possibly relating to the presence of fresher deposits atop the more historic and contaminated black silt. The presence of anthropogenic contamination is expected in urban environments. By harnessing the known chemical signatures of various anthropogenic contaminants and distribution of other C groups, differentiating between BC and other carbonaceous particles is possible.

Evaluating the presence of IC, TOC, RC and EPA PAHs alongside BC allowed for additional degrees of experimental control. Method 8270 and Kahn (1988) are standard applications for ecological risk assessments and investigations. However, analytical methods such as CTO-375 and LOI are considered more ‘arbitrary’ due to the greater risk of human error involved in sample preparation and calculation. Review of the final laboratory package provided by IAL included sample-specific TOC response curve chromatograms. TOC response curve chromatograms are often included with any commercial laboratory TOC request for QA/QC purposes. Generally, these chromatograms are disregarded unless a QA/QC issue appears. However, upon closer inspection it was evident that they also can support the likely presence of BC when overlaying TOC and BC response curves together as shown in Figure 38.

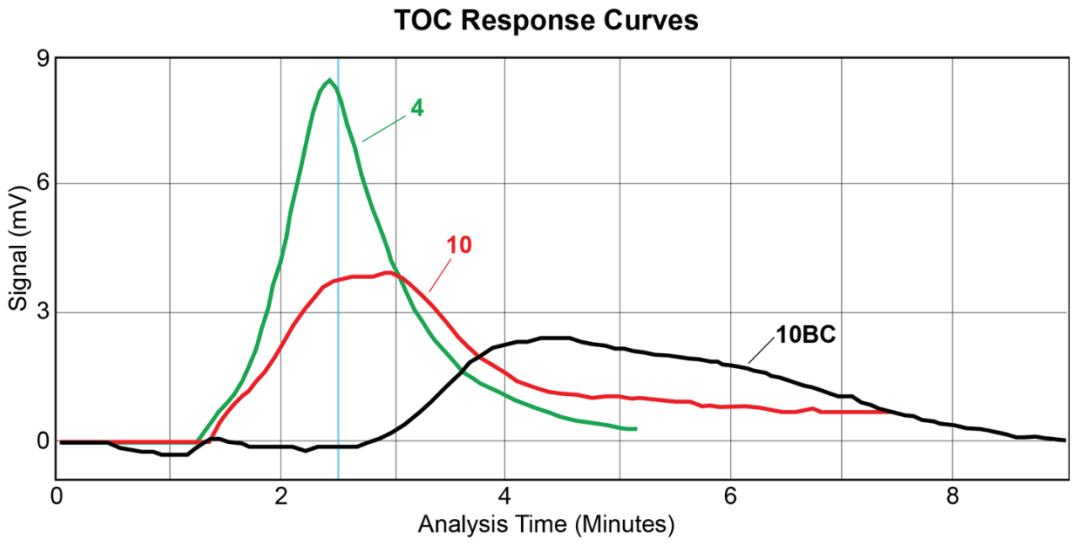

Figure 38. TOC and modified TOC response curves. The green curve represents the typical TOC curve. The average TOC curve was narrow, peaking before 3 minutes. The red curve represents sample HACK19_10, the outlier, which showed a very broad peak, maximizing later, at nearly 4 minutes. The black curve is the post 375 ºC carbonaceous residue which did not combust at 375 ºC. The behavior of the black broad, late peak is consistent with BC characteristics (i.e. resistant, eluting much later compared to other C forms) (Kruge, 2020).

The late eluting mixture denoted as 10BC represents the modified TOC for BC analysis run. The behavior is consistent with what is expected. BC is comprised of refractory C, which has already survived high temperature heating (pyrolytic processes). Therefore, BC particles should peak late. Such run behavior also confirms the applicability of the methods included in this study for BC quantification.

4.2 BC and Other Contaminants of Concern Distribution

The association and shared physiochemical properties of BC and other contaminants of concern were evaluated to further understand the relationships / processes which govern their

transport, deposition and accumulation. Figure 39 illustrates the similar fluctuations in terms of concentrations for TOC, BC, ΣEPA PAHs and the PHN index ratio.

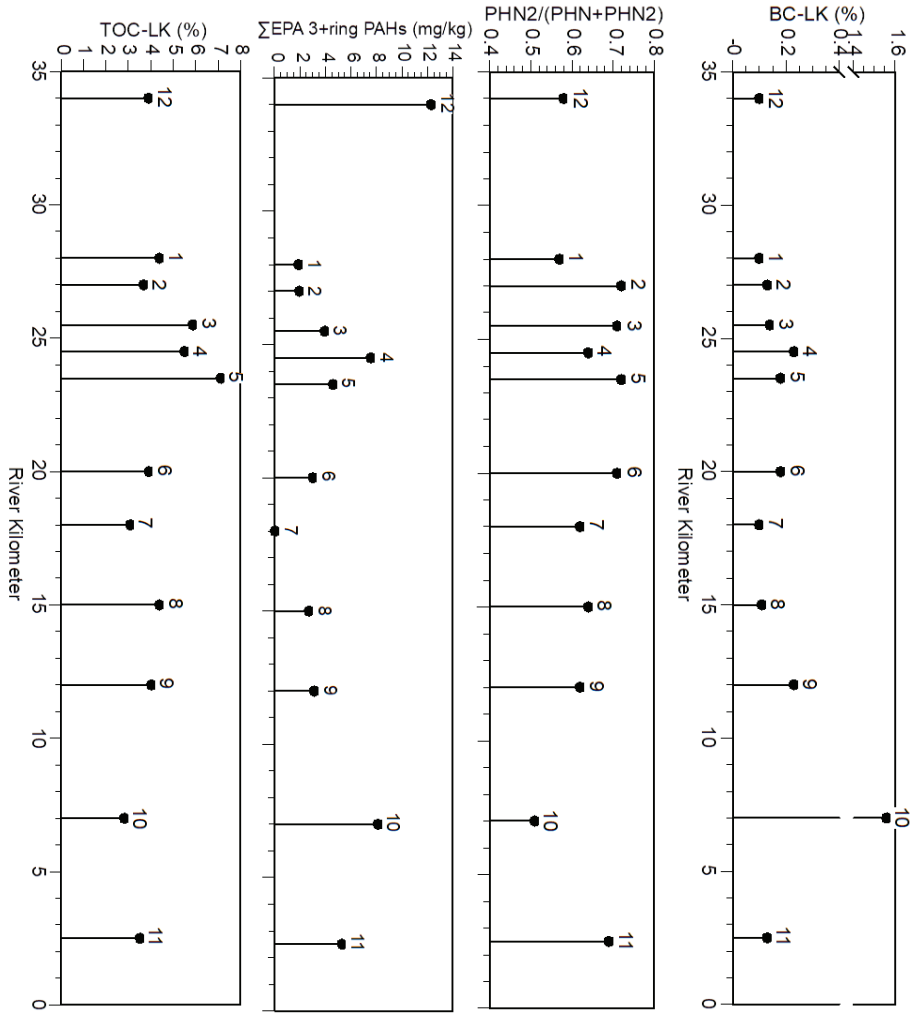

Figure 39. Spatial distribution of TOC (%), ΣEPA PAHs (mg/kg), PHN series ratio, and BC (%) plotted against rkm. Fluctuations follow a similar trend across the board apart from HACK19_10 as observed by the line break for BC-LK (%).

The spike observed in HACK19_10 for BC is also supported by the very low (< 0.6) PHN series value indicative of pyrogenic influence and the relatively high spike observed for ΣEPA PAHs. The presence of pyrolytic PAHs not only confirm the presence of BC as a result of co-

emission, but also point to their likely origins. Significant BC generation occupies high temperature burning, as do 3+ ring PAHs.

The spatial distribution of BC compared to metals of concern did not reveal any significant patterns (Figure 40). However, the petroleum ratio for V and Ni (V/(V+Ni)) and biomarker ratio for VGII (VG(VG+I) showed strong similarities. Overall, the current data for BC and metals is not strong enough to determine whether any significant relationships and correlations exist, most likely due to the relatively small sample group (n = 12). Metal contamination throughout the Lower Hackensack River is apparent though.

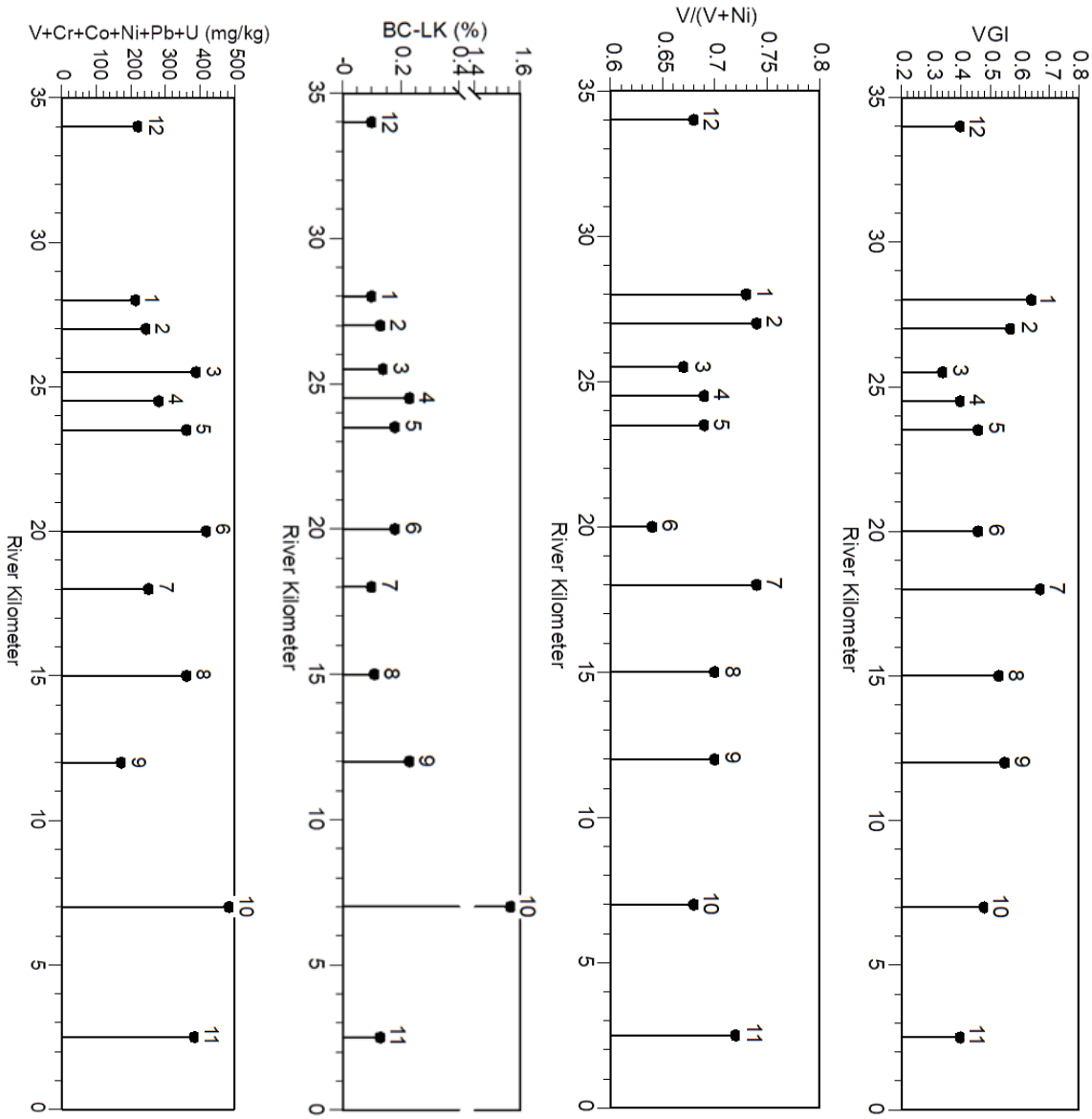

Figure 40. Spatial distribution of metals of concern (mg/kg) and BC (%). VGI and V/NI ratio values are also included. Results are shown against rkm. General fluctuating trend is observed. Overall, however, it does not appear BC totals are following the same distribution as metals of concern.

4.3 Potential Pollutant Sources

Various coal-burning and oil-burning electrical utilities formerly or currently operate along the lower shores of the Lower Hackensack River (E&E, 2015). The light, smooth, spherical particles observed dominating the lower river sediments during SEM analysis appear consistent with the findings of various coal ash studies (Cowan 2015 & 2017) and urban/industrial combustion particulate waste matter (SUNY-UMU, *n.d.*). A 2012 study by Yu *et al.* involving SEM analysis of fly ash samples collected from two Chinese coal burning power stations reported very similar findings in terms of surface morphology.

Possible sources for the spherical particles observed in study samples include the former Hudson Generation Station (Jersey City, NJ), this historically adjacent Malanka Landfill, and the various historical refineries and shipping yards which historically dotted the shores of the Lower Hackensack River for the better part of the last century (E&E, 2015).

The former Hudson Generating Station dominates the eastern lower riverbend and is located approximately 5 km upstream of Newark Bay (PSEG, 2019). The primary historic site operations included two coal burning power plants which ran from 1960s to 2017, capable of producing upwards of 680 Megawatts (MW) of electricity each (PSEG, 2019). The former power plant also supported natural gas burning as a secondary fuel (EPA, 2017). Cooling at the power plant was provided by the Lower Hackensack River (E&E, 2015).

Generally, particle morphology of combustion phase impurities in coal emerge as completely spherical particles when viewed with SEM analysis, while petroleum oil related combustion processes often result in porous, well-rounded, indented particles (SUNY-UMU, 2020; Hower et al., 2017; Niyogi et al., 2011). Sample HACK19_10 which was collected near

the former Hudson Generating Station shores, was particularly littered with varying sizes of 'white', perfectly spherical to oval particles (Figure 35) indicative of historic fly ash particulate wastes and contamination. Extremely high temperatures are required for an array of pulverized-fuel combustion plants such as the former Hudson Generating Station (Hower et al., 2017). Fly ash particles are pyrogenic by-products, like BC. HACK19_10 also reported the greatest amount of % BC as compared to other sample sites (Table 9) and was determined to be pyrogenic in origin (Figure 30). The presence of the spherical particles was initially thought of as BC, however, as elemental analysis revealed, the particles were comprised mostly of Si, Al, Fe, and other inorganic elements. Ultimately, though SEM analysis did reveal the visual presence of BC with positive identification and characterization accomplished between SEM-BSE and SEM-EDS.

Petrogenic sources contribute significant proportions of 2 to 3 ring PAHs and their alkylated substitutions to urban waterways (Uhler et al., 2005). Likely petrogenic sources observed along the river include the former Hess Terminal (HACK19_04) and the numerous petroleum terminals which straddle the shores of Port Newark. Chronic releases of petroleum products have plagued the Lower Hackensack River for centuries due to its proximity and association with various shipping containers (EPA, 2017). Environmental forensics when combined with BC quantification can help improve pollution control strategies for various petroleum, chemical and combustion related industries by fingerprinting releases back to original parent materials and by using BC as the vessel for characterization and quantification of other contaminants of concern.

4.3.1 Tidal Variations of Contaminant Concentrations

Previous hydrodynamic studies involving the Lower Hackensack River such as Miskewitz et al., (2005) and Weis et al., (2005), found the varying tidal influences of Newark Bay, the Lower Hackensack River and overarching Hudson-Raritan Estuary are likely responsible for the significant variations of heavy metal concentrations observed throughout the river in addition to the chronic release of various wastes from various point (i.e., direct discharges of oil) and non-point sources (i.e., stormwater/sewage effluents). Historic industrial discharges and effluents related to various industrial processes chronically plagued the surface sediment bed of the Lower Hackensack River (EPA, 2017). Industry related hazardous petroleum and/or chemical wastes were routinely stockpiled in multiple, large lagoons or pits, often positioned only several m from riverbanks, providing excellent pathways for various industry related hazardous materials directly into the waterways (Figure 41). Figure 42 illustrates the gravitational circulation and tidal currents at the Mouth of Newark Nay. The saltwater and strong tidal currents are responsible for the fate and transport of numerous organic and inorganic pollutants (Sherstha et al., 2010). BC quantification provides an additional evaluative lens when investigating fate and transport systems due to the efficient bonding of various PAHs to BC matrixes and BC's relative resistance to further chemical and biological degradation (Agarwal and Bucheli, 2011).

Figure 41. Historical aerial (1978) of the lower river portion looking south towards Kearny, portions of Jersey City and Newark Bay. Former petroleum related industries line the meandering river edges. Structures related to the former Kopper's Coke coal coking operations are observed in the lower right handle of the photograph. Further downstream and across the other side of Kopper's Coke are several large petroleum related holding tanks. The smokestacks of the former PSE&G coal powered Kearny Generating Station are observed in the distant. The various bridges associated with the Hackensack River Vertical Lift Bridges Historic District are also shown (U.S. Library of Congress, 1978). Development often extended directly to the river shorelines. Coal embargos would routinely travel from Newark Bay upstream to the various industrial shores of the properties shown in the image above (EPA, 2017; Murphy et al., 2011).

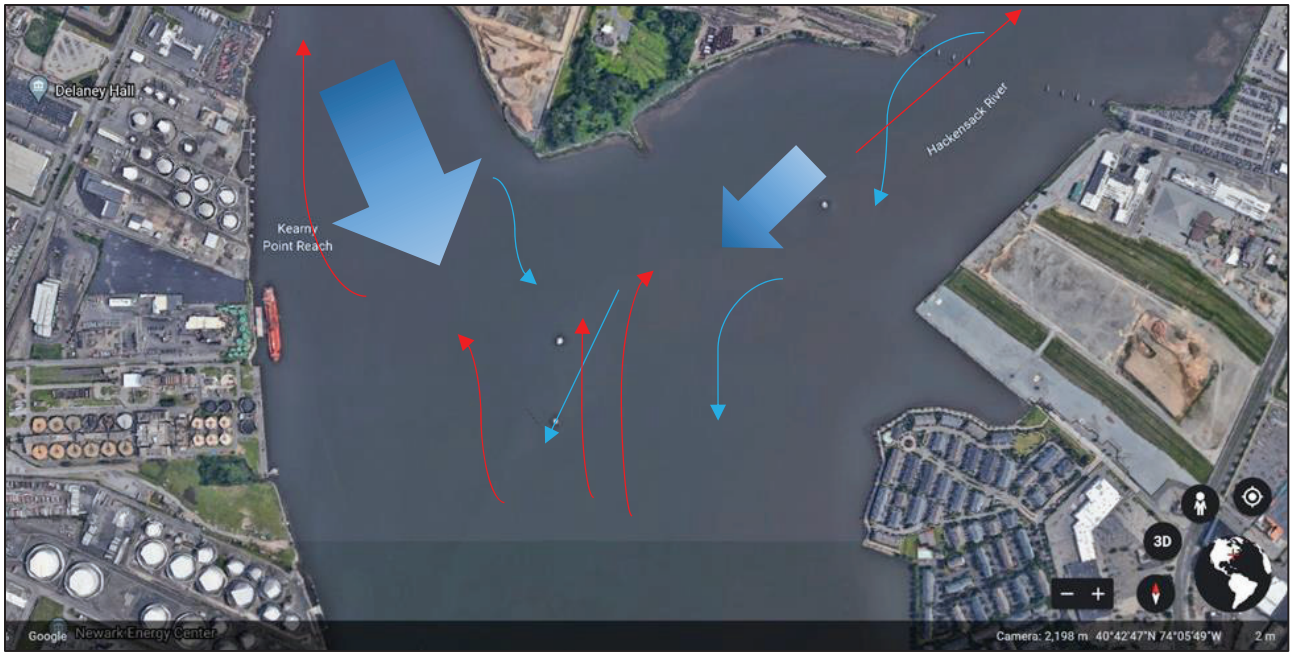

Figure 42. Schematic of gravitational circulation and tidal currents at the Mouth of Newark Bay. Freshwater flows are in blue, the size of the open arrows reflects the relative magnitude of the flows. Red arrows represent saltwater inflows. Petroleum related tank terminals are observed along the western shores of Newark Bay. Source: Google Earth, 2020 & Shrethsa et al. (2014).

5.0 Conclusion

PAH quantification and characterization can assist investigation of BC distribution due to co-emission and efficient sorption properties of PAHs to BC particles (Agarwal and Bucheli, 2011). However, sorption processes alone do not control the complete fate transport of particles in complex dynamic systems, such as the Lower Hackensack River. In the similar manner, PAH compounds are associated with specific characteristics and chemical signatures, the differentiated structures and chemical characteristic of BC when identified and accurately investigated can provide crucial information regarding the geochemical and physical processes governing its distribution and other persistent organic pollutants. Results from this study also show the beneficial use of including BC quantification alongside TOC analysis and the various checks and balances provided by use of pyrolytic-PAH data and EPA PAH data.

Py-GC-MS is not routinely included in ecological risk assessments and investigations. However, TOC via Kahn (1988) and EPA Method 8270 are. As this study shows, careful manipulation of both standardized methods (TOC & EPA-PAHs) alongside Py-GC-MS allows for the inclusion of commonly missed pyrolytic compounds such as BC and numerous alkylated homologues.

Previous sediment and characterization studies of the Lower Hackensack River focused primarily on characterizing EPA PAHs, extractable petroleum hydrocarbons, PCBs, heavy metals (i.e., Cr, Pb, Hg, etc.,) dioxins and so on (E&E, 2015). If the rapid and successful screening tools conducted with Py-GC-MS in this small study were applied to a sample set of hundreds (i.e., EPA's 2016 SIR sediment data), numerous chemical signatures would arise allowing for further understanding regarding whole system processes. Evaluation of specific

homologues (i.e., PHN series) could help reduce overlapping signals that might have been entirely excluded from the initial EPA-PAH evaluation.

BC quantification involving a modified Kahn (1988) approach ultimately provided successful (Figure 38). Acid digestion followed by combustion at 375 ^{o}C resulted in the incomplete destruction of organic matter as expected. The combusted residues that were then pyrolyzed and quantified using element analysis ultimately confirmed the presence of BC within RC groups. Elemental mapping of suspected BC particles further refined evaluation efforts by confirming the predominance of C compounds.

Future work should include the collection of a much larger sample set ($n \geq 100$) to accommodate statistical analysis for correlation determinations. Also, future work should include subsurface sampling to investigate the settling of BC and other hydrophobic compounds in TOC-enriched (>5 %) sediments. Three-point sampling may also be advantageous for future work to account for potential sediment drifts.

Quantifying and investigating the biophysiochemical properties and relative abundance of BC in natural environments, such as the Lower Hackensack River, is crucial for ecological system assessment and investigations. The general exclusion of BC quantification in soil and sediment investigations is ironic as it is shown to be a useful geochemical marker for historical inputs. Hopefully, continued efforts regarding BC and its potential use for environmental fingerprinting will continue as analytical complexities are reduced.

References:

Agency for Toxic Substances and Disease Registry (ATSDR). (2005) *Napthalene, 1-Methylnapthalene, and 2-Methylnaphthalene.* August 2005, Public Heath Statement.

Bucheli, T. D., Blum, F., Desaules, A., & Gustafsson, Ö. (2004). Polycyclic aromatic hydrocarbons, black carbon, and molecular markers in soils of Switzerland. *Chemosphere* **56**(11):1061-1076. doi:10.1016/j.chemosphere.2004.06.002

Chen, X., Yang, L., Myneni, S. C. B., & Deng, Y. (2019). Leaching of polycyclic aromatic hydrocarbons (PAHs) from sewage sludge-derived biochar. *Chemical Engineering Journal*, *373*, 840–845. https://doi-org.ezproxy.montclair.edu/10.1016/j.cej.2019.05.059

Dai, M., Kang, Y., Wang, X., Li, A., Song, Q., Dai, M., & Feng, H. (2008). Black carbon and polycyclic aromatic hydrocarbons (PAHs) in surface sediments of China's marginal seas. *Chinese Journal of Oceanology and Limnology* ***27***(2): 297-308.

Ecology and Environment, Inc. (2015). Lower Hackensack River Bergen and Hudson Counties, New Jersey: Preliminary Assessment (Report No. 15-03-0008). Retrieved from https://www.epa.gov/sites/production/files/201511/documents/r_hackensack_river_pa_09292015.pdf

Environmental Protection Agency, Region 2 (2017). Final Expanded Site Inspection Report for the Lower Hackensack River Bergen and Hudson Counties New Jersey (Site ID No: NJN000201845). Retrieved from https://semspub.epa.gov/work/02/515540.pdf

Environmental Protection Agency, Region 2 (2016). *Record of Decision Standard Chlorine Chemical Company, Inc., Town of Kearny, Hudson County, New Jersey.* September 2016. (# 393188). https://semspub.epa.gov/work/02/393188.pdf

Emsbo-Mattingly, S.D., Uhler, A.D., Stout, S.A., McCarthy, K.J., Douglas, G.S., Brown, John, Boehm, Paul (2001). Polycyclic aromatic hydrocarbon (PAH) chemistry of MGP tar and source identification in sediment. page 1-1 to 1-41. In, *Sediment Guidance Compendium, EPRI Technical Report 1005216,* Electric Power Research Institute, Palo Alto, CA.

Federal Registar (2012). 117.723 Hackensack River, Title 33: Navigation and Navigable Waters Part 117—*Drawbridge Operations Regulations,* US Government Printing Office, October 20, 2012, retrieved 2012-10-20, viewed 2020-04-02

Forbes, M., Raison, R., & Skjemstad, J. (2006). Formation, transformation and transport of black carbon (charcoal) in terrestrial and aquatic ecosystems. *Science of the Total Environment* **370**:190-206. doi:10.1016/j.scitotenv.2006.06.007

Glaser, B., Haumaier, L., Guggenberger, G., & Zech, W. (1998). Black carbon in soils: the use of benzenecarboxylic acids as specific markers. *Organic Geochemistry* **29**:811-819. doi:10.1016/S0146-6380(98)00194-6

Hackensack Riverkeeper, Our Mission (n.d.) Retrieved from https://www.hackensackriverkeeper.org/about-us/our-mission/

Hagmann D.F., Kruge M.A., Cheung M., Mastalerz M., Gallego J.L.R., Singh J.P., Krumins J.A., Li X., Goodey N. (2019) Environmental forensic characterization of former rail yard soils located adjacent to the Statue of Liberty in the New York/New Jersey harbor. Science of the Total Environment 690:1019-1034.

Hagmann, D. F., Kruge, M. A., Goodey, N. M., & Krumins, J. A. (2020). Characterization of coal particles in the soil of a former rail yard and urban brownfield: Liberty State Park, Jersey City (NJ), USA. *International Journal of Coal Geology*, *217*.

Heiri, O., Lotter, A., & Lemcke, G. (2001). Loss on ignition as a method for estimating organic and carbonate content in sediments: reproducibility and comparability of results. *JOURNAL OF PALEOLIMNOLOGY*, *25*(1), 101–110.

Hower, J. C., Groppo, J. G., Graham, U. M., Ward, C. R., Kostova, I. J., Maroto-Valer, M. M., & Dai, S. (2017). Coal-derived unburned carbons in fly ash: A review. *International Journal of Coal Geology*, *179*, 11–27.

Kahn, L. (1988) Determination of Total Organic Carbon in Sediment (Lloyd Kahn Method). July 27, 1988. U.S. Environmental Protection Agency, Region II, Monitoring Management Branch, Edison, New Jersey.

Killops, S. D., & Killops, V. J. (2013). Introduction to organic geochemistry. John Wiley & Sons, 393 p.

Knicker, H. (2011). Pyrogenic organic matter in soil: Its origin and occurrence, its chemistry and survival in soil environments. *Quaternary International*, *243*(2), 251–263.

Kolay, P. K., & Bhusal, S. (2014). Recovery of hollow spherical particles with two different densities from coal fly ash and their characterization. *Fuel*, *117*(Part A), 118–124.

Konsevick, E., Bragin, A, B., (2010) Chemical characteristics of sediment of the Lower Hackensack River, New Jersey, *Proceedings of the Annual International Conference on Soils, Sediments, Water and Energy:* 15(25), 304-334. Available at: https://scholarworks.umass.edu/soilsproceedings/vol15/iss1/25

Kruge M.A. (2015) Analytical pyrolysis principles and applications to environmental science In, M. Barbooti, ed., *Environmental Applications of Instrumental Chemical Analysis*. Ch. 15, p. 533-569.

Kruge M.A., Gallego J.L.R., Lara-Gonzalo A., Esquinas N. (2018) Environmental forensics study of crude oil and petroleum product spills in coastal and oilfield settings: Combined insights from conventional GC-MS, thermodesorption-GC-MS and pyrolysis-GC-MS. In, Stout S., Wang Z., eds., Oil Spill Environmental Forensics Case Studies. Butterworth-Heinemann (Elsevier), Oxford (UK), pp. 131-156.

Kruge M.A., Lara-Gonzalo A., Gallego J.L.R. (2020) Environmental forensics of complexly contaminated sites: A complimentary fingerprinting approach. Environmental Pollution. 263B:114645.

Langa, M. (2017). Superfund at Risk Under New Administration. Retrieved from https://www.hackensackriverkeeper.org/wp-content/uploads/2014/06/news_Summer_2017.pdf

Lara-Gonzalo A., Kruge M.A., Lores I., Gutiérrez B., Gallego J.L.R. (2015) Pyrolysis-GC-MS for the rapid environmental forensic screening of contaminated brownfield soil. Organic Geochemistry 87:9-20.

Library of Congress Prints and Photographs Division. Reproduction No., HAER NJ,9-KEAR, 3-2*, Vertical Lift Bridges Spanning the Hackensack River, Looking Northeast,* (1978). Historic American Engineering Record Collections. Retrieved from: http://hdl.loc.gov/loc.pnp/hhh.nj0967/photos.113452p

Mattingly, S. E., Stout, S. A., McCarthy, K. S., Douglas, G. S., Brown, J. S., & Boehm, P. D. (2001). Polycyclic Aromatic Hydrocarbons (PAH) Chemistry of MGP Tar and Source Identification in Sediment. *Sediments Guidance Compendium,* 1–38.

Mcardle, J. (2011, July 8). *Jersey City Power Plant Cleans Up Emissions but Can't Escape Activists' Wrath.* The New York Times. Retrieved from https://archive.nytimes.com/www.nytimes.com/gwire/2011/07/08/08greenwire-jersey-city-power-plant-cleans-up-emissions-bu-54513.html

Miskewitz, R., Su, T. L., Hires, R. I., Dimou, K., & Korfiatis, G. P. (2005). Tidal Variations of Heavy Metal Concentrations in the Hackensack River, New Jersey, USA. *Journal of Marine Environmental Engineering*, *7*(4), 241–248.

Murphy, III, W., Ward, W. B., Murphy IV, W., Nolen-Hoeksema, R., Art, M., & Rosales, D. A. (2011). Sediment, Sedimentation, and Environments of the Lower Hackensack River and Newark Bay Estuary Complex. *Proceedings of the Western Dredging Association (WEDA XXXI) Technical Conference and Texas A&M University (TAMU 42) Dredging Seminar,* Nashville, Tennessee, June 5-8, 2011.

Natural Atlas (2020). Retrieved from https://naturalatlas.com/rivers/hackensack-932297

New Jersey Department of Environmental Protection (NJDEP). (2013). *Development of Impact to Ground Water Soil Remediation Standards Using the Soil-Water Partition Equation, -* Guidance Document, Version 2.0. Retrieved from https://www.nj.gov/dep/srp/guidance/rs/partition_equation.pdf

NOAA, Office of Response and Restoration (2015). *Largest oil spills affecting us water from 1969 to present.* Retrieved from https://response.restoration.noaa.gov/oil-and-chemical-spills/oil-spills/largest-oil-spills-affecting-us-waters-1969.html

Niyogi, A., Pati, J., Patel, S., Panda, D., & Patil, S. (2011). Anthropogenic and impact spherules: Morphological similarity and chemical distinction - A case study from India and its implications. *Journal of Earth System Science*, *120*(6), 1043–1054. https://doi-org.ezproxy.montclair.edu/10.1007/s12040-011-0125-y

Oen, A. M., Cornelissen, G., & Breedveld, G. D. (2006). Relation between PAH and black carbon contents in size fractions of Norwegian harbor sediments. *Environmental Pollution* **141**: 370-380. doi:10.1016/j.envpol.2005.08.033

O'Neill, J. M. (2017, February 10). Stew of contaminants found in Hackensack riverbed tests. *northjersey.com*. Retrieved from https://www.northjersey.com/story/news/environment/2017/02/10/stew-contaminates-found-hackensack-riverbed-tests/97548744/

O'Laughlin, C., van Proosdij, D., & Milligan, T. (2014). Research papers: Flocculation and sediment deposition in a hypertidal creek. *Continental Shelf Research*, *82*72-84. doi:10.1016/j.csr.2014.02.012

Olsen, K.K., 2014, Organic geochemical investigations of urban sediments by pyroysis-gas chromatography/mass spectroscopy. PhD Dissertation, Montclair State University, Montclair (NJ), 531 p.

Peters, K.E., Walters, C.C., Moldowan, J.M., 2005. *The Biomarker Guide*. Vols. 1 & 2, Cambridge University Press, Cambridge, 1155 p.

Rosenmeier & Abbott. (2005). Loss on Ignition protocol. *S.O.P. – Loss on Ignition.*

Sánchez-García, L., de Andrés, J. R., Gélinas, Y., Schmidt, M. W., & Louchouarn, P. (2013). Different pools of black carbon in sediments from the Gulf of Cádiz (SW Spain): Method comparison and spatial distribution. *Marine Chemistry* **151**:13-22. doi:10.1016/j.marchem.2013.02.006

Sánchez-García, L., Cato, I., & Gustafsson, Ö. (2010). Evaluation of the influence of black carbon on the distribution of PAHs in sediments from along the entire Swedish continental shelf. *Marine Chemistry*, **119**(1-4), 44-51. doi:10.1016/j.marchem.2009.12.005

Sanders, P.F., 2003. Ambient levels of metals in New Jersey soils. Environmental Assessment and Risk Analysis Element Research Project Summary. New Jersey Dept. of Environmental Protection, Division of Science, Research & Technology, Trenton, N.J.

Shrestha, G., Traina, J. S., & Swanston, W. C (2010). Black carbon's properties and role in the environment: a comprehensive review. *Sustainability* **2**: 294-320. doi:10.3390/su2010294

Schumacher, A, B. (2002). Methods for the determination of total organic carbon (TOC) in soils and sediments. Ecological Risk Assessment Group. *Office of Research and Development.* U.S. Environmental Protection Agency. NCEA-C-1282.

Shrestha, L.P, Su, H. S., James, C. S., Shaller, J. P., Doroudian, M., Firstenberg, E. C., Thompson, T. C. (2014). Conceptual site model for Newark Bay, hydrodynamics and sediment transport. *Marine Science and Engineering*, 2: 123-139. doi: 10.3390/jmse2010123

Staniszewska, M., Burska, D., Sapota, G., Bogdaniuk, M., Borowiec, K., Nosarzewska, I., & Bolałek, J. (2011). The relationship between the concentrations and distribution of organic pollutants and black carbon content in benthic sediments in the Gulf of Gdańsk, Baltic Sea. *Marine Pollution Bulletin*, *62*(7), 1464-1475. doi:10.1016/j.marpolbul.2011.04.013

State University of New York (SUNY) Upstate Medical University. Particle Morphology (n.d.). https://www.upstate.edu/pathenvi/basics/particle_morphology.php

Stoffyn-Egli, P., Potter, M.T., Leonard, D. J., Pocklington, R. (1997). The identification of black carbon particles with the analytical scanning electron microscope: methods and initial results. *The Science and the Total Environment*, **198**: 211-223.

Stout, S. A., Emsbo-Mattingly, S. D., Douglas, G. S., Uhler, A. D., & McCarthy, K. J. (2015). Beyond 16 Priority Pollutant PAHs: A Review of PACs used in Environmental Forensic Chemistry. *Polycyclic Aromatic Compounds*, **35**(2–4), 285–315. doi:10.1080/10406638.2014.891144

Tissot, B.P., Welte, D.H., 1984. *Petroleum Formation and Occurrence.* Springer, 702 p.

Tobiszewski, M., & Namieśnik, J. (2012). PAH diagnostic ratios for the identification of pollution emission sources. *Environmental Pollution* **162***:*110-119. doi:10.1016/j.envpol.2011.10.025

Uhler, A. D., Emsbo-Mattingly, S., Bo Liu, Hall, J. . L. W., & Burton, D. T. (2005). An Integrated Case Study for Evaluating the Impacts of an Oil Refinery Effluent on Aquatic Biota in the Delaware River: Advanced Chemical Fingerprinting of PAHs. *Human & Ecological Risk Assessment*, *11*(4), 771–836.

United States Fish & Wildlife Service (USFWS). (2007). The Hackensack Meadowlands Initiative, Preliminary conservative planning for the Hackensack Meadowlands, Hudson and Bergen

Counties, New Jersey. March 2007. Retrieved from: http://www.fws.gov/northeast/njfieldoffice/

Wang Z. and Fingas M.F. (2003) Development of oil hydrocarbon fingerprinting and identification techniques. *Marine Pollution Bulletin* **47**:423-452.

Wang Z. and Stout S.A. (2007) *Oil Spill Environmental Forensics*, 554 pages, Academic Press.

Weis, J. S., Skurnick, J., & Weis, P. (2004). Studies of a contaminated brackish marsh in the Hackensack Meadowlands of Northeastern New Jersey: benthic communities and metal contamination. *Marine Pollution Bulletin*, *49*(11/12), 1025.

Yunker, M. B., Macdonald, R. W., Vingarzan, R., Mitchell, R. H., Goyette, D., & Sylvestre, S. (2002). PAHs in the Fraser River basin: a critical appraisal of PAH ratios as indicators of PAH source and composition. *Organic Geochemistry* **33**: 489-515. doi:10.1016/S0146-6380(02)00002-5

APPENDIX A:
Py-GC-MS Chromatograms

Appendix
Pyrolysis-Gas Chromatography-Mass Spectrometry
Total Ion Chromatograms - Peak Identification

Aliphatic hydrocarbons

+n	normal alkanes (n = carbon number)
^n	normal alk-1-enes (n = carbon number)

Isoprenoid hydrocarbons (biomass markers)

Pr:1	prist-1-ene
NPhy	neophytadiene

Petroleum biomarkers

Ts	C_{27} hopane (18α(H),21β(H)-22,29,30-trisnorhopane)
Hn	other hopanes (n = carbon number)

Monoaromatic hydrocarbons (produced during pyrolysis)

B0	benzene
B1	toluene
EB	ethylbenzene
mX	*meta*-xylene (1,3-dimethylbenzene)
pX	*para*-xylene (1,4-dimethylbenzene)
B2:	styrene

Polycyclic aromatic hydrocarbons (PAHs)

N0	naphthalene
mN	methylnaphthalenes
PHN	phenanthrene
FLA	fluoranthene
PYR	pyrene
RET	retene (1-methyl-7-isopropyl phenanthrene) (wood smoke marker)
BAN	benzo[*a*]anthracene
CHR	chrysene
BFLA	benzofluoranthene isomers (undifferentiated)

Simple phenols

F0	phenol
3mF	3-methylphenol
4mF	4-methylphenol
F2	4-ethylphenol
F2:	4-vinylphenol

Methoxyphenols (lignin pyrolysis markers)

G0	guaiacol
G1	methylguaiacol
G2:	vinylguaiacol
G3:	propenyl guaiacol
S2:	vinylsyringol
S3:	propenyl syringol

Polysaccharide markers

FCA0	furfural
FCA1	methylfurfural

Fatty acid (microbial biomass marker)

CA16	hexadecanoic acid

Nitrogen compounds (protein and microbial biomass markers)

Pd	pyridine
IL	indole
IL1	methylindole
DKDP	diketodipyrrole
ANn	alkylnitriles (n = carbon number)

Sulfur compounds

DMDS	dimethyldisulfide
T1	2-methylthiophene
S8	elemental sulfur (S_8)

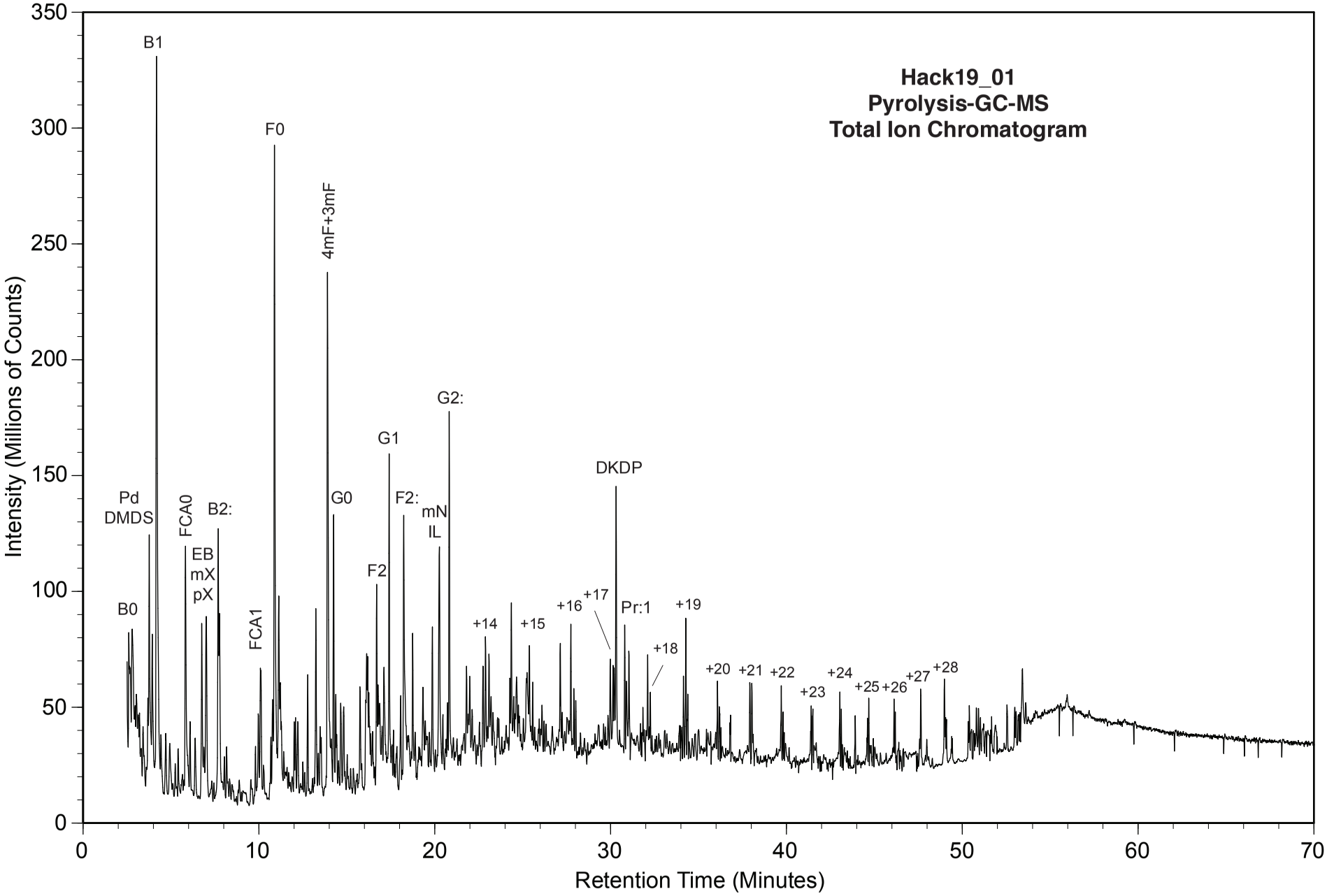
Hack19_01
Pyrolysis-GC-MS
Total Ion Chromatogram
Intensity (Millions of Counts)
Retention Time (Minutes)
0
50
100
150
200
250
300
350
0
10
20
30
40
50
60
70
B1
F0
4mF+3mF
G2:
G1
DKDP
Pd
DMDS
FCA0
B2:
G0
F2:
mN
IL
F2
EB
mX
pX
B0
FCA1
+14
+15
+16
+17
Pr:1
+18
+19
+20
+21
+22
+23
+24
+25
+26
+27
+28

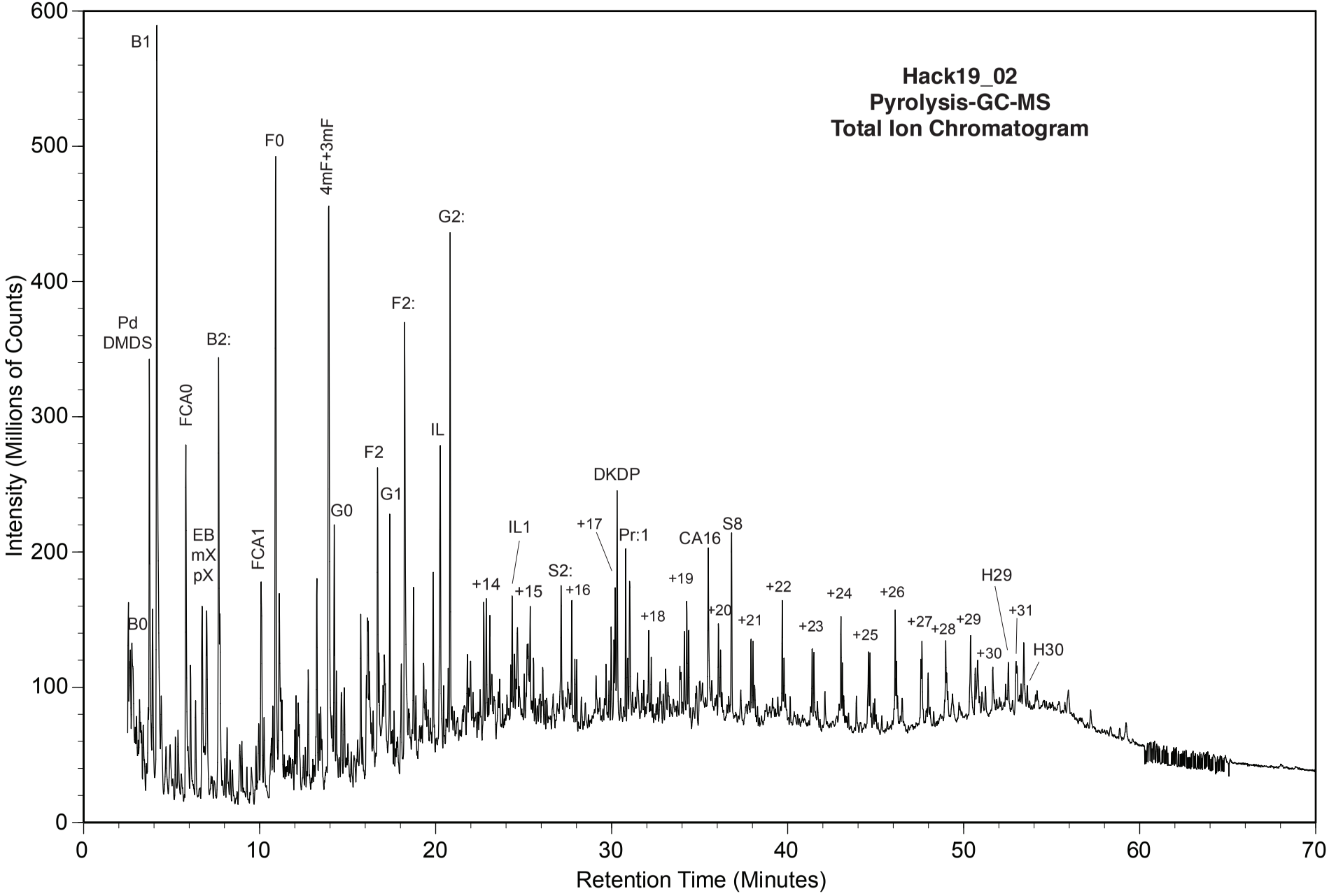
Hack19_02
Pyrolysis-GC-MS
Total Ion Chromatogram
Intensity (Millions of Counts)
Retention Time (Minutes)
0
100
200
300
400
500
600
0
10
20
30
40
50
60
70
B1
Pd
DMDS
B0
FCA0
EB
mX
pX
B2:
FCA1
F0
4mF+3mF
G0
F2
G1
F2:
IL
G2:
IL1
+14
+15
S2:
+16
+17
DKDP
Pr:1
+18
+19
CA16
+20
S8
+21
+22
+23
+24
+25
+26
+27
+28
+29
+30
H29
+31
H30

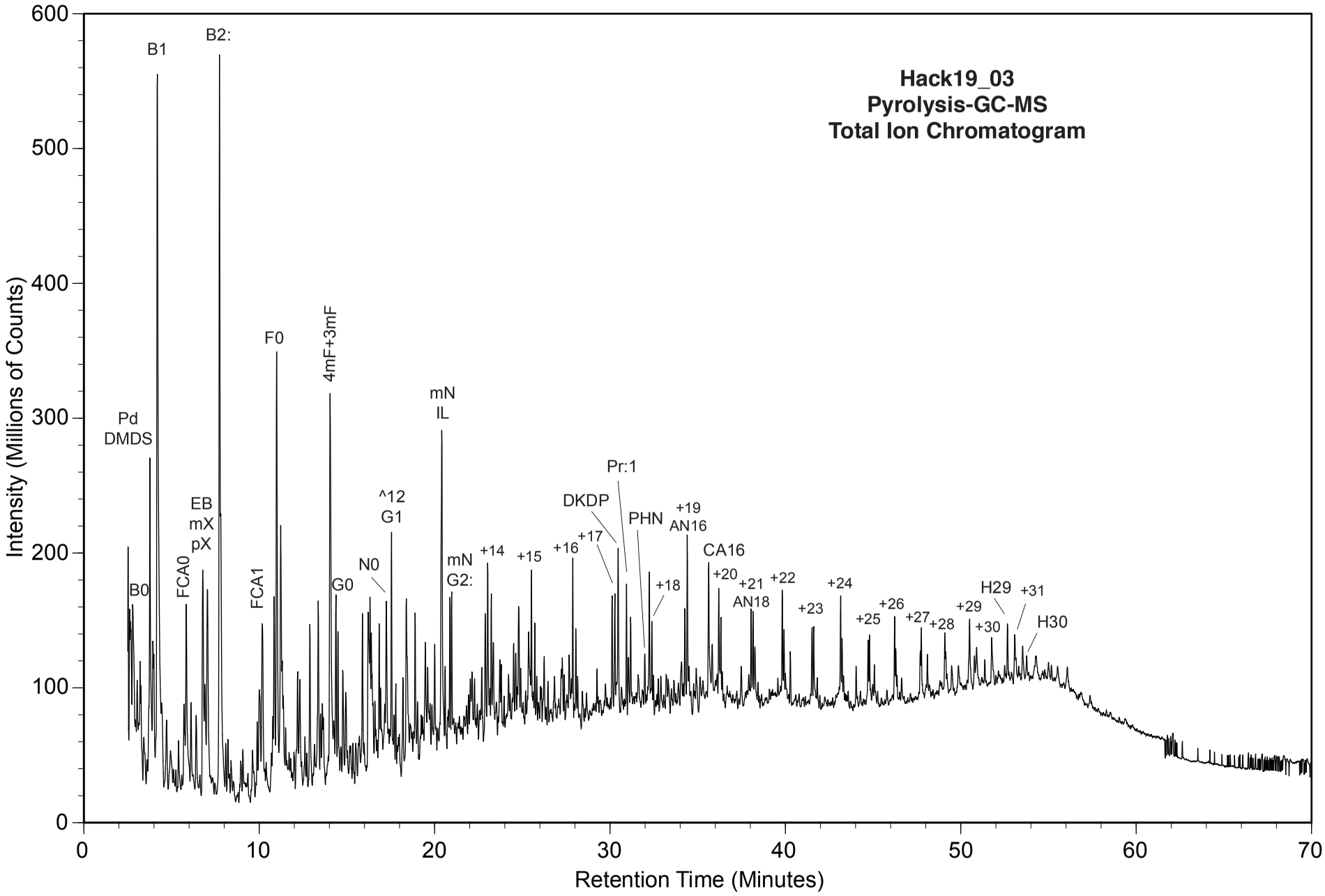
Hack19_03
Pyrolysis-GC-MS
Total Ion Chromatogram
Intensity (Millions of Counts)
Retention Time (Minutes)
0
100
200
300
400
500
600
0
10
20
30
40
50
60
70
Pd
DMDS
B0
B1
FCA0
EB
mX
pX
B2:
FCA1
F0
G0
4mF+3mF
N0
^12
G1
mN
IL
mN
G2:
+14
+15
+16
+17
DKDP
Pr:1
PHN
+18
+19
AN16
CA16
+20
+21
AN18
+22
+23
+24
+25
+26
+27
+28
+29
+30
H29
+31
H30

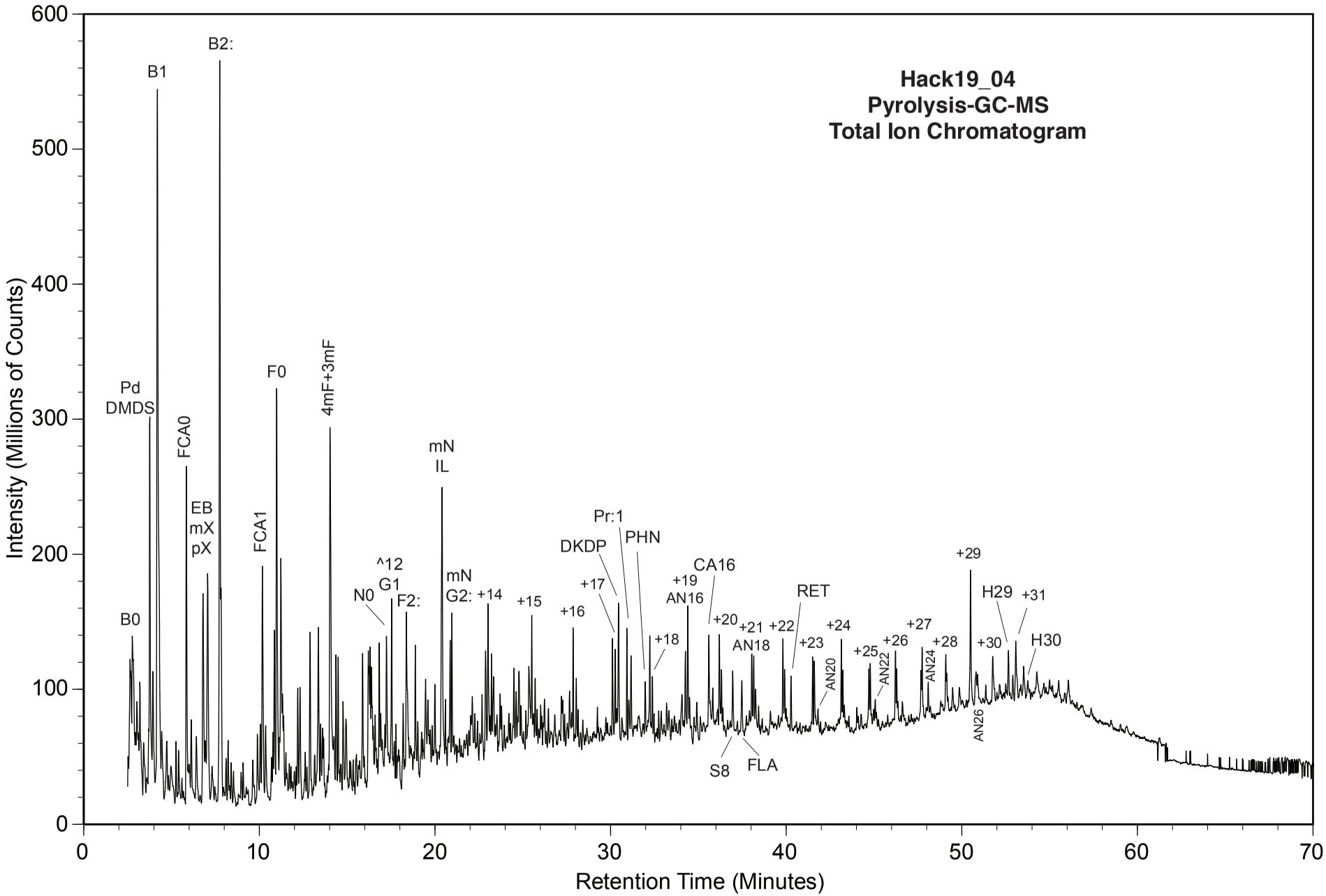
Hack19_04
Pyrolysis-GC-MS
Total Ion Chromatogram
Intensity (Millions of Counts)
Retention Time (Minutes)
0
100
200
300
400
500
600
0
10
20
30
40
50
60
70
B0
Pd
DMDS
B1
B2:
FCA0
EB
mX
pX
FCA1
F0
4mF+3mF
N0
^12
G1
F2:
mN
IL
mN
G2:
+14
+15
+16
DKDP
+17
Pr:1
PHN
+18
+19
AN16
CA16
+20
+21
AN18
+22
RET
+23
AN20
+24
+25
AN22
+26
+27
AN24
+28
+29
AN26
+30
H29
+31
H30
S8
FLA

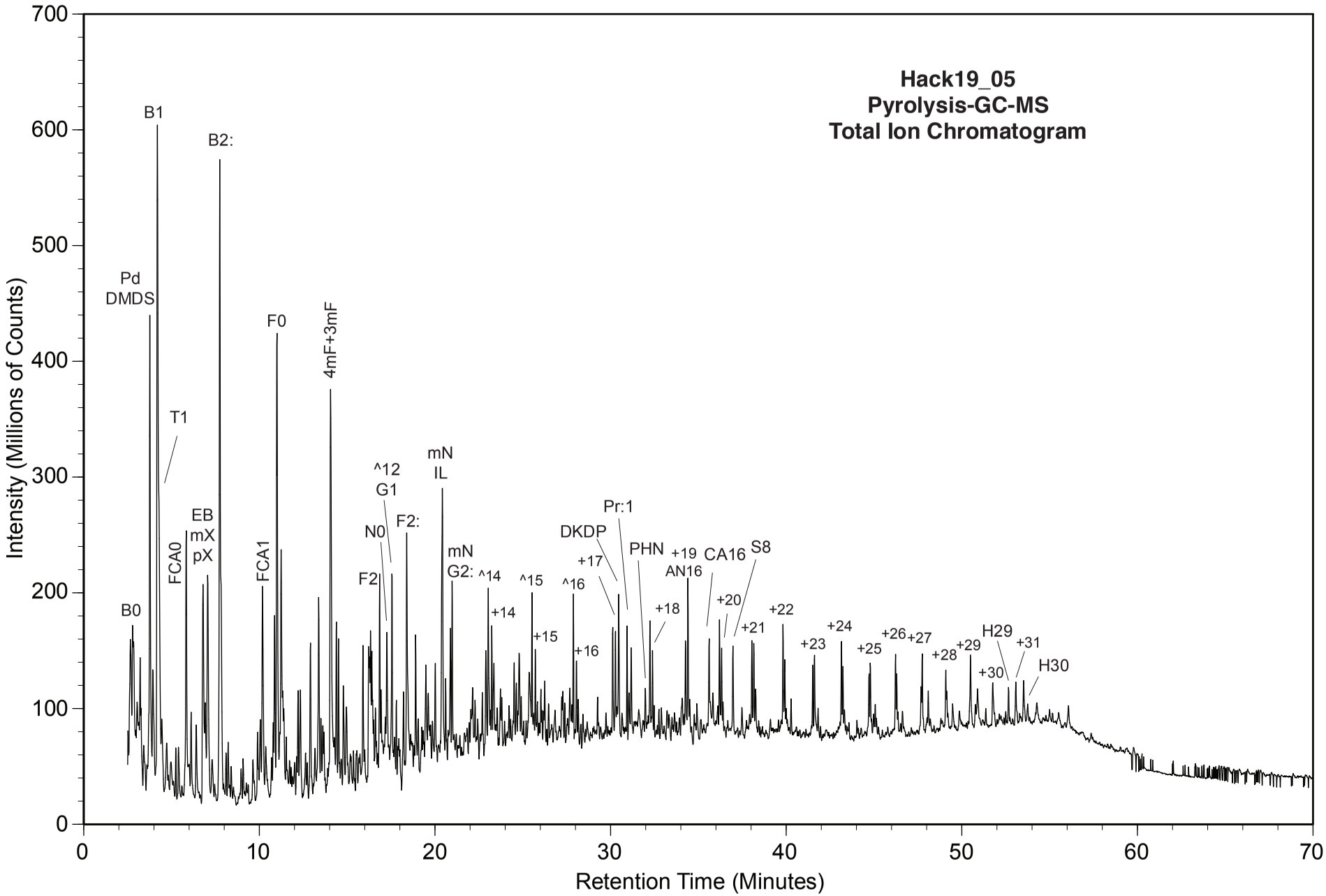
Hack19_05
Pyrolysis-GC-MS
Total Ion Chromatogram
Intensity (Millions of Counts)
Retention Time (Minutes)
0
100
200
300
400
500
600
700
0
10
20
30
40
50
60
70
B0
Pd
DMDS
B1
T1
FCA0
EB
mX
pX
B2:
FCA1
F0
4mF+3mF
F2
N0
^12
G1
F2:
mN
IL
mN
G2:
^14
+14
^15
+15
^16
+16
DKDP
+17
Pr:1
PHN
+18
+19
AN16
CA16
+20
S8
+21
+22
+23
+24
+25
+26
+27
+28
+29
+30
H29
+31
H30

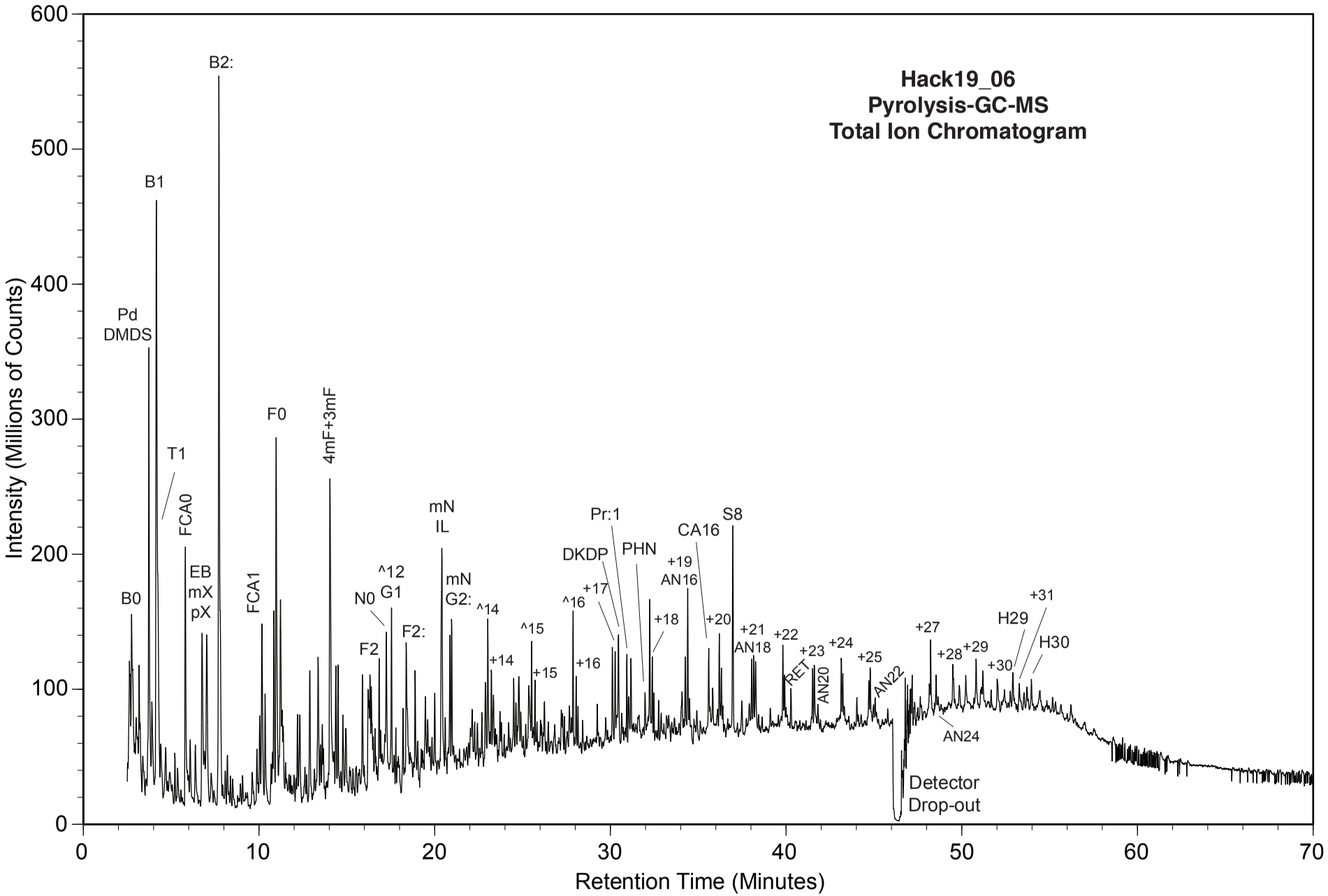
Hack19_06
Pyrolysis-GC-MS
Total Ion Chromatogram
Intensity (Millions of Counts)
Retention Time (Minutes)
0
100
200
300
400
500
600
0
10
20
30
40
50
60
70
B0
Pd
DMDS
B1
T1
FCA0
EB
mX
pX
B2:
FCA1
F0
4mF+3mF
N0
F2
^12
G1
F2:
mN
IL
mN
G2:
^14
+14
^15
+15
^16
+16
DKDP
Pr:1
+17
PHN
+18
+19
AN16
CA16
+20
S8
+21
AN18
+22
RET
+23
AN20
+24
+25
AN22
+27
+28
+29
+30
H29
+31
H30
AN24
Detector
Drop-out

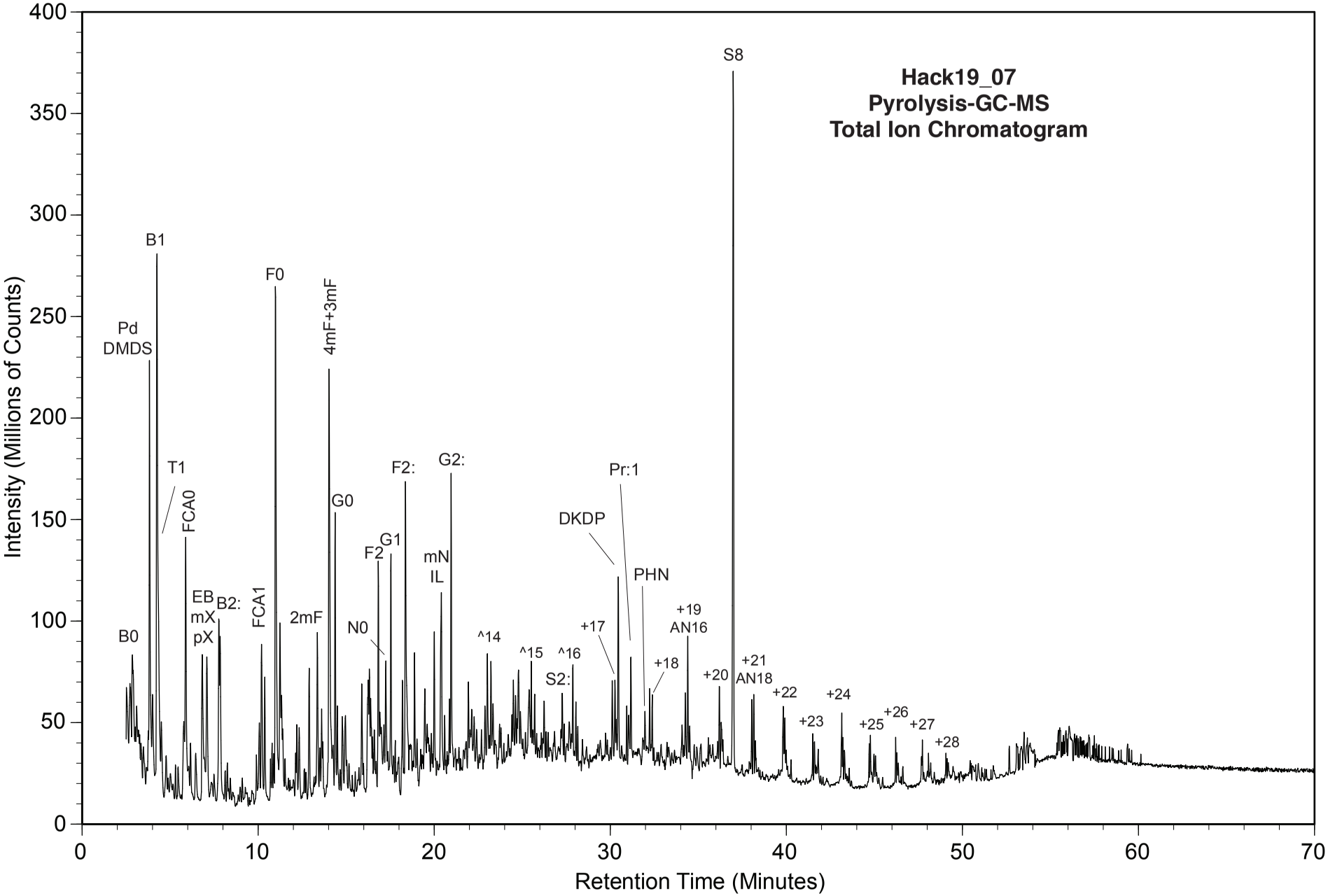
Hack19_07
Pyrolysis-GC-MS
Total Ion Chromatogram
Intensity (Millions of Counts)
Retention Time (Minutes)
0
50
100
150
200
250
300
350
400
0
10
20
30
40
50
60
70
S8
B1
F0
4mF+3mF
Pd
DMDS
T1
FCA0
F2:
G2:
G0
Pr:1
DKDP
G1
F2
mN
IL
PHN
EB
mX
pX
B2:
FCA1
2mF
N0
+19
AN16
B0
^14
+17
^15
^16
+18
+20
+21
AN18
S2:
+22
+24
+23
+25
+26
+27
+28

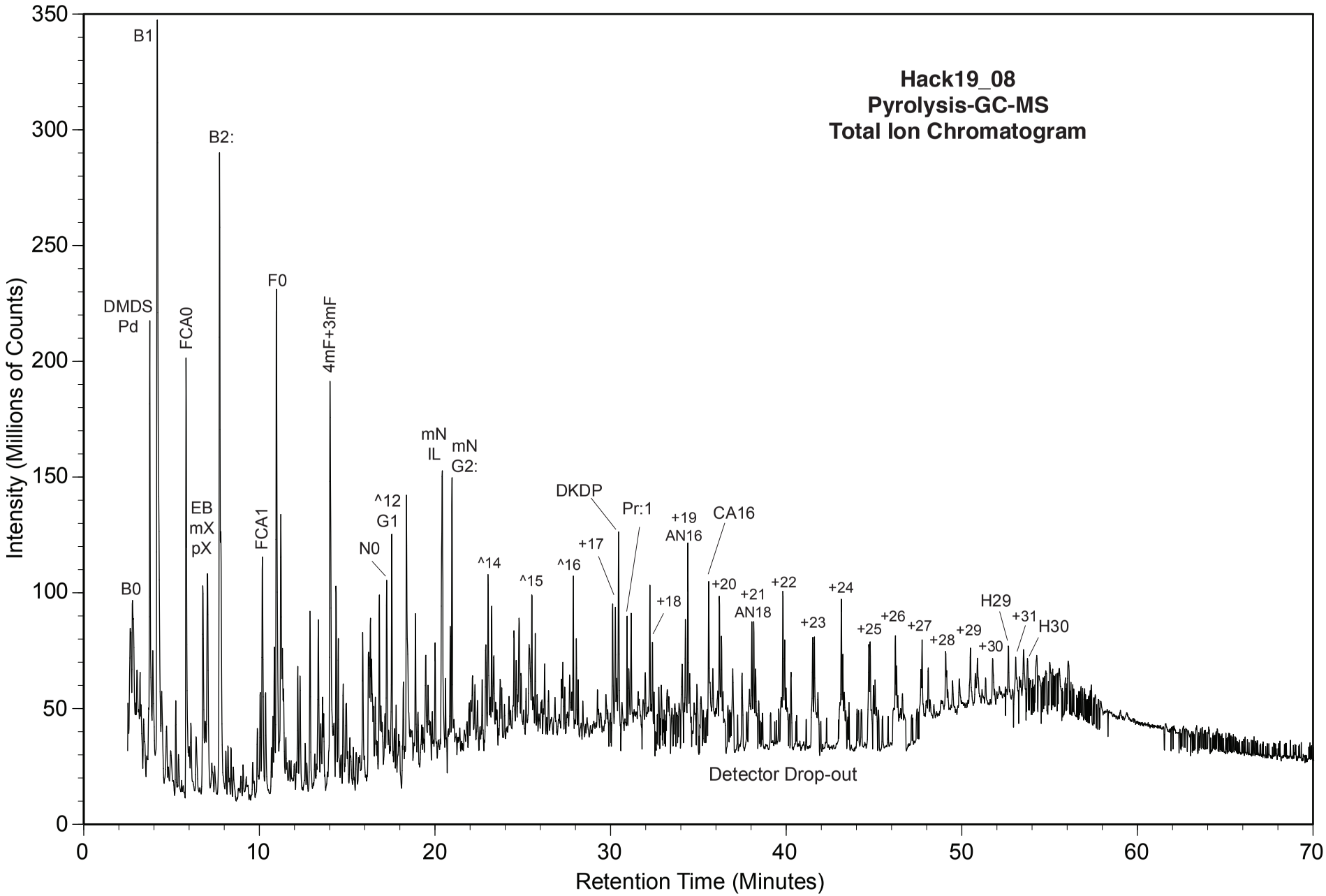
Hack19_08
Pyrolysis-GC-MS
Total Ion Chromatogram
Intensity (Millions of Counts)
Retention Time (Minutes)
0
50
100
150
200
250
300
350
0
10
20
30
40
50
60
70
B1
B2:
DMDS
Pd
FCA0
F0
4mF+3mF
EB
mX
pX
FCA1
B0
N0
^12
G1
mN
IL
mN
G2:
^14
^15
^16
DKDP
+17
Pr:1
+18
+19
AN16
CA16
+20
+21
AN18
+22
+23
+24
+25
+26
+27
+28
+29
+30
H29
+31
H30
Detector Drop-out

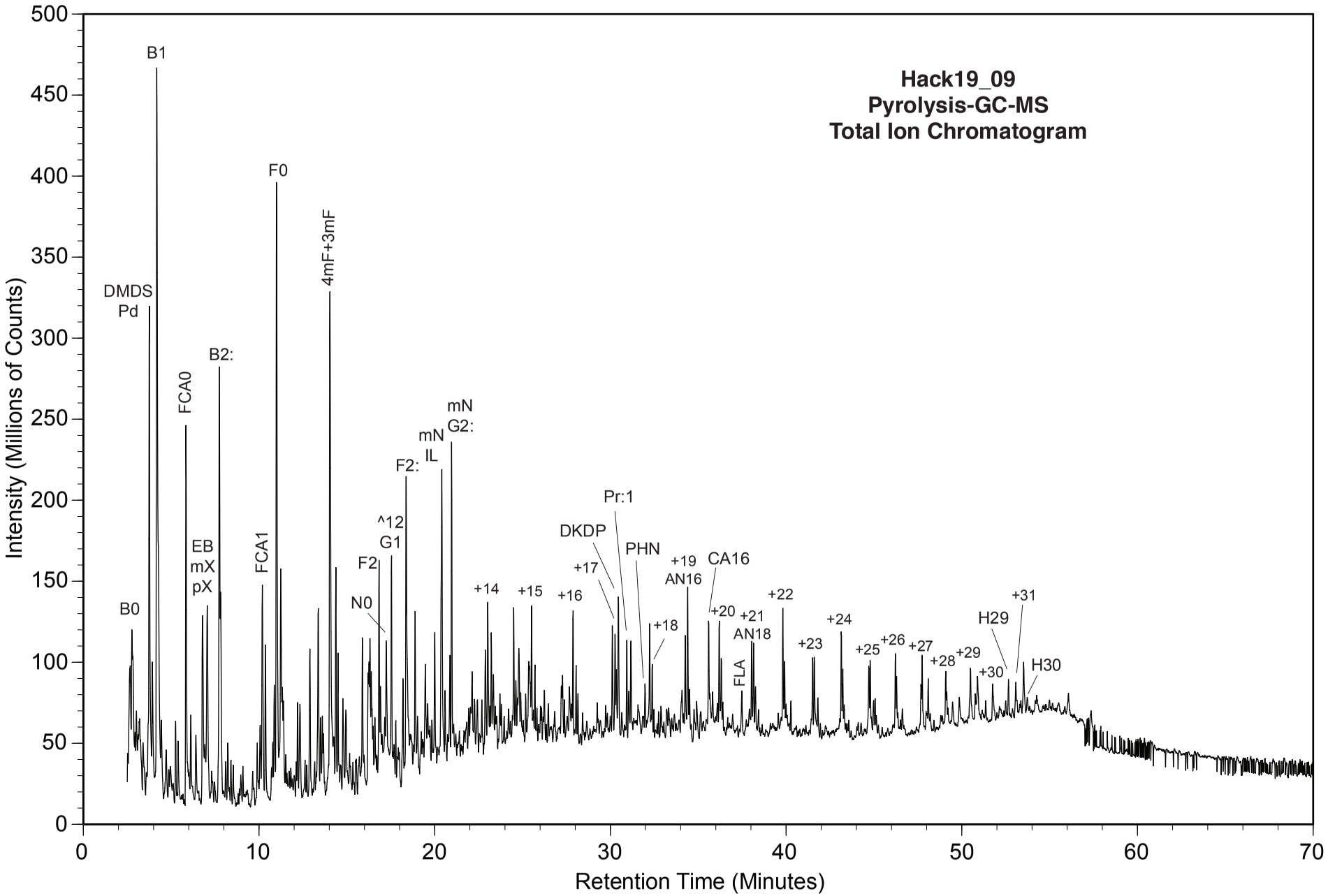
Hack19_09
Pyrolysis-GC-MS
Total Ion Chromatogram
Intensity (Millions of Counts)
Retention Time (Minutes)
0
50
100
150
200
250
300
350
400
450
500
0
10
20
30
40
50
60
70
B0
B1
DMDS
Pd
FCA0
EB
mX
pX
B2:
FCA1
F0
4mF+3mF
N0
F2
^12
G1
F2:
mN
IL
mN
G2:
+14
+15
+16
+17
DKDP
Pr:1
PHN
+18
+19
AN16
CA16
+20
+21
AN18
FLA
+22
+23
+24
+25
+26
+27
+28
+29
+30
H29
+31
H30

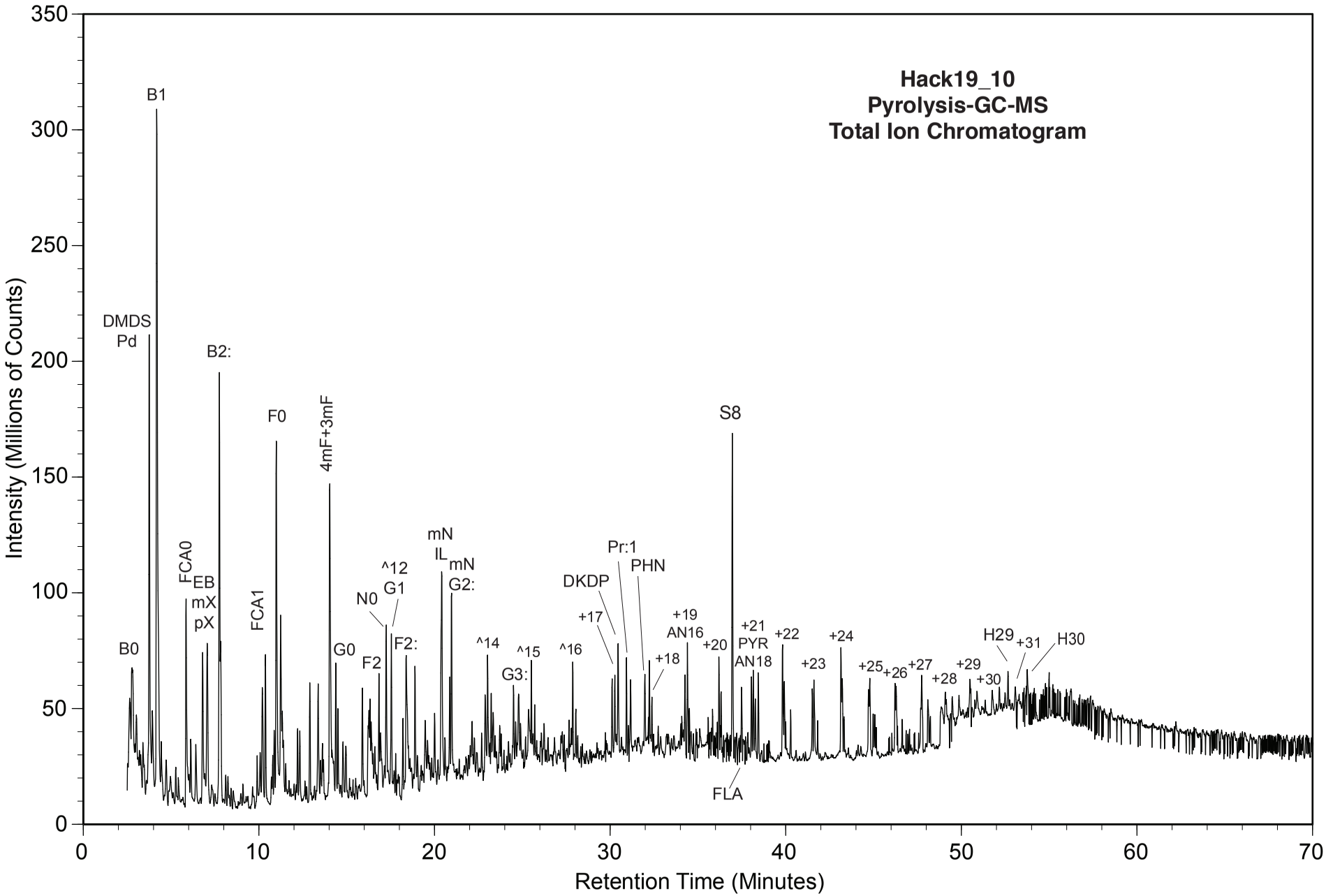
Hack19_10
Pyrolysis-GC-MS
Total Ion Chromatogram
Intensity (Millions of Counts)
Retention Time (Minutes)
0
50
100
150
200
250
300
350
0
10
20
30
40
50
60
70
B0
B1
DMDS
Pd
FCA0
EB
mX
pX
B2:
FCA1
F0
4mF+3mF
G0
N0
F2
^12
G1
F2:
mN
IL
mN
G2:
^14
G3:
^15
^16
DKDP
+17
Pr:1
PHN
+18
+19
AN16
+20
S8
FLA
+21
PYR
AN18
+22
+23
+24
+25
+26
+27
+28
+29
+30
H29
+31
H30

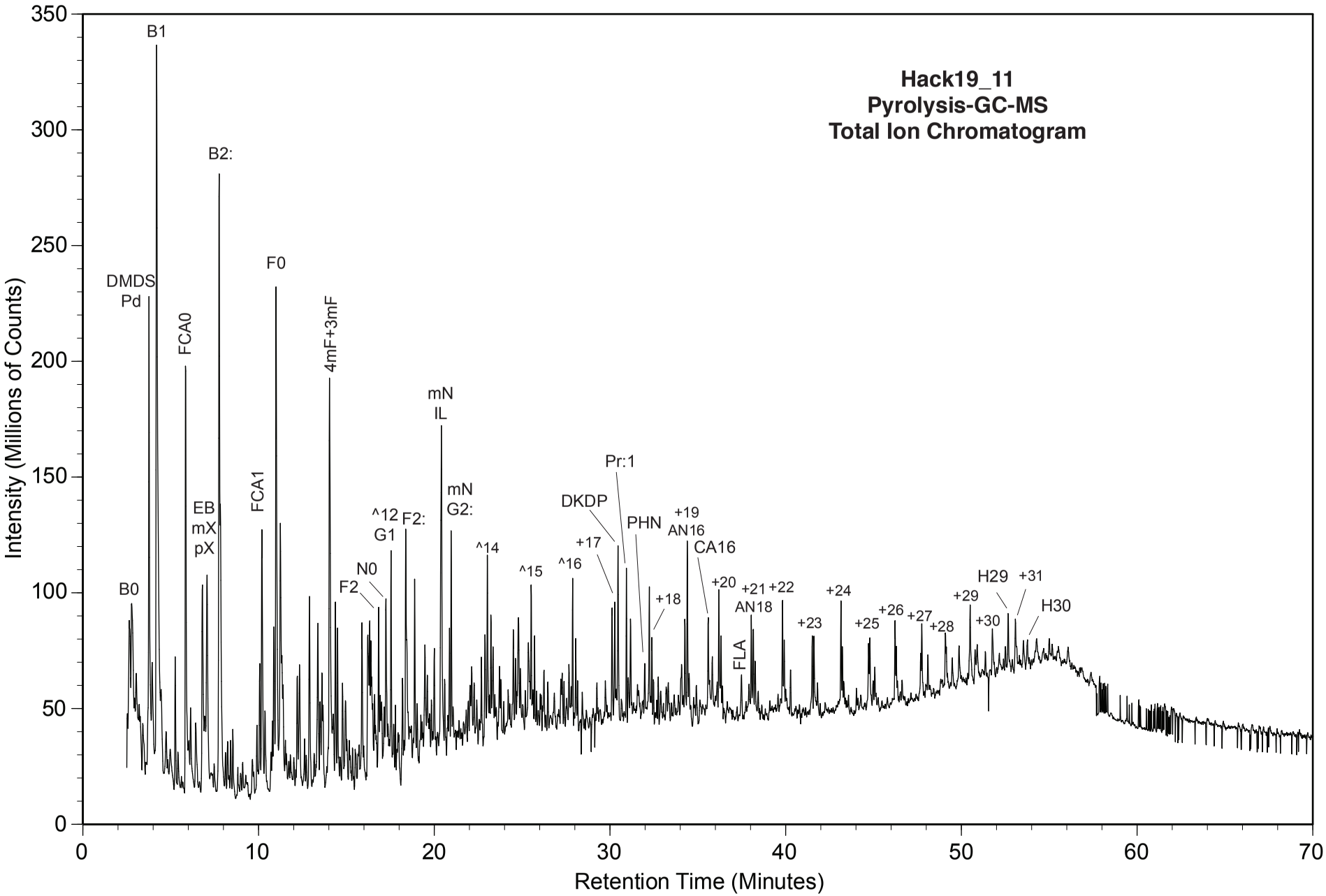
Hack19_11
Pyrolysis-GC-MS
Total Ion Chromatogram
Intensity (Millions of Counts)
Retention Time (Minutes)
0
50
100
150
200
250
300
350
0
10
20
30
40
50
60
70
B0
B1
DMDS
Pd
FCA0
B2:
EB
mX
pX
FCA1
F0
4mF+3mF
F2
N0
^12
G1
F2:
mN
IL
mN
G2:
^14
^15
^16
+17
DKDP
Pr:1
PHN
+18
+19
AN16
CA16
+20
+21
AN18
+22
FLA
+23
+24
+25
+26
+27
+28
+29
+30
H29
+31
H30

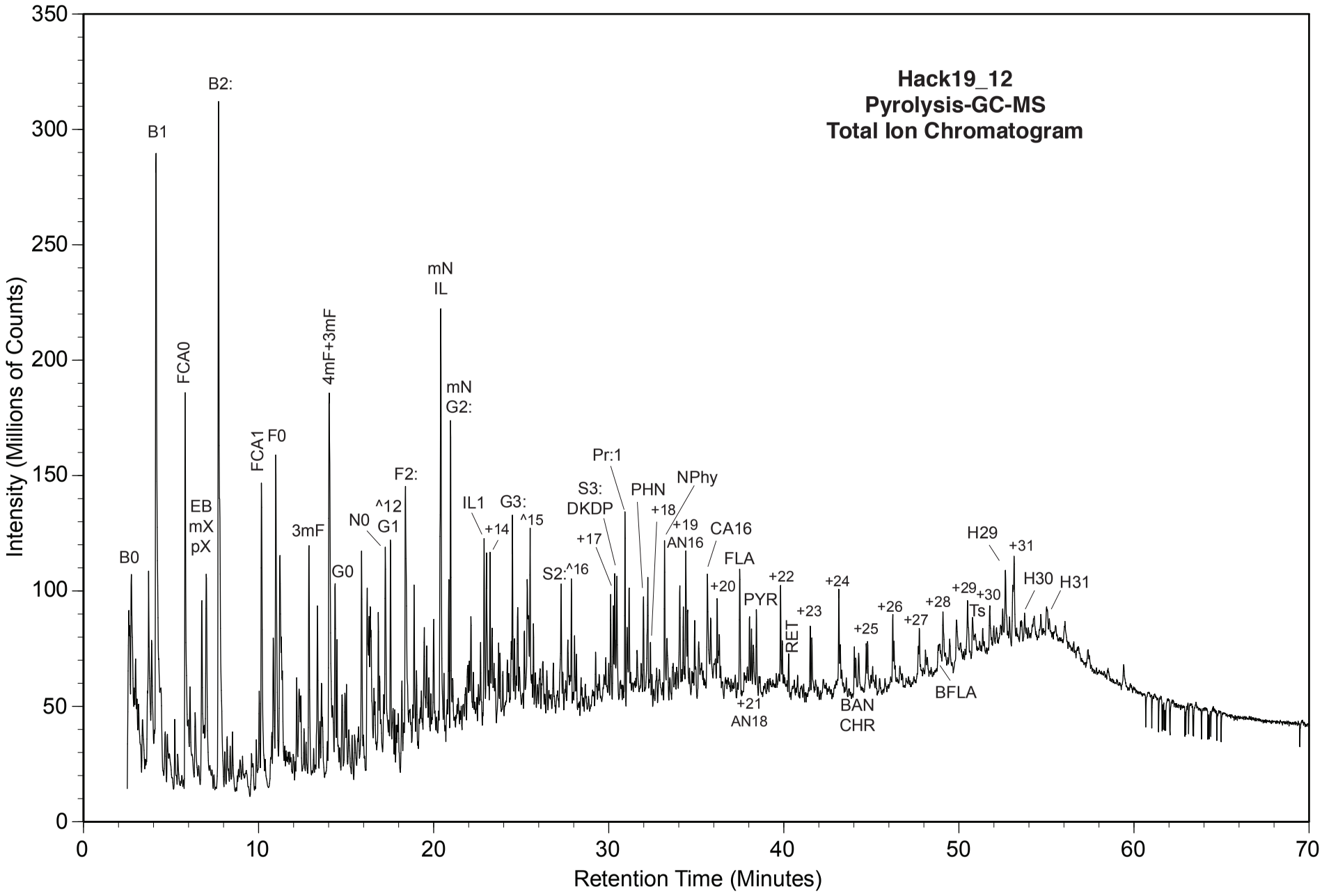
Hack19_12
Pyrolysis-GC-MS
Total Ion Chromatogram
Intensity (Millions of Counts)
Retention Time (Minutes)
0
50
100
150
200
250
300
350
0
10
20
30
40
50
60
70
B0
B1
B2:
FCA0
EB
mX
pX
FCA1
F0
3mF
4mF+3mF
G0
N0
^12
G1
F2:
mN
IL
mN
G2:
IL1
+14
G3:
^15
S2:^16
S3:
DKDP
+17
Pr:1
PHN
+18
NPhy
+19
AN16
CA16
+20
FLA
PYR
+21
AN18
+22
RET
+23
+24
BAN
CHR
+25
+26
+27
+28
BFLA
+29
Ts
+30
H29
+31
H30
H31

APPENDIX B:
Commercial Laboratory Report

Integrated Analytical Laboratories
Compound list for GC-MS analyses

Target Compounds (PAHs)
Naphthalene
2-Methylnaphthalene
Acenaphthylene
Acenaphthene
Fluorene
Phenanthrene
Anthracene
Fluoranthene
Pyrene
Benzo[*a*]anthracene
Chrysene
Benzo[*b*]fluoranthene
Benzo[*k*]fluoranthene
Benzo[*a*]pyrene
Indeno[l,2,3-*cd*]pyrene
Dibenz[*a,h*]anthracene
Benzo[*ghi*]perylene

Internal Standards
(Note: hydrogen replaced by deuterium ("d") to make these compounds distinguishable by mass spectrometry.)
l,4-Dichlorobenzene-d4
Naphthalene-d8
Acenaphthene-d10
Phenanthrene-d10
Chrysene-d12
Perylene-d12
l,4-Dioxane-d8

System Monitoring Compounds
2-Fluorophenol
Phenol-d5
l,4-Dioxane-d8
Nitrobenzene-d5
2-Fluorobiphenyl
2,4,6-Tribromophenol
Terphenyl-d14

Quantitation Report (QT Reviewed)

Data Path : C:\msdchem\1\data\19-11-08C\
Data File : C7407.D
Acq On : 8 Nov 2019 18:11
Operator : EDM
Sample : HACK_19-,E19-07990-001,Xs,15.10g,42.9,0.5
Misc : 191106-01,11/06/19,10/28/19,1
ALS Vial : 29 Sample Multiplier: 1

Quant Time: Nov 11 11:05:29 2019
Quant Method : C:\MSDCHEM\1\METHODS\CS2919.M
Quant Title : BNA CALIBRATION METHOD
QLast Update : Fri Nov 08 08:29:50 2019
Response via : Initial Calibration

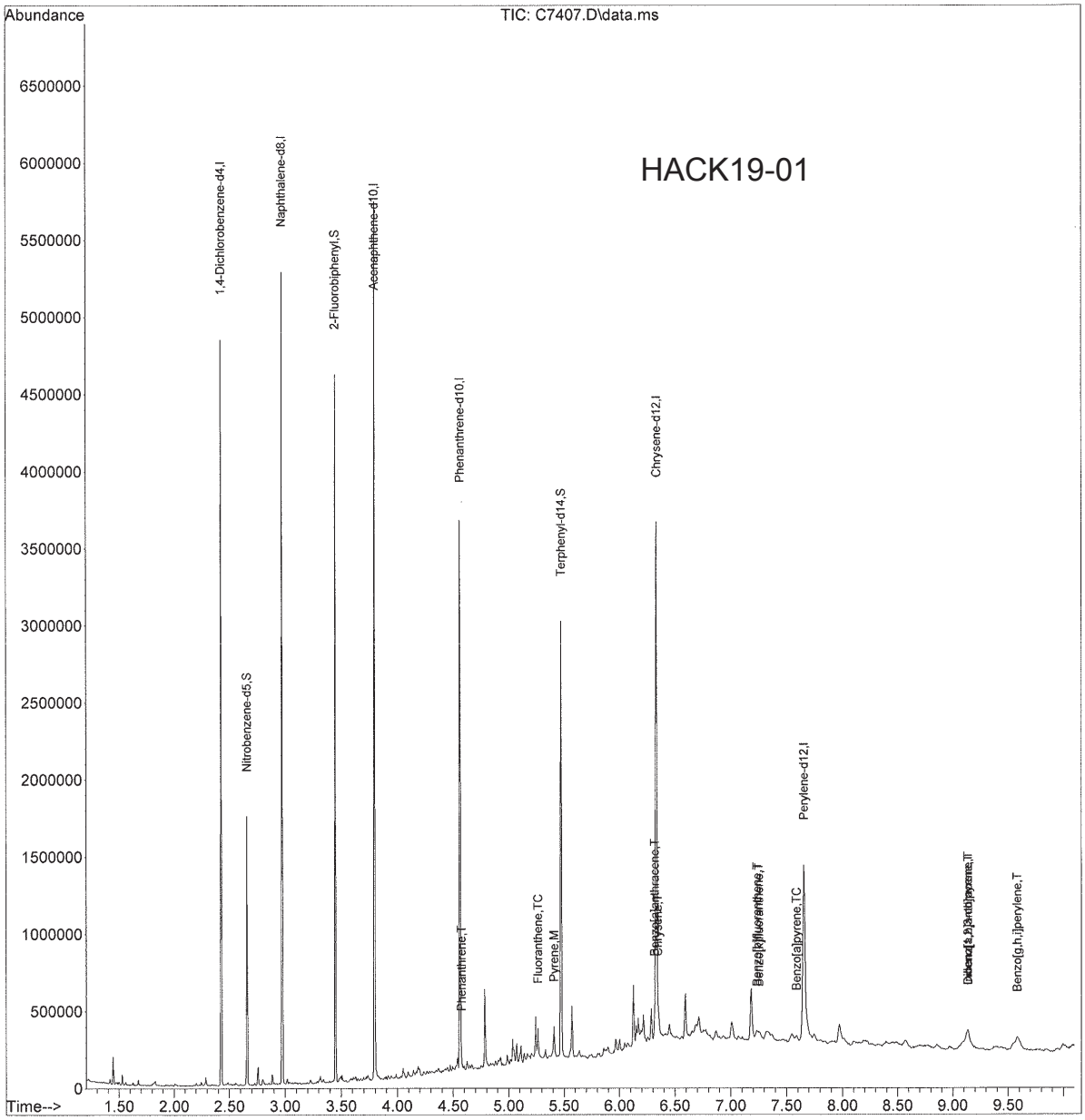

INTEGRATED ANALYTICAL LABORATORIES, LLC

Quantitation Report (QT Reviewed)

Data Path : C:\msdchem\1\data\19-11-08C\
Data File : C7408.D
Acq On : 8 Nov 2019 18:26
Operator : EDM
Sample : HACK_19-,E19-07990-002,Xs,15.1g,1.80,0.5
Misc : 191106-01,11/06/19,10/28/19,1
ALS Vial : 30 Sample Multiplier: 1

Quant Time: Nov 11 11:09:56 2019
Quant Method : C:\MSDCHEM\1\METHODS\CS2919.M
Quant Title : BNA CALIBRATION METHOD
QLast Update : Fri Nov 08 08:29:50 2019
Response via : Initial Calibration

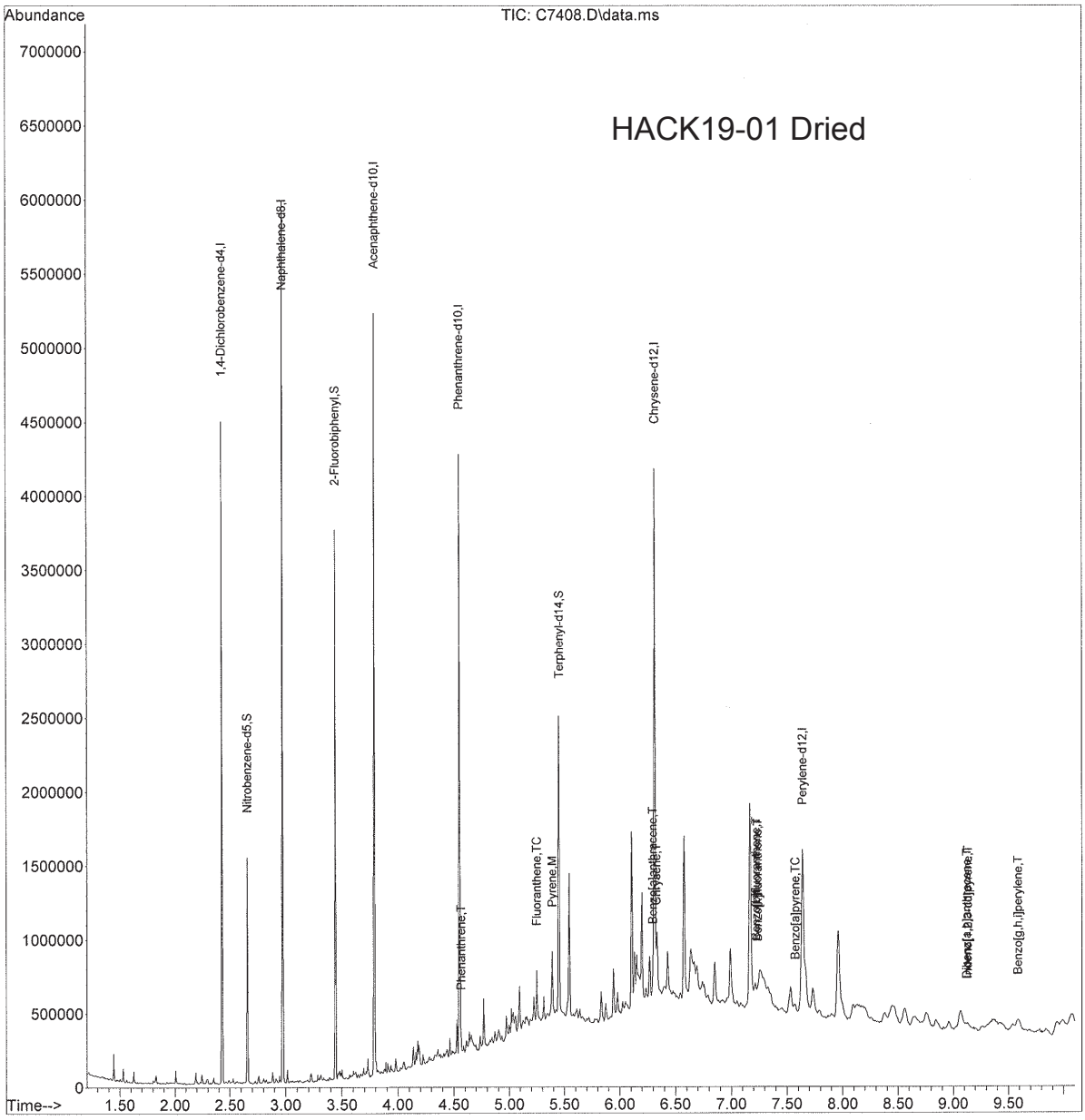

INTEGRATED ANALYTICAL LABORATORIES, LLC

Quantitation Report (QT Reviewed)

Data Path : C:\msdchem\1\data\19-11-08C\
Data File : C7409.D
Acq On : 8 Nov 2019 18:42
Operator : EDM
Sample : HACK_19-,E19-07990-004,Xs,15.3g,2.00,0.5
Misc : 191106-01,11/06/19,10/28/19,1
ALS Vial : 31 Sample Multiplier: 1

Quant Time: Dec 05 12:03:04 2019
Quant Method : C:\MSDCHEM\1\METHODS\CS2919.M
Quant Title : BNA CALIBRATION METHOD
QLast Update : Fri Nov 08 08:29:50 2019
Response via : Initial Calibration

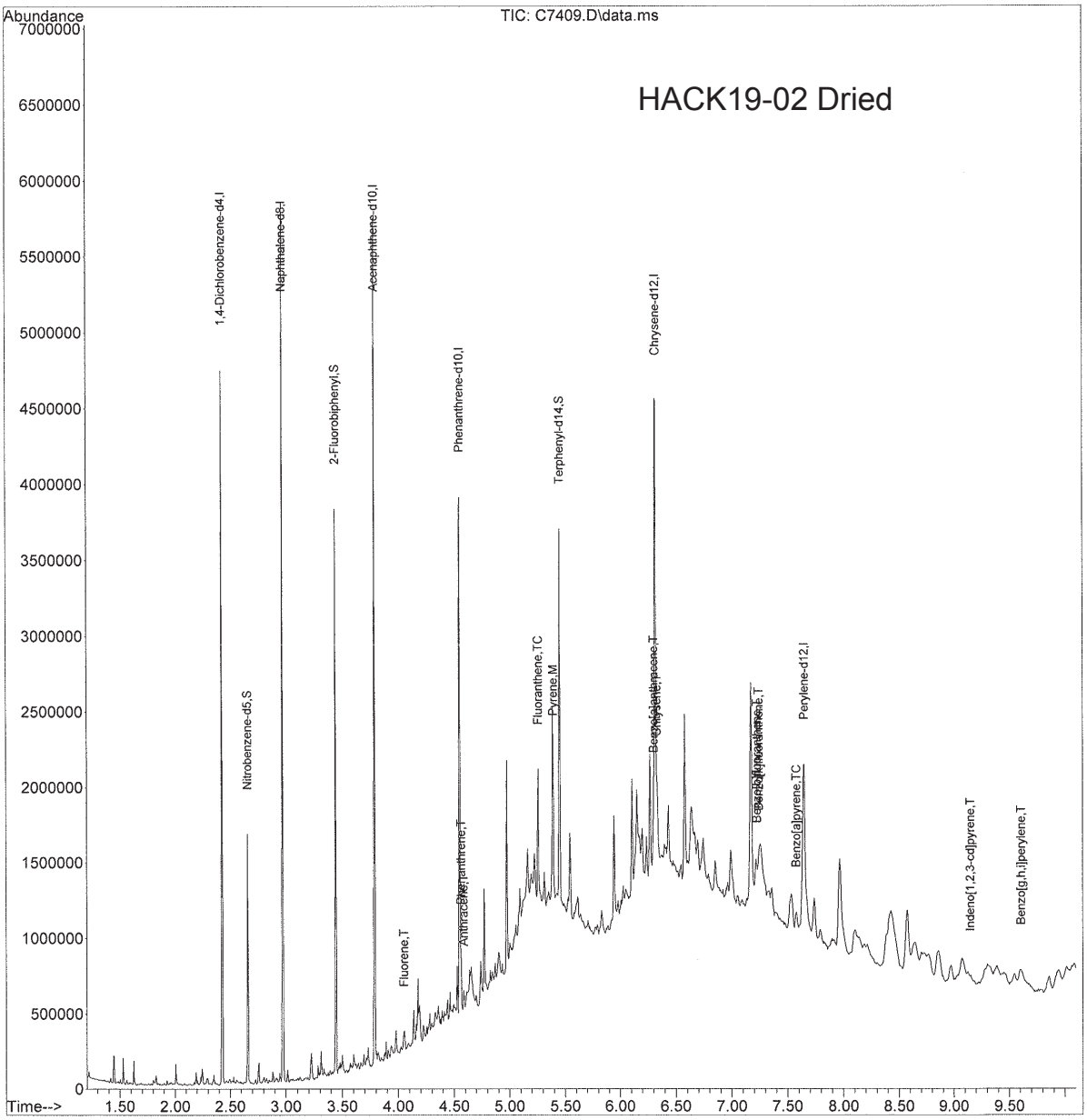

CS2919.M Thu Dec 05 12:03:12 2019 MSDC Page: 2

Quantitation Report (QT Reviewed)

Data Path : C:\msdchem\1\data\19-11-08C\
Data File : C7410.D
Acq On : 8 Nov 2019 18:57
Operator : EDM
Sample : HACK_19-,E19-07990-005,Xs,15.1g,67.5,0.5
Misc : 191106-01,11/06/19,10/28/19,1
ALS Vial : 32 Sample Multiplier: 1

Quant Time: Nov 11 11:16:17 2019
Quant Method : C:\MSDCHEM\1\METHODS\CS2919.M
Quant Title : BNA CALIBRATION METHOD
QLast Update : Fri Nov 08 08:29:50 2019
Response via : Initial Calibration

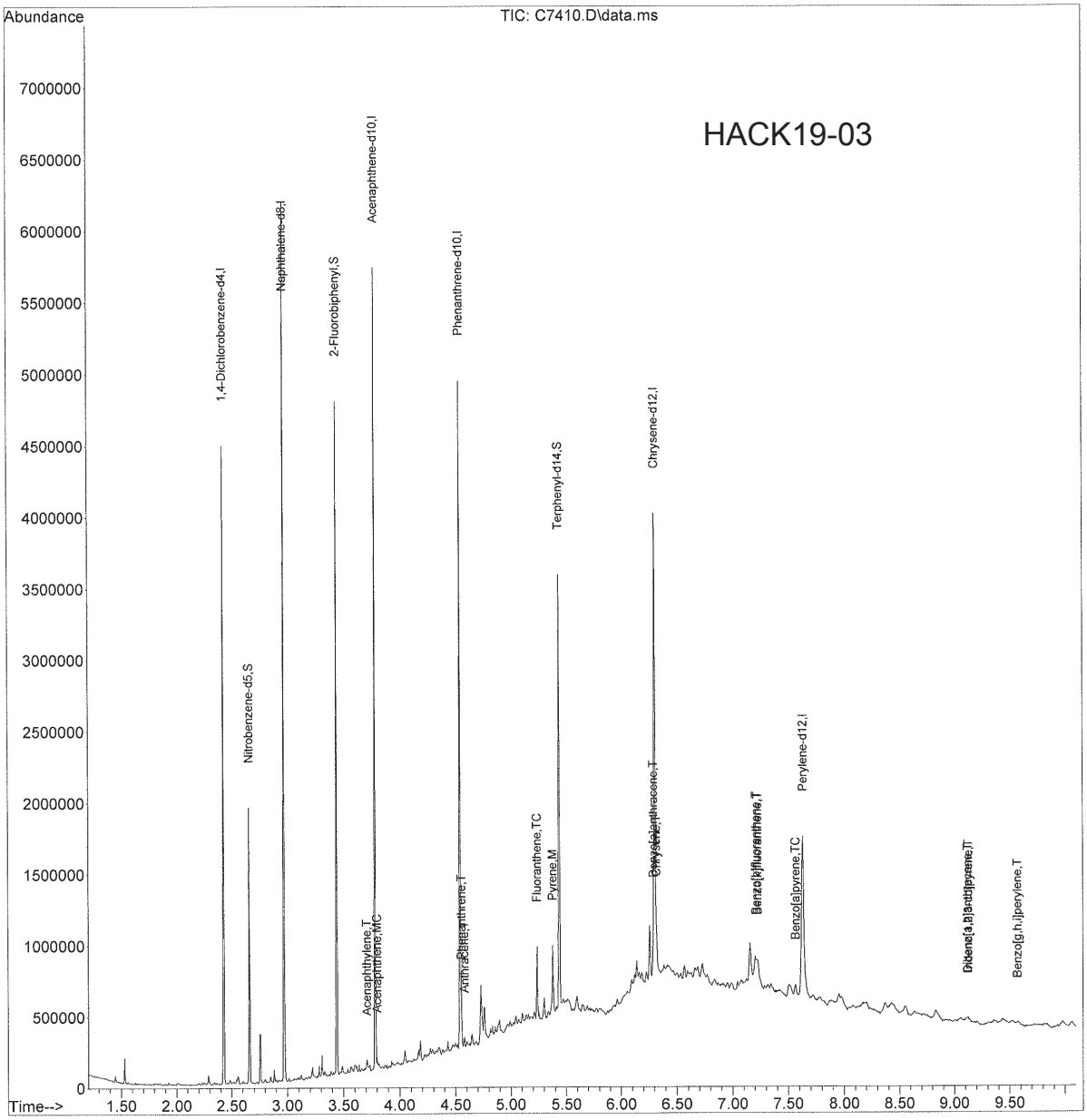

CS2919.M Mon Dec 02 14:25:42 2019 MSDC Page: 2

INTEGRATED ANALYTICAL LABORATORIES, LLC

Quantitation Report (QT Reviewed)

Data Path : C:\msdchem\1\data\19-11-08C\
Data File : C7411.D
Acq On : 8 Nov 2019 19:12
Operator : EDM
Sample : HACK_19-,E19-07990-006,Xs,15.4g,66.5,0.5
Misc : 191106-01,11/06/19,10/28/19,1
ALS Vial : 33 Sample Multiplier: 1

Quant Time: Nov 11 11:24:28 2019
Quant Method : C:\MSDCHEM\1\METHODS\CS2919.M
Quant Title : BNA CALIBRATION METHOD
QLast Update : Fri Nov 08 08:29:50 2019
Response via : Initial Calibration

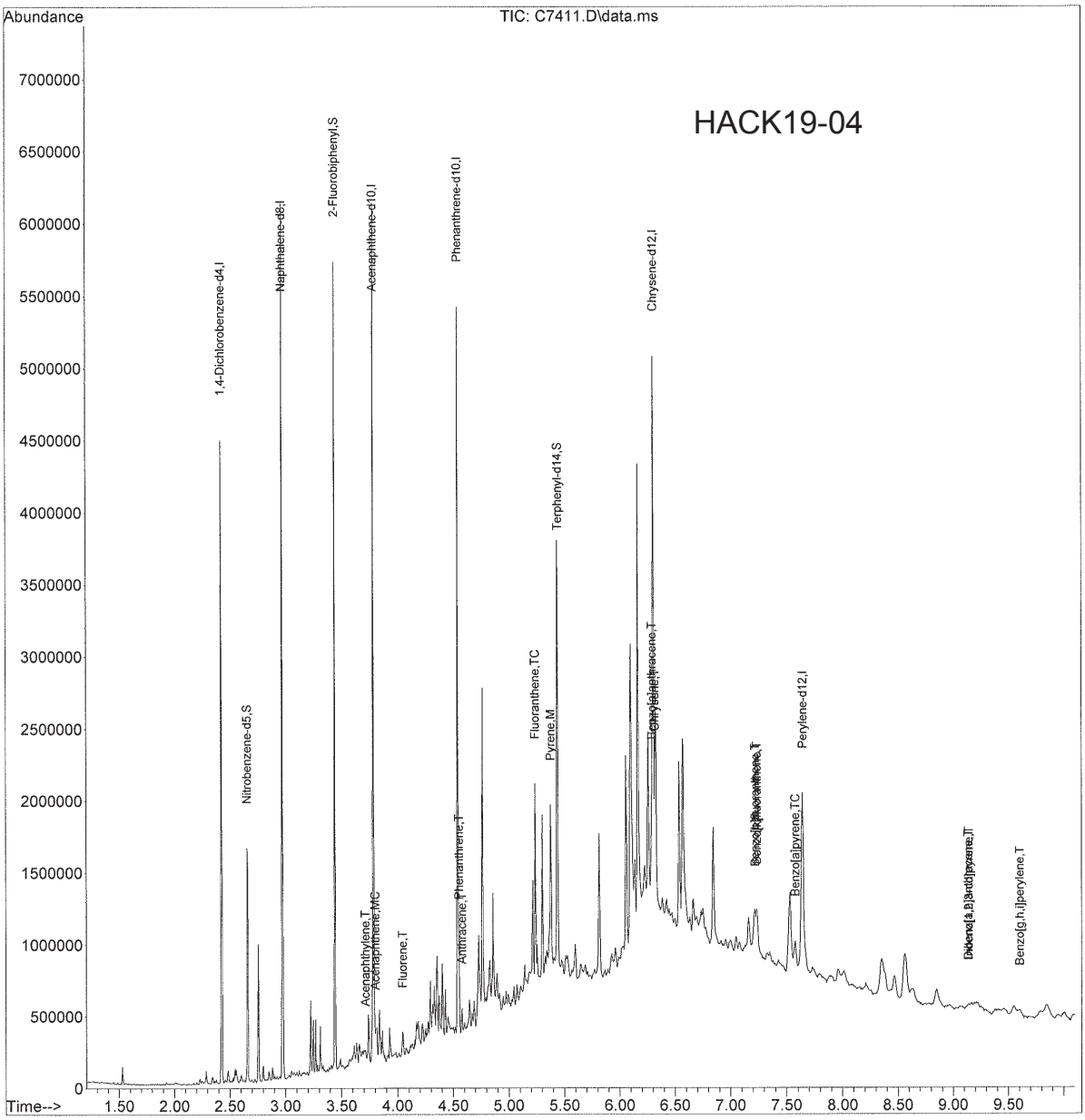

INTEGRATED ANALYTICAL LABORATORIES, LLC

Quantitation Report (QT Reviewed)

Data Path : C:\msdchem\1\data\19-11-08C\
Data File : C7412.D
Acq On : 8 Nov 2019 19:27
Operator : EDM
Sample : HACK_19-,E19-07990-007,Xs,15.3g,68.7,0.5
Misc : 191106-01,11/06/19,10/28/19,1
ALS Vial : 34 Sample Multiplier: 1

Quant Time: Nov 11 11:26:06 2019
Quant Method : C:\MSDCHEM\1\METHODS\CS2919.M
Quant Title : BNA CALIBRATION METHOD
QLast Update : Fri Nov 08 08:29:50 2019
Response via : Initial Calibration

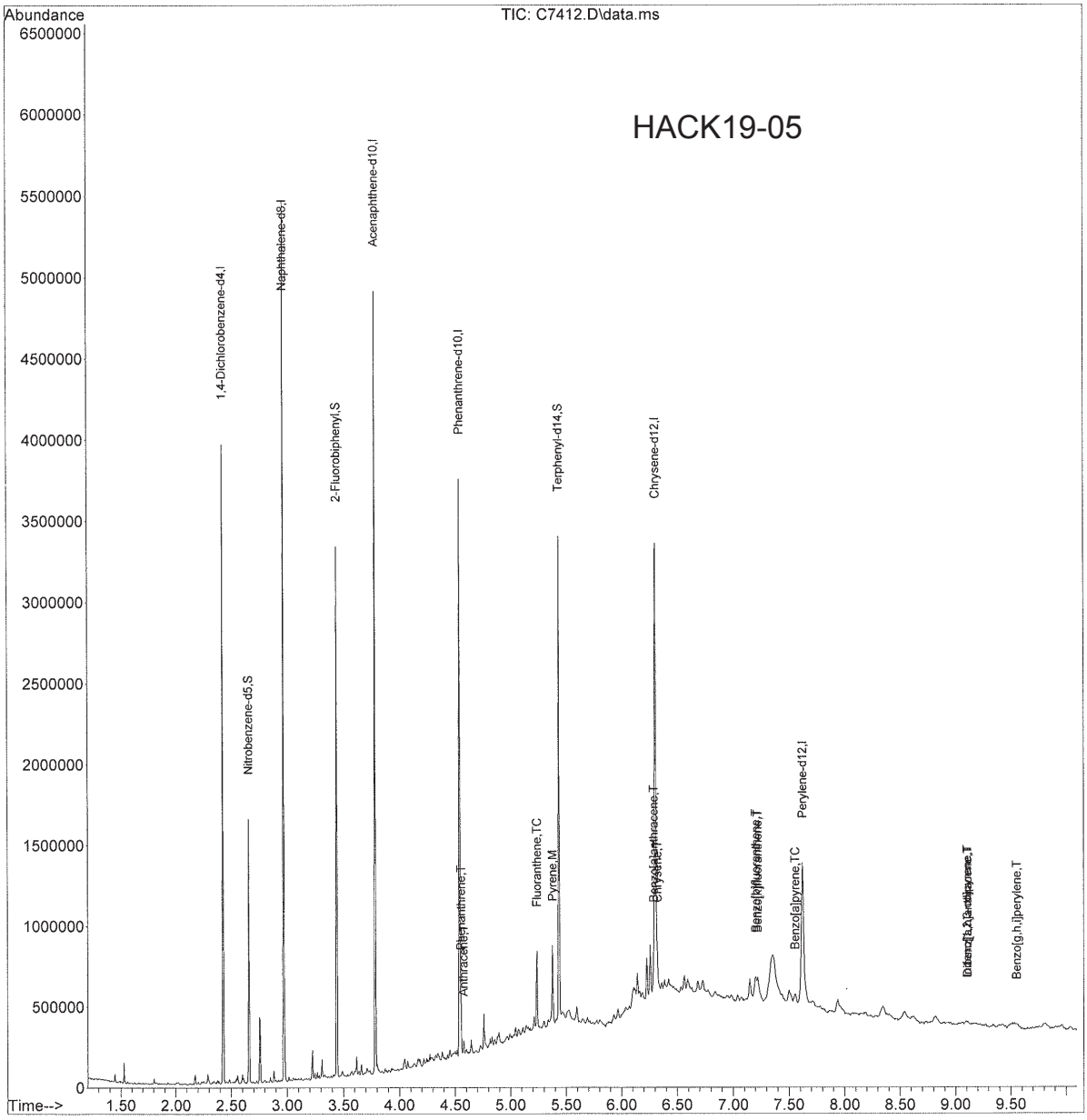

CS2919.M Mon Dec 02 14:26:41 2019 MSDC Page: 2

Quantitation Report (QT Reviewed)

Data Path : C:\msdchem\1\data\19-11-08C\
Data File : C7420.D
Acq On : 8 Nov 2019 21:29
Operator : EDM
Sample : HACK_19.,E19-07990-015,Xs,15.3g,68.7,0.5
Misc : 191106-01,11/06/19,10/28/19,1
ALS Vial : 42 Sample Multiplier: 1

Quant Time: Nov 11 11:55:28 2019
Quant Method : C:\MSDCHEM\1\METHODS\CS2919.M
Quant Title : BNA CALIBRATION METHOD
QLast Update : Fri Nov 08 08:29:50 2019
Response via : Initial Calibration

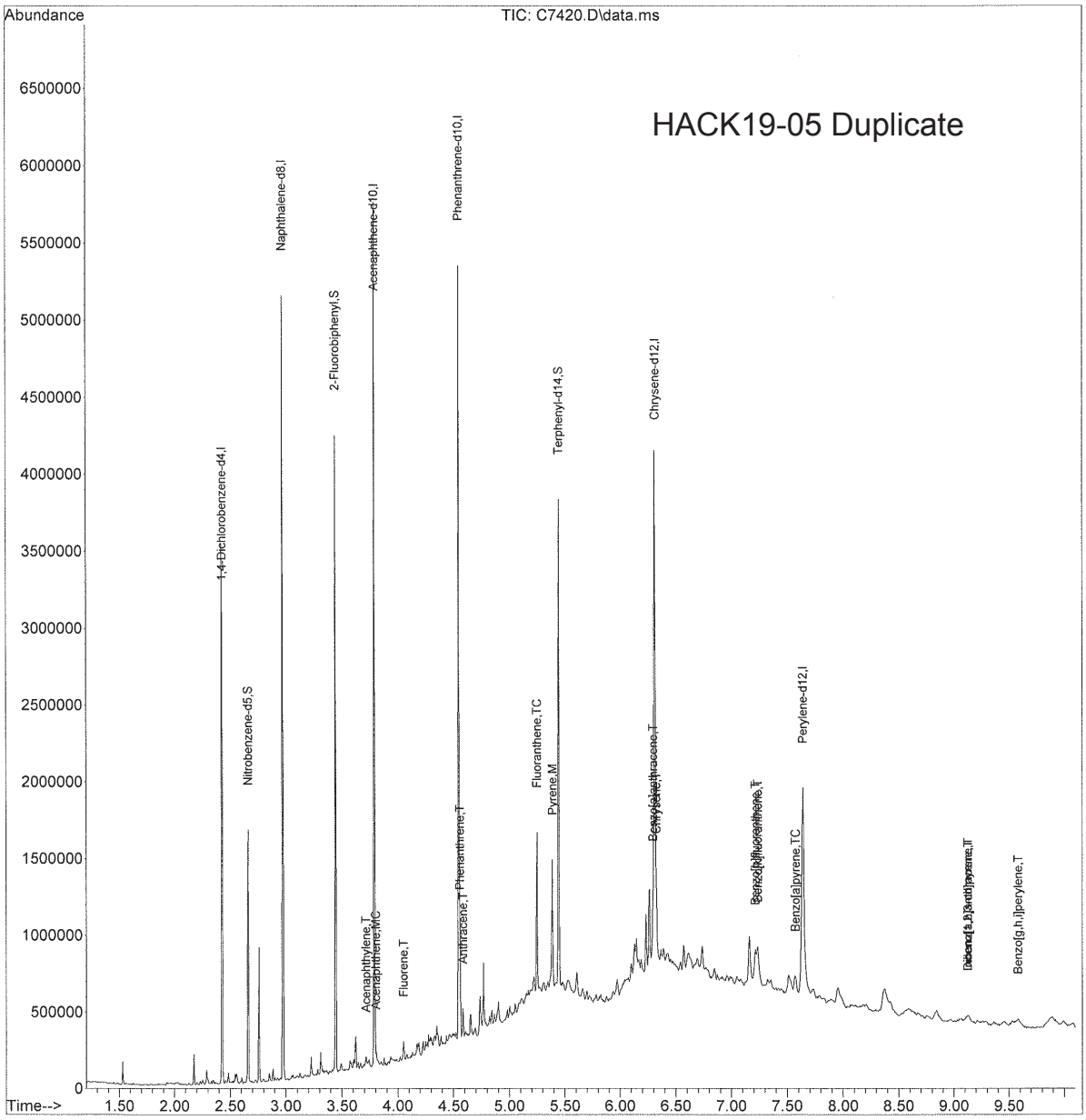

Quantitation Report (QT Reviewed)

Data Path : C:\msdchem\1\data\19-11-08C\
Data File : C7413.D
Acq On : 8 Nov 2019 19:42
Operator : EDM
Sample : HACK_19-,E19-07990-008,Xs,15.7g,62.0,0.5
Misc : 191106-01,11/06/19,10/28/19,1
ALS Vial : 35 Sample Multiplier: 1

Quant Time: Nov 11 11:29:00 2019
Quant Method : C:\MSDCHEM\1\METHODS\CS2919.M
Quant Title : BNA CALIBRATION METHOD
QLast Update : Fri Nov 08 08:29:50 2019
Response via : Initial Calibration

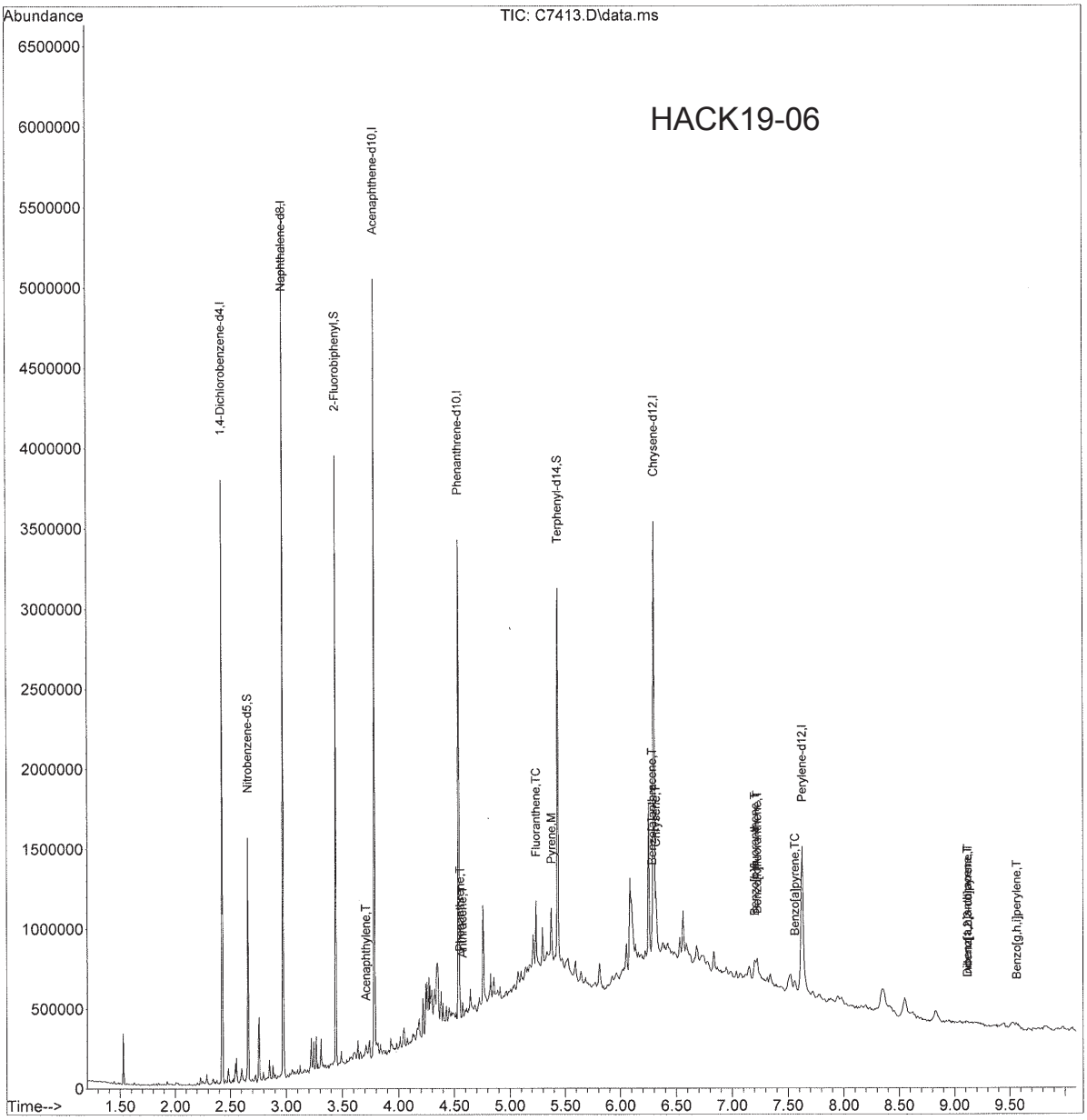

Quantitation Report (QT Reviewed)

Data Path : C:\msdchem\1\data\19-11-08C\
Data File : C7414.D
Acq On : 8 Nov 2019 19:58
Operator : EDM
Sample : HACK_19-,E19-07990-009,Xs,15.1g,54.9,0.5
Misc : 191106-01,11/06/19,10/28/19,1
ALS Vial : 36 Sample Multiplier: 1

Quant Time: Nov 11 11:30:36 2019
Quant Method : C:\MSDCHEM\1\METHODS\CS2919.M
Quant Title : BNA CALIBRATION METHOD
QLast Update : Fri Nov 08 08:29:50 2019
Response via : Initial Calibration

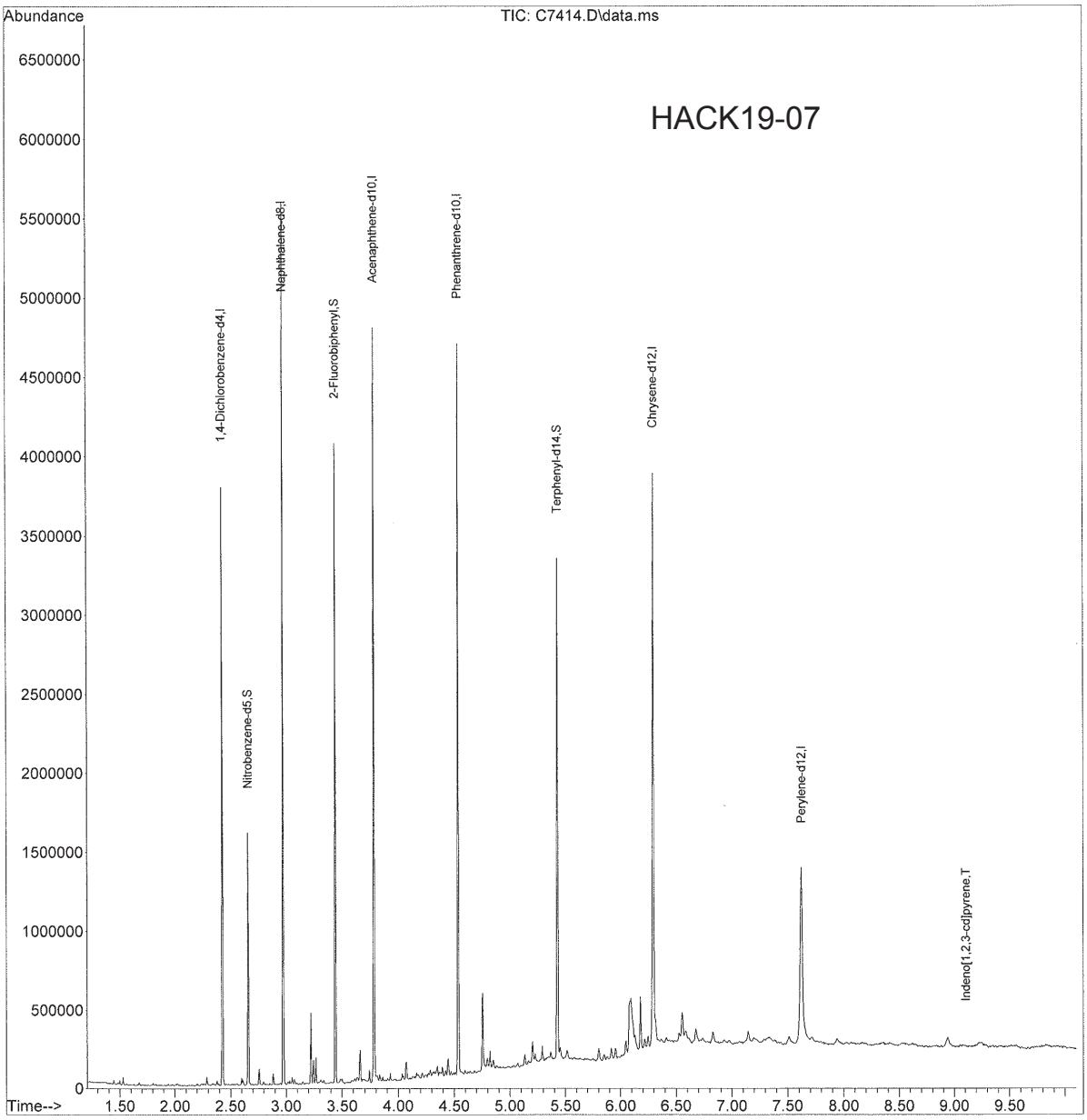

CS2919.M Mon Dec 02 14:27:04 2019 MSDC Page: 2

Quantitation Report (QT Reviewed)

Data Path : C:\msdchem\1\data\19-11-08C\
Data File : C7415.D
Acq On : 8 Nov 2019 20:13
Operator : EDM
Sample : HACK_19-,E19-07990-010,Xs,15.8g,57.0,0.5
Misc : 191106-01,11/06/19,10/28/19,1
ALS Vial : 37 Sample Multiplier: 1

Quant Time: Nov 11 11:45:07 2019
Quant Method : C:\MSDCHEM\1\METHODS\CS2919.M
Quant Title : BNA CALIBRATION METHOD
QLast Update : Fri Nov 08 08:29:50 2019
Response via : Initial Calibration

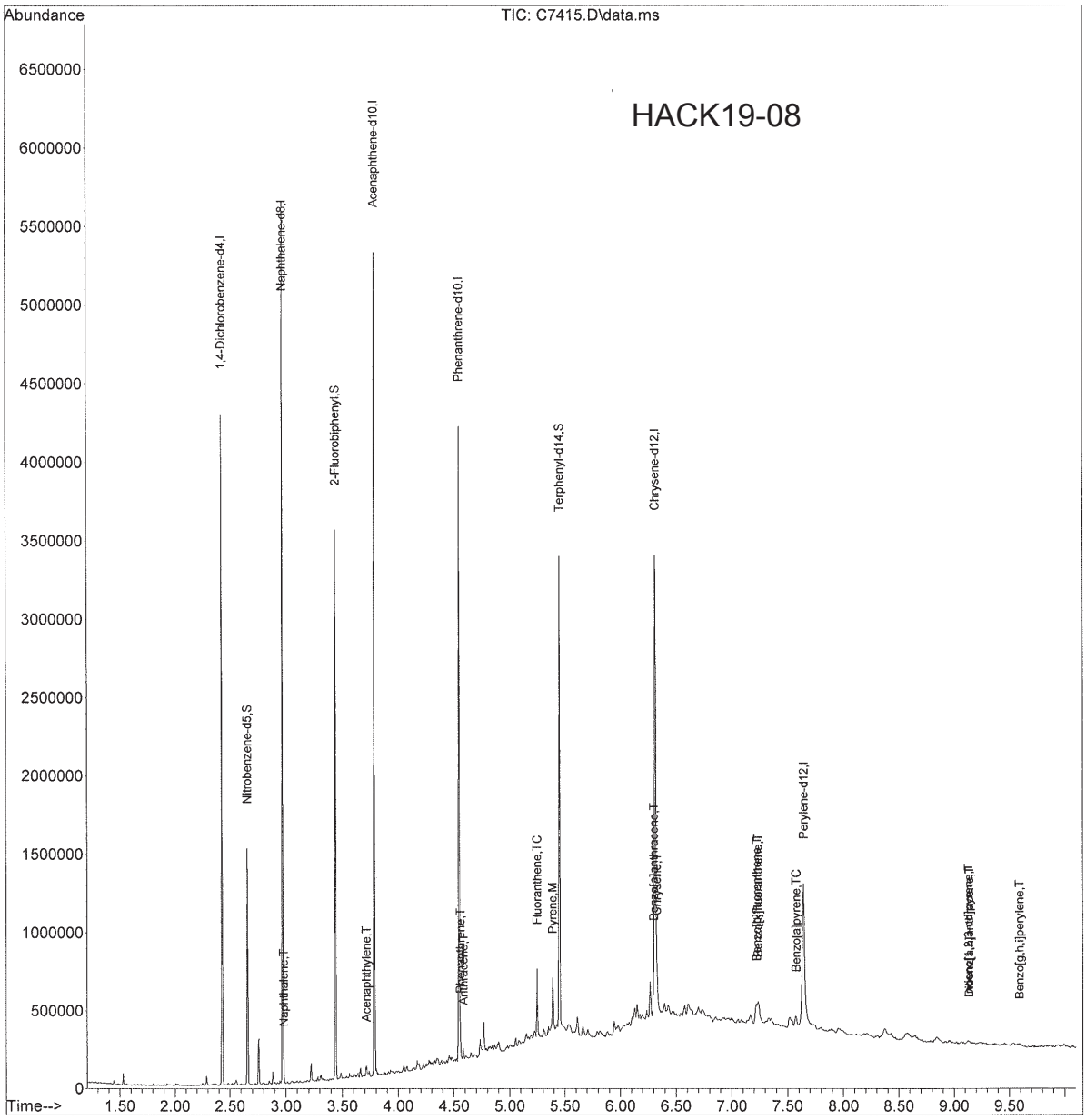

Quantitation Report (QT Reviewed)

Data Path : C:\msdchem\1\data\19-11-08C\
Data File : C7416.D
Acq On : 8 Nov 2019 20:28
Operator : EDM
Sample : HACK_19-,E19-07990-011,Xs,15.0g,52.0,0.5
Misc : 191106-01,11/06/19,10/28/19,1
ALS Vial : 38 Sample Multiplier: 1

Quant Time: Nov 11 11:46:39 2019
Quant Method : C:\MSDCHEM\1\METHODS\CS2919.M
Quant Title : BNA CALIBRATION METHOD
QLast Update : Fri Nov 08 08:29:50 2019
Response via : Initial Calibration

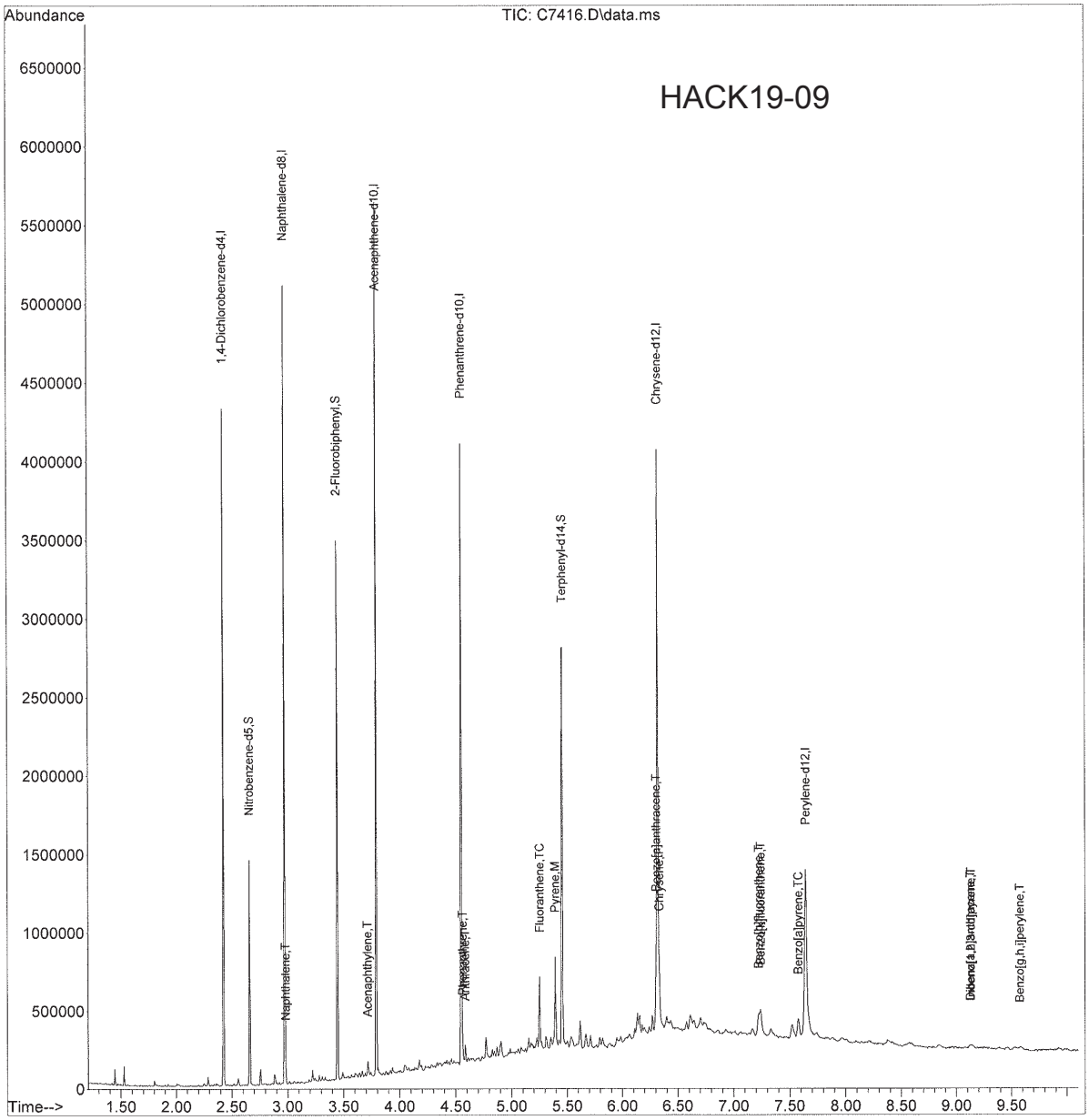

Quantitation Report (QT Reviewed)

Data Path : C:\msdchem\1\data\19-11-08C\
Data File : C7417.D
Acq On : 8 Nov 2019 20:43
Operator : EDM
Sample : HACK_19-,E19-07990-012,Xs,15.2g,38.2,0.5
Misc : 191106-01,11/06/19,10/28/19,1
ALS Vial : 39 Sample Multiplier: 1

Quant Time: Nov 11 11:48:41 2019
Quant Method : C:\MSDCHEM\1\METHODS\CS2919.M
Quant Title : BNA CALIBRATION METHOD
QLast Update : Fri Nov 08 08:29:50 2019
Response via : Initial Calibration

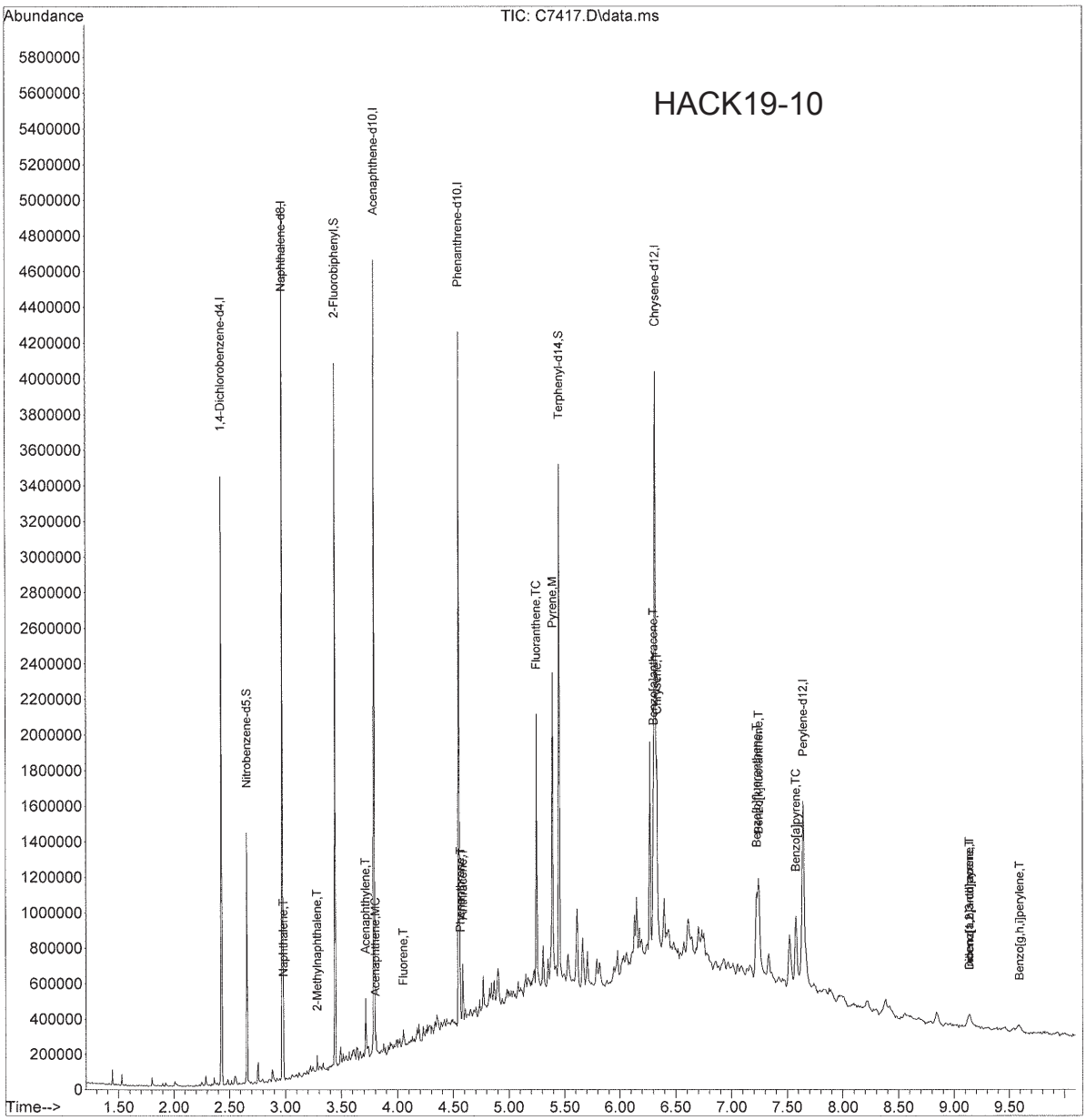

INTEGRATED ANALYTICAL LABORATORIES, LLC

Quantitation Report (QT Reviewed)

Data Path : C:\msdchem\1\data\19-11-08C\
Data File : C7421.D
Acq On : 8 Nov 2019 21:44
Operator : EDM
Sample : HACK_19,E19-07990-16,Xs,15.2g,38.2,0.5
Misc : 191106-01,11/06/19,10/28/19,1
ALS Vial : 43 Sample Multiplier: 1

Quant Time: Nov 11 11:58:13 2019
Quant Method : C:\MSDCHEM\1\METHODS\CS2919.M
Quant Title : BNA CALIBRATION METHOD
QLast Update : Fri Nov 08 08:29:50 2019
Response via : Initial Calibration

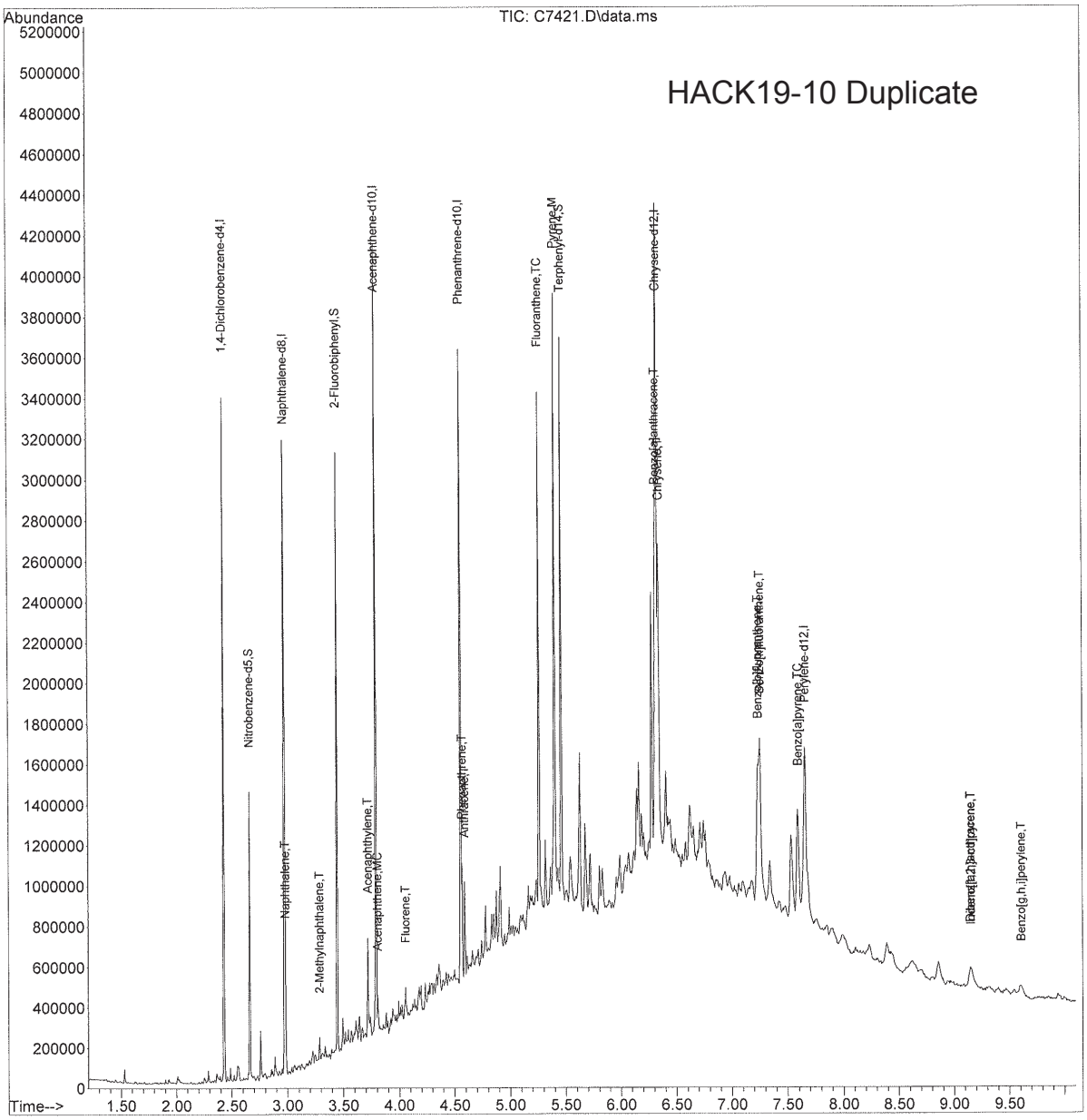

CS2919.M Mon Dec 02 14:28:34 2019 MSDC Page: 2

Quantitation Report (QT Reviewed)

Data Path : C:\msdchem\1\data\19-11-08C\
Data File : C7418.D
Acq On : 8 Nov 2019 20:59
Operator : EDM
Sample : HACK_19-,E19-07990-013,Xs,15.3g,64.3,0.5
Misc : 191106-01,11/06/19,10/28/19,1
ALS Vial : 40 Sample Multiplier: 1

Quant Time: Nov 11 11:51:06 2019
Quant Method : C:\MSDCHEM\1\METHODS\CS2919.M
Quant Title : BNA CALIBRATION METHOD
QLast Update : Fri Nov 08 08:29:50 2019
Response via : Initial Calibration

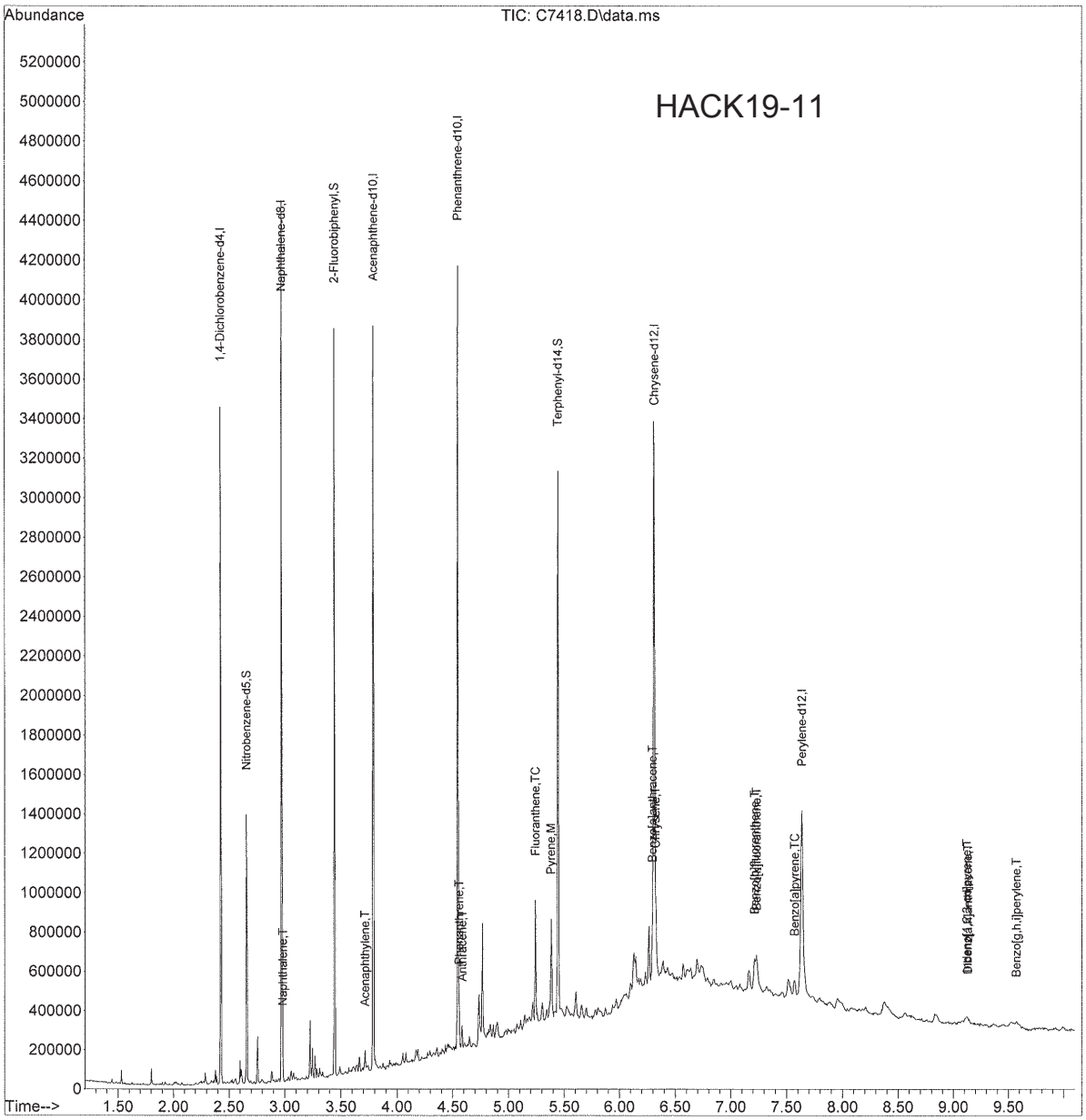

Quantitation Report (QT Reviewed)

Data Path : C:\msdchem\1\data\19-11-08C\
Data File : C7419.D
Acq On : 8 Nov 2019 21:14
Operator : EDM
Sample : HACK_19-,E19-07990-014,Xs,15.3g,47.0,0.5
Misc : 191106-01,11/06/19,10/28/19,1
ALS Vial : 41 Sample Multiplier: 1

Quant Time: Nov 11 11:53:54 2019
Quant Method : C:\MSDCHEM\1\METHODS\CS2919.M
Quant Title : BNA CALIBRATION METHOD
QLast Update : Fri Nov 08 08:29:50 2019
Response via : Initial Calibration

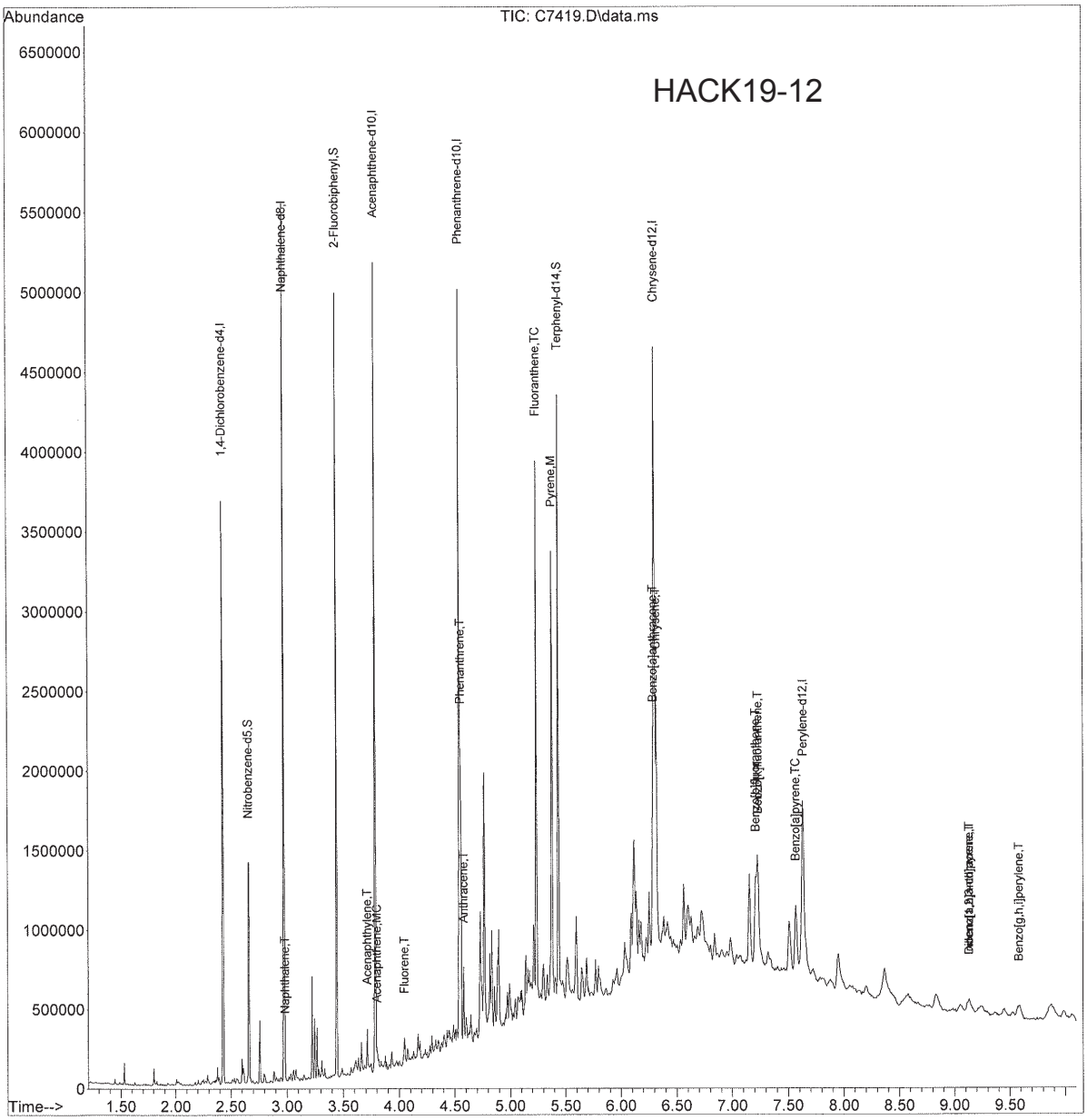

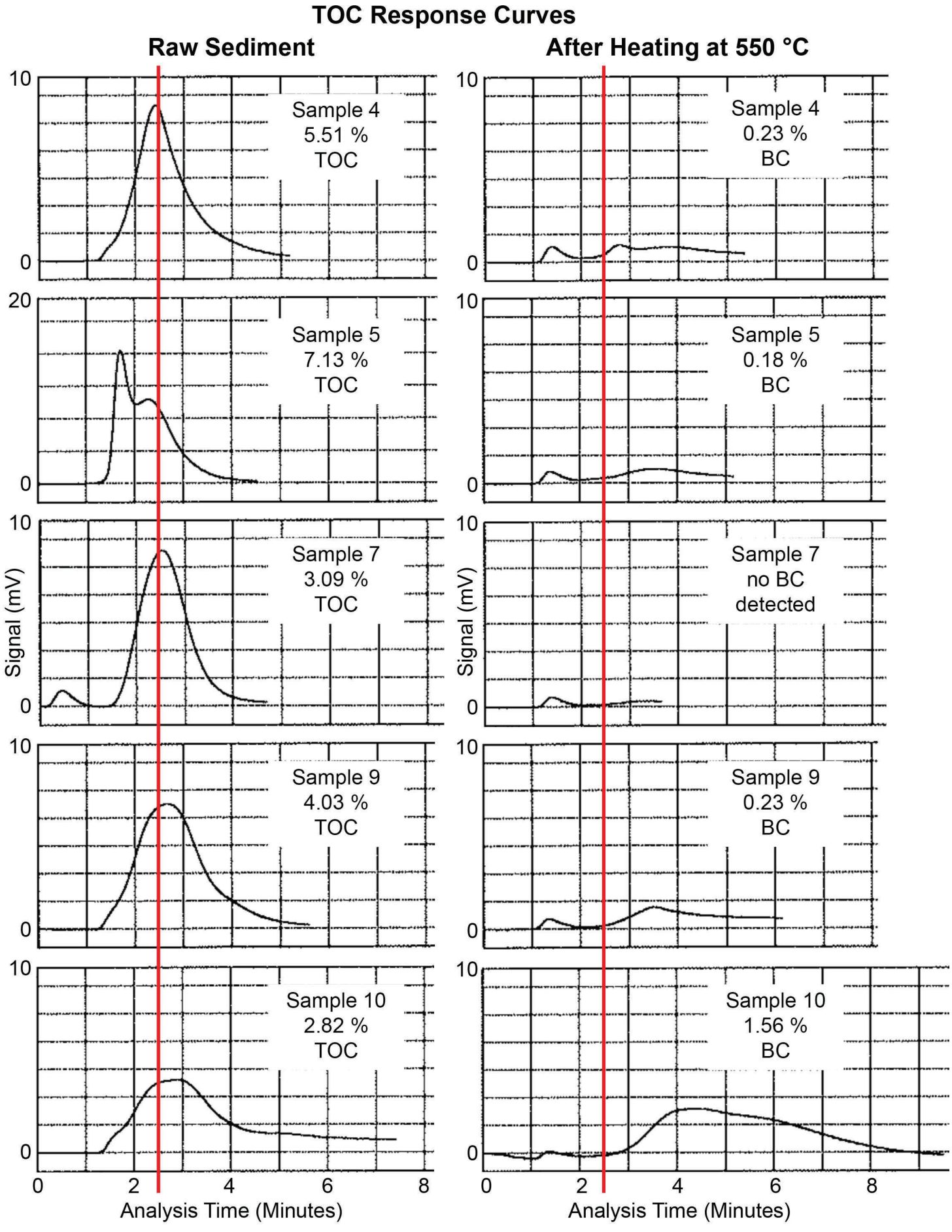
TOC Response Curves
Raw Sediment
After Heating at 550 °C
Sample 4
5.51 %
TOC
Sample 4
0.23 %
BC
Sample 5
7.13 %
TOC
Sample 5
0.18 %
BC
Sample 7
3.09 %
TOC
Sample 7
no BC
detected
Sample 9
4.03 %
TOC
Sample 9
0.23 %
BC
Sample 10
2.82 %
TOC
Sample 10
1.56 %
BC
Signal (mV)
Analysis Time (Minutes)